ACS OMEGA

Open Access

http://pubs.acs.org/journal/acsodf

Review

Label-Free Biochemical Sensing Using Processed Optical Fiber Interferometry: A Review

Rajan Jha,* Pintu Gorai, Anand Shrivastav, and Anand Pathak

Cite This: *ACS Omega* 2024, 9, 3037−3069

Read Online

ACCESS | Metrics & More | Article Recommendations

ABSTRACT: Over the last 20 years, optical fiber-based devices have been exploited extensively in the field of biochemical sensing, with applications in many specific areas such as the food processing industry, environmental monitoring, health diagnosis, bioengineering, disease diagnosis, and the drug industry due to their compact, label-free, and highly sensitive detection. The selective and accurate detection of biochemicals is an essential part of biosensing devices, which is to be done through effective functionalization of highly specific recognition agents, such as enzymes, DNA, receptors, etc., over the transducing surface. Among many optical fiber-based sensing technologies, optical fiber interferometry-based biosensors are one of the broadly used methods with the advantages of biocompatibility, compact size, high sensitivity, high-resolution sensing, lower detection limits, operating wavelength tunability, etc. This Review provides a comprehensive review of the fundamentals as well as the current advances in developing optical fiber interferometry-based biochemical sensors. In the beginning, a generic biosensor and its several components are introduced, followed by the fundamentals and state-of-art technology behind developing a variety of interferometry-based fiber optic sensors. These include the Mach−Zehnder interferometer, the Michelson interferometer, the Fabry−Perot interferometer, the Sagnac interferometer, and biolayer interferometry (BLI). Further, several technical reports are comprehensively reviewed and compared in a tabulated form for better comparison along with their advantages and disadvantages. Further, the limitations and possible solutions for these sensors are discussed to transform these in-lab devices into commercial industry applications. At the end, in conclusion, comments on the prospects of field development toward the commercialization of sensor technology are also provided. The Review targets a broad range of audiences including beginners and also motivates the experts helping to solve the real issues for developing an industry-oriented sensing device.

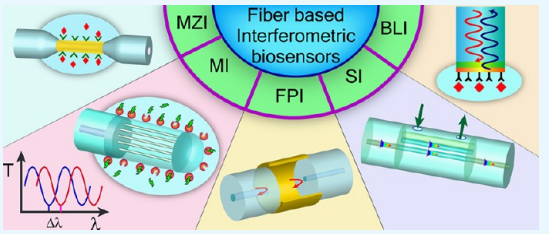

1. INTRODUCTION

Biosensing technology comprises advanced detection methods with innovative analytical developments for the recognition of several biological elements covering a broad spectrum of applications. Some of these are clinical diagnostics, environmental monitoring, and agricultural applications. Among them, the most recent field of biochemical detection is clinical diagnostics tests, where precise measurement of different biochemicals associated with human physiological processes is always essential to help keep our bodies fit and healthy.[1,2] Pharmaceutical application is another important sector involving various types of medicines, vitamins, and drugs for preventing and curing several diseases, where accurate measurements and detection of different reagents are required to obtain the best results.[3] One of the serious problems in recent years has been environmental pollution due to the addition of different toxic pollutants into natural water resources or air. These are mainly different biochemicals produced naturally or in several manmade processes. Therefore, exact monitoring of these toxic biochemicals is essential to control environmental pollution and maintain the safe stable state of the ecosystem.[4] Adulteration due to different harmful biochemicals like flavor, color, and food dyes is happening in an uncontrolled way to improve the food quality artificially. In many cases, the safe limit of these adulterants is exceeded, which causes food poisoning and various other severe health issues. Thus, nowadays food safety is also a major issue for human civilization. Last but not least, humanity is facing large health, social, and economic negative impacts due to the origin and transportation of the coronavirus and its several mutants.[5,6] Hence, viral diagnosis is also a very highly demanding field for biosensing applications.

At present, many transducing methods are being developed or utilized toward biosensing, such as plasmonic,[7] electrochemical,[8] thermometric,[9] piezoelectric,[10] and magnetic methods.[11] Among them, optical fiber-based biochemical

Received: June 6, 2023
Revised: December 8, 2023
Accepted: December 12, 2023
Published: January 11, 2024

sensors have attracted huge attention from the science community because of the outstanding features of optical fibers like compact size, superior biocompatibility, remote operation potential, and multiplexing detection capability. For biomedical application, we would like to mention that the most applied biomedical use of optical fiber is in endoscopy, as it provides an extra benefit of light propagation with bending so imaging of cells, tissues, and other biological components within the human body becomes possible. Conventional silica fiber is not a very biocompatible material, but specially fabricated fibers such as polymer fiber and hydrogel-based fiber have been proven good candidates with better biocompatibility. Hence, these can be used for in vivo monitoring of biological analytes along with their remote sensing capability. Regarding the immunity to electromagnetic interference, as we know, light propagation in optical fiber occurs through the total internal reflection (TIR) phenomenon, where most of the light is guided through a high index core with a small attenuation through the cladding. This light is strongly isolated from the additional ambient electric/magnetic field and no light can be externally coupled through the fiber, which makes the light unaffected by external electromagnetic interference or perturbation. Additionally, the light propagation through the fiber with minimum loss without bending and external electromagnetic interference keeps the signal highly stable. The above-mentioned advantages provide optical fiber an additional advantage compared to traditional substrates for optical sensing.

Several technical methods for the fabrication of optical fiber-based biochemical sensors are proposed in the literature, including fiber Bragg gratings (FBGs),[12] long-period gratings (LPGs),[13] surface-enhanced Raman scattering (SERS),[14] surface plasmon resonance (SPR),[15] lossy-mode resonance (LMR),[16] and optical fiber interferometry.[17] A broad range of research papers, reviews, and books have been published comprising the fields of FBGs, SPR, and SERS for biosensing applications[18−20] without covering the field of fiber optic interferometry. Hence, the present Review has a strong focus on optical fiber interferometry along with a discussion on the fundaments of advanced developments. Specifically in the case of fiber optic interferometry, the advantages are higher sensitivity (as it is sensitive toward the phase change of the light propagating through the sensing layer), higher sensing resolution (as the fwhms are comparatively lower than those of conventional fiber sensors), and hence lower detection limits, higher operating wavelength tunability (one can choose the operating wavelength based on the application), and a wide dynamical range. The recent decade has witnessed substantial progress in optical fiber interferometric-based devices, especially for biosensing and lasing applications.[21,22] These interferometric devices intrinsically can identify the analytes with significantly zero selectivity based on the refractive index variation of the surroundings, which limits their applications toward biosensing applications that require high sensitivity along with high detection specificity. To overcome this challenge, an efficient method is to functionalize the interferometric sensing platform using a highly specific recognition layer toward the target molecule to be detected. The selectivity for such a sensor can be improved by immobilizing a variety of sensing materials, including antibodies,[23] aptamers,[24] enzymes,[25] nucleic acids,[26] and molecular imprinting polymer (MIPs),[27] on the sensor surface.

A working mechanism of a generic biosensor using a fiber-based interferometric platform is as follows. The target biomolecule interacts, covalently or noncovalently, with the highly specific sensing layer immobilized over the interferometric platform by changing its refractive index. This is then translated through the change in the characteristics of the light propagating through the fiber in terms of effective refractive index (RI) variation, spectral absorption, phase, and polarization. These parameters are then translated into optical signals and measured at the output end of the fiber interferometric platform using a spectrometer, optical spectrum analyzer (OSA), interrogator, etc. The sensitivity of these sensors can be enhanced by several interferometric platforms[28] through increasing the loading capacity of the guest molecules and incorporating nanostructures and absorbing 2D materials such as carbon nanotubes,[29] graphene,[30] nanoparticles,[31] quantum dots.[32−34] A broad range of interferometric-based biochemical sensors have been successfully developed and demonstrated by researchers, leading the technology toward more reliable, sensitive, and industry-enabled devices.

The present Review covers an exhaustive survey of fundamentals and technological advancements in fiber optic interferometric sensors, especially for biosensing applications. There are few review articles available in the literature, they are but limited to the physical measurements or some extent for chemical sensors.[35−37] For fundamental aspects, five types of interferometric-based biochemical sensors, namely Mach−Zehnder interferometer, Fabry−Perot interferometer, Michelson interferometer, Sagnac interferometer, and biolayer interferometer, are overviewed in terms of sensing structure, operating principles, and biosensing application fields. Furthermore, the advantages and disadvantages of these interferometric-based biochemical sensors are evaluated in this paper, covering examples of the various reported studies. Later, a summarized overview of the paper along with advancements in technology and future perspectives are exploited.

2. A GENERIC BIOSENSOR

A conventional biosensor consists of three major segments. The first is the target analyte that is to be detected, the second one is the recognition layer or sensing element that binds with the target analyte, and the last one is the transducing element. When the target analyte is recognized and bounded by the sensing element of the sensor through specific molecular interactions, a change in its physical properties, such as color, refractive index, mass, pH, and conductivity, or even in its chemical properties takes place. A few examples of sensing elements or receptors such as antibodies, enzymes, DNAs, nucleic acids, aptamers, and molecular imprinting polymer (MIP) have a selective interaction toward target molecules. Transducer elements translate these changes in the sensing region into some monitorable signal using some physical methods including electrochemistry (identification of changes in electrical properties), quartz crystal microbalance (QCM, mass sensitive method), surface plasmon resonance (SPR, for determination of RI changes), absorption, and scattering. Hence, by observing these changes, one can identify the presence of target analytes to achieve recognition. This is the basic sensing mechanism of any biochemical sensor. Figure 1 presents a basic structural concept about general biosensors. Depending upon the nature of sensing elements, biochemical sensors can be classified into the following categories.

https://doi.org/10.1021/acsomega.3c03970
ACS Omega 2024, 9, 3037−3069

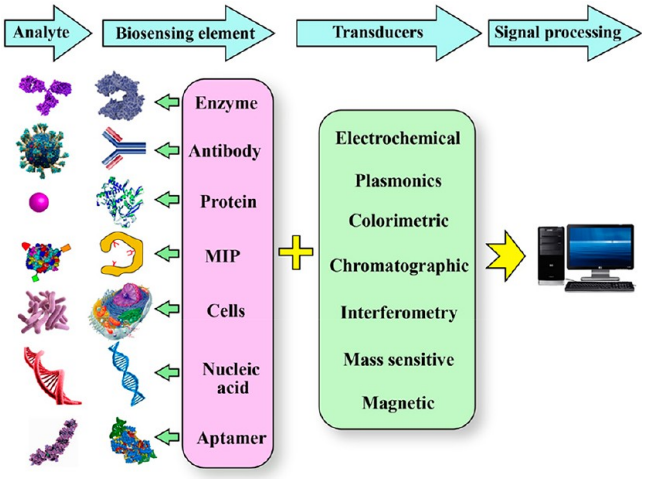

Figure 1. A general pictorial representation of the biochemical sensor.

2.1. Immunosensors. Immunosensors are classified for the identification of a selective immunoreaction between the target antigen and corresponding antibodies via the formation of a stable immunocomplex. In such sensors, one element acts as a sensing agent, which is used to immobilize the transducing platform, while another acts as a target analyte. The transducing element converts an antibody−antigen binding event to a measurable physical signal. The antibodies are generally synthesized within the human body or any other living animal called the host. In this synthesis process, the antigen is inserted in the host body, and then the natural immune system of the host fights to protect the body from the guest antigen by producing the specific antibody.[38] The antigen−antibody interaction is highly specific, with high affinity toward the target analyte. Due to the novel characteristics of immunosensors such as selectivity, sensitivity, reversibility, real-time performance, and miniature ability, they have become popular for the measurement of different pathogenic micro-organisms responsible for the diseases, such as proteins, enzymes, viruses, bacteria, and hormones.

2.2. Aptamer-Based Sensors. Aptamers are some good examples of functional molecules for the in vitro selection of different biochemicals with high specificity. These recognizing elements have been used mainly in electrochemical, optical, or mass-sensitive analytical techniques for the development of biosensors. In 1990, two groups independently developed in vitro selection and amplification for the isolation of RNA sequences that could specifically bind to target molecules.[39] These functional RNA oligonucleotides were then termed aptamers. Later, DNA-based aptamers were also found. Aptamer technology has received tremendous attention in the scientific and industrial communities for the development of biosensors and bioassays due to its small size, cost-effectiveness, and chemical stability. The aptamers can be synthesized from commercial sources with high reproducibility. Hence, for high specificity and affinity, they can be used for in vitro detection of any given target, ranging from small molecules to large proteins and even cells. This makes it possible to develop a wide range of aptamer-based biosensors.[40,41]

2.3. Enzymatic Sensors. Enzymes are classified as chemical reagents or analytical catalysts playing a pivotal role in specific chemical interaction kinetics with the target analyte. The combination of an enzyme as a recognition material with a transducer to obtain the outcome as a function of the target analyte concentration is called an enzymatic biosensor. A few examples of enzymes used for biosensor fabrication are glucose oxidase (GOx) for glucose detection,[42] cholesterol oxidase for cholesterol sensing,[43] and acetylcholinesterase for neurotransmitter activity detection.[44] The chemical interactions between the enzyme and corresponding analyte are generally highly specific, such as in the case of glucose, with glucose oxidase (GOx), gluconolactone, and hydrogen peroxide (H_2O_2) formed. Gluconolactone is hydrolyzed to gluconic acid ($gluconate^-$ and H^+ ions), while H_2O_2 also dissociates to oxygen molecules, H^+ ions, and electrons. This is a reversible process, and only glucose can interact with GOx, which makes the sensor specific.[45] The same stands for other enzymatic biomolecules. The enzyme-based immunoassay is commonly designated as an enzyme-linked immunoassay (ELISA).[46] Efficient processing to optimize the immobilization and enzyme concentration over the transducing surface leads to increased catalytic performance and specificity. The immobilization process follows several analytical techniques like absorption, sol−gel method, polymeric film growth, or covalent binding.[47,48] Out of these, the easiest technique for immobilizing the enzyme around the sensing probe region is absorption. This is done by simply dipping the sensing probe surface into the enzyme solution. In this immobilization technique, the enzyme coating is produced in an irregular fashion that sometimes affects the efficient selective binding of the target analyte. The sol−gel method is another approach to increase the homogeneity of the enzyme-entrapped sensing layer, which is done by adding enzyme in a sol−gel precomplex during gel formation. As a result, the entrapped enzyme does not lose its selective binding affinity, resulting in enhanced binding sensitivity toward the target analyte.[49] Currently, the integrated approach of the sol−gel method and nanotechnology has proven to be an efficient probe functionalization method in biochemical sensor fabrication.[50] The probe functionalization process using enzymes is also done through covalent binding with an optical fiber surface. In this case, the functionalization is done using a water-insoluble linking agent. Amino acid is a good example of a linking agent that does not affect the binding process of an enzyme. Hence, this covalent binding technique itself shows very stable performance and enhances the sensor's shelf life significantly.

2.4. Cell-Based Biosensors. Another category for biosensor characterization based on the sensing layer is cell-based biosensors, which are fabricated through genetic modification of living cells. The sensing surface is functionalized using these modified cells. The sensing mechanism relies on the interaction of the living cell with the target analyte, resulting in adaptation and survival depending upon the ambient atmospheric conditions. These functionalized cells are very sensitive to any change in external analyte and produce readable output in terms of shape and size of cells, fluorescence, color change, and morphological modification in the cell membrane. These sensors are compact, easy to handle, cost-effective, highly sensitive, and selective toward biological target analytes.[51] These sensors facilitate the collection of information about the sensing analyte based on the morphological changes, and cell interactions through attachment/detachment or even through cell death.[52]

2.5. Molecular Imprinted Polymer (MIP) Based Sensors. Molecularly imprinted polymers (MIPs) are artificial molecular receptors having synthetically and complementarily

https://doi.org/10.1021/acsomega.3c03970
ACS Omega 2024, 9, 3037−3069

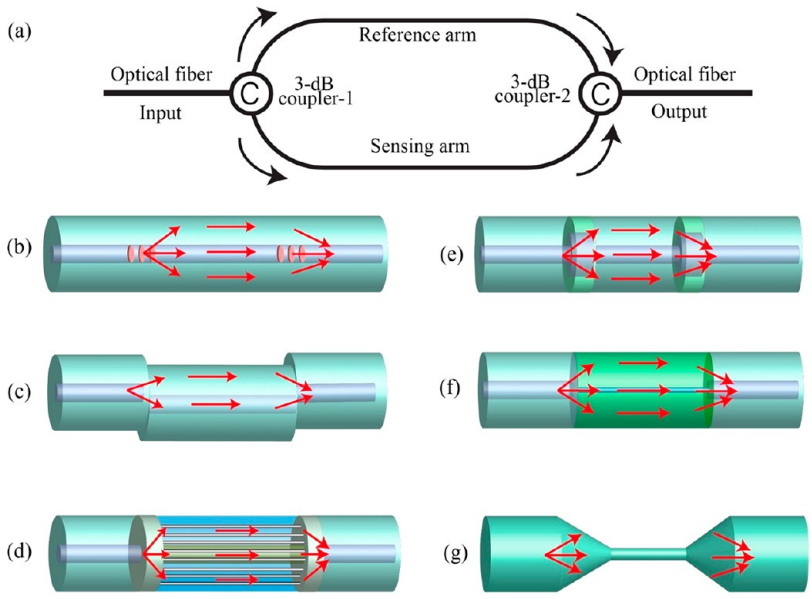

Figure 2. Schematic diagram of an optical fiber-based MZI. (a) The basic structure of a dual-arm-based MZI. In-line fiber-based MZI for different configurations using (b) long period grating (LPG), (c) fiber core mismatching, (d) air-hole collapsing of the photonic crystal fiber (PCF), (e) multimode fiber (MMF) segment, (f) thin core fiber (TCF) segment, and (g) micro/nanostructured fiber combinations.

prepared molecular mimics in a special polymeric medium. The synthesis procedure consists of mixing a certain amount of template (target analyte) with the functional monomer, having noncovalent/covalent molecular interaction in between. This template−monomer complex is then polymerized in the presence of a subsequent cross-linking agent and initiator. The polymerization process ensures the template molecule is frozen at a certain position within the polymer backbone. In particular, when the solvent is removed (which can break the template−monomer bond), the template detached from this position leads to the formation of three-dimensional complementary scaffolds of the template molecule within the polymer structure. These void sites have a highly specific binding affinity toward the target template and work as receptors in the sensing medium. The sensing mechanism of MIP-based biochemical sensors is similar to the previously mentioned recognizing elements with comparable binding affinity for the target analyte. However, these are more robust, durable, cost-effective, reusable, and suitable for working in harsh environmental conditions.[15,53]

2.6. Deoxyribonucleic Acid (DNA) Based Biosensors. DNA-based biochemical sensors have shown significant potential as candidates for next-generation biochemical detection devices due to their robust chemical properties and customizable biosensing functions. The major advantages of such sensors are their biocompatibility, thermal stability, cost-effective small structure, wide detection range, and durable lifetime. DNA and its assembly structure can be applied to detect specific targets, including nucleic acids, proteins, metal ions, and small biological molecules.[54,55] The basic principle of these sensors is the interaction of the target analyte with DNA. These interactions result in a structural change in DNA and its base sequence, leading to a change in the replication of DNA. Depending on the working mechanism, the DNA-based sensors can be classified as functional DNA strand-based biosensors, DNA hybridization-based biosensors, and DNA template-based biosensors.[56] In functional DNA strand-based biosensors, the sensing probe is formed by the functionalization of DNA strands like DNA aptamer and DNAzyme. The basic operation of a DNA hybridization-based biosensor is the complementary coupling among the specific single-stranded DNA (ssDNA) sequences (the target) within the analyte. These biosensors are complementary tools for the study of biomolecular interaction mechanisms and target nucleic acid fragments. In DNA template-based biosensors, different programmable structures as produced through DNA hybridization process are used for probe fabrication in order to selectively detect the target analyte. These sensors show some great application potential in disease detection and molecular kinetics measurements

3. OPTICAL FIBER INTERFEROMETRY

During the last few decades, optical fiber interferometry has emerged as an extensively adopted technique in several applications, ranging from biochemical engineering to nanoscience and technology, due to its highly sensitive in situ, contactless, and hassle-free measurement potential. Additionally, the integration of fiber optic interferometry with the advancement of computational analysis has made it possible to achieve an accurate and excellent sensing platform. The sensing mechanism using these types of sensors depends on the accurate identification of intensity, phase, wavelength, or polarization of propagating light passing near the domains of the sensing region. A variety of interferometric sensors have been developed for detecting several physical, chemical and biological entities.[17,28,57] Conventionally, four types of fiber optic interferometers are available, namely Mach−Zehnder, Michelson, Sagnac, and Fabry−Perot interferometers.[58] Among them, Mach−Zehnder and Michelson's interferometers are used frequently for multiparameter sensing purposes due to their compact, flexible, and reconfigurable structure. Apart from the sensitivity enhancement facility of these sensors through functionalization of the probe, the use of the sensing material makes them popular in many application fields.

In the case of optical fiber-based interferometry, the performance of sensors depends on the interference between

https://doi.org/10.1021/acsomega.3c03970
ACS Omega 2024, 9, 3037−3069

higher-order cladding modes with a fundamental core mode. This modal interference can be expressed by two-beam interferometry, where two coherent light beams interfere with each other and produce constructive and destructive interference depending upon the phase difference between them. If I_1 and I_2 correspond to the intensities of two coherent interfering beams, the resulting interference intensities can be shown by the following relation"

$$I = I_1 + I_2 + 2\sqrt{I_1 I_2}\cos\phi$$

Here, ϕ denotes the phase difference between the two interfering beams and can be obtained as

$$\phi = \frac{N\pi n_{\text{eff}} L}{\lambda}$$

Here, N is an integer whose value depends on the adopted interferometric technique. In the case of Fabry−Perot interference (FPI), the value of N is equal to 4, while in the Mach−Zehnder interferometer (MZI) its value is 2. n_{eff} is an effective refractive index as seen by two propagating interfering beams, and L is the length of the sensing region. Thus, any perturbation in the external sensing medium alters the value of n_{eff}, which subsequently shifts the interference dip wavelength. Hence, through precise monitoring of this shift, any change in the external medium can be measured.

This is a basic principle of optical fiber-based interferometry for sensing applications. The following section of the Review will address the discussion of several types of such transducing platforms covering the fundamentals and workflows for biosensing applications. In this category, the first type of interferometric platform is the Mach−Zehnder interferometer, as discussed below.

3.1. Mach−Zehnder Interferometer-Based Biochemical Sensors. Mach−Zehnder interferometers (MZIs) are frequently used in a broad spectrum of sensing application fields due to their miniaturized configuration, easy handling, and simple fabrication processes. In a conventional era, MZIs consisted of two independent arms, namely, the reference arm and the sensing arm, as illustrated in Figure 2a. The input incident light propagating through the fiber gets divided into two arms through a fiber coupler, followed by recombination at another end. At the recombination point, due to the optical path change, a phase change occurs between the two different arms that leads to interference after the superposition of these two coherent light beam, propagating through the arms. To utilize this mechanism for sensing applications, the reference arm is kept isolated from the surrounding medium, and the sensing arm is deposited with the specific biomolecule layer and then exposed to the biochemical sample to be detected. The binding of target biochemicals with the sensing arm changes the effective refractive index (RI) of the sensing region and induces an optical path difference (OPD) between two interfering coherent light beams, resulting in a variation in the interference signal. This basic scheme of using two separate arms in the MZIs is rapidly replaced with the advent of long-period fiber gratings (LPGs), micro/nanostructured optical fiber, cascading of the heterocore fiber structure, offsetting the fiber core, and combinations of specialty fiber. This structural modification makes the sensor compact in structure and miniature in nature. Figure 2b−g shows different methods for achieving in-line MZI.[28] A brief description of the working principle of each modulation-based MZI is given as follows.

3.1.1. Long Period Grating-Based MZI. One of the effective ways of achieving MZI is by incorporating integration with LPG. It is a periodic modulation of mode propagation constant formed mainly through the modification of RI of the core of the fiber. The MZI structure can be obtained by cascading serially two LPGs along normal SMF, as shown in Figure 2b. In this configuration, at the first point, the light propagating through LPG provides the excitation of higher-order cladding mode along with the fundamental core modes. Then, in the second section of LPG, the core and cladding modes again get coupled and, due to changes in effective refractive indices of core and cladding modes, a phase difference occurs. The phase difference results in the occurrence of an interference pattern. The mode coupling depends on the following phase-matching condition:

$$\lambda_i = [n_{\text{co}}(\lambda) - n_{\text{cl}}^i(\lambda)]\Lambda$$

Here $n_{\text{co}}(\lambda)$ is the effective RI for core mode, $n_{\text{cl}}^i(\lambda)$ is the i^{th} cladding mode at wavelength λ, and Λ is the period of LPG.[59] Here, we would like to mention that the effective index of the cladding modes is strongly dependent upon the surrounding environmental changes since light is guided more near the fiber surface. Any change in the refractive index of the surroundings leads to a shift in the interference patterns and results in its applications in the sensing field. The LPG's period plays a very crucial role to obtain a high-contrast interference pattern.

3.1.2. Offset Fiber-Based MZI. Figure 2c represents the in-line fiber-based MZI structure, which was fabricated through offset splicing of a small section of SMF between two SMFs pigtails. The light initially propagating through the fiber's core gets split between the core mode and higher-order cladding modes at the first offset region. These two modes propagate through the offset SMF and recombine with some phase difference at the second spliced region. The superposition of these two propagating modes produces a stable interference pattern at the output. The shift in the interference dip wavelength is sensitive to the external medium and thus can be used for sensing purposes.[60]

3.1.3. Single Mode Fiber (SMF)−Photonic Crystal Fiber (PCF)−SMF-Based MZI. Another important technique to obtain an in-line fiber-based MZI platform is to use a heterofiber structure of specialty fiber along with conventional SMF. One such specialty fiber is photonic crystal fiber (PCF) used to make a compact in-line MZI. The schematic image of this transducer is shown in Figure 2d. The PCF section is spliced in between normal SMF using a fusion splicer. The splicing of SMF and PCF fused the air channels around the splicing points and produces collapsed regions. The first collapsed region diffracts the input light and acts as a beam splitter. The diffracted light enters the cladding region and excites higher-order cladding modes. These cladding modes propagate through the PCF and again recombine with the core mode at the second collapsed region. The superposition of these interfering modes produces interference. The shape, length, and structure of PCF play an important role in interference sensitivity and also application.[61]

3.1.4. SMF−Multimode Fiber (MMF)−SMF-Based MZI. The fiber-based in-line MZI can also be obtained using multimode fiber (MMF) in combination with single-mode fiber (SMF). The schematic image of the MMF-based fiber transducer is shown in Figure 2e. In this case, two small strips of MMFs are spliced in-line to obtain an SMF−MMF−SMF−MMF−SMF structure. Here first MMF splits the light and

https://doi.org/10.1021/acsomega.3c03970
ACS Omega 2024, 9, 3037−3069

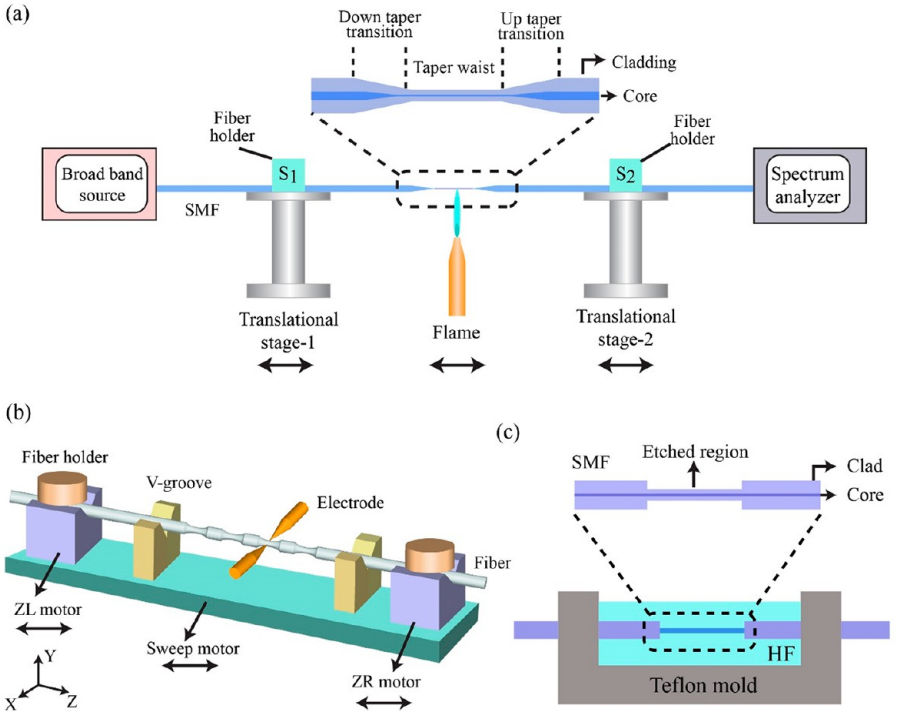

Figure 3. Different experimental procedures for the fabrication of optical micro/nanofiber. (a) Schematic image of the flame and brush technique. (b) Fusion splicer-based tapering technique. (c) Schematic diagram of microfiber fabrication process using the chemical etching technique.

excites the higher-order cladding modes inside SMF. These modes propagate through SMF and recombine with the fundamental core mode at the second MMF. Finally, the combined light produces interference spectra at the output. This combinational fiber structure can be used for sensing applications.[62] The excitation of the higher order cladding mode can be obtained using a thin core fiber (TCF) in combination with normal SMF.

3.1.5. SMF−Thin Core fiber (TCF)−SMF-Based MZI. Figure 2 f shows the schematic view of an in-line fiber-based MZI structure using a thin core fiber (TCF). The fundamental core mode of light inside the SMF splits at the first splicing point and excites higher-order modes. A small part of light propagates through the core of TCF, and another part propagates through the cladding region. At the second splicing point the higher-order modes again recombine with the core mode. This facilitates a stable interference spectrum at the output.[63]

3.1.6. Tapering the SMF/Microfiber-Based MZI. In addition to the above-discussed methods, a broadly used structure for an in-line fiber-based compact MZI platform is microstructure fiber, as shown in Figure 2g. This is usually obtained by tapering the conventional SMF up to a certain diameter (usually less than 10 μm). In normal SMF, the light propagates through the core as a fundamental core mode. Now, if the diameter of SMF decreases gradually, then in the down-tapered transition region it starts to support higher-order excited modes along with the fundamental core mode. The cladding modes propagate through the clad of the microfiber and recombine at the up-tapered transition region. This structure gives a stable interference pattern for the superposition of these modes. The interference pattern is very much sensitive to external perturbations like RI, strain, and temperature. Hence, this microfiber-based MZI transducer can be used for such sensing applications.[64] In these modified in-line compact MZIs, the sensing and reference arms have the same physical path length. The modal dispersion of light occurs in these fiber structures, which excites the higher-order cladding modes along with the fundamental core mode. These modes propagate through different dielectric regions of these fiber structures and suffer from an extra path difference. Hence, the superposition of these interfering modes produces a stable interference fringe pattern at the output transmitted spectra. Now, to use this modified structure for biosensing purposes, the transducing surface is functionalized with different recognizing elements. The binding of the target biochemical with these recognizing elements effectively changes the effective RI of the sensing region. This change in the effective index alters the cladding mode propagation significantly. This change in the effective index results in a shift in the output in terms of wavelength and also in intensity. Thus, through monitoring this spectral shift, the presence of a measurable entity can be found.

To analyze the light-guiding properties in a specific structure, researchers use several mathematical models based on the finite element method (FEM) and finite difference time domain (FDTD) methods for solving Maxwell equations without any approximations using several software like COMSOL and LUMERICAL. More detailed information on this can be found in reports as well as during the special paper discussion at several places in the manuscript.

3.2. Micro/nanostructured Fiber (MNF) Based MZI Biochemical Sensor: Fabrication. Generally, a significant portion of the light propagating through the fiber is confined in its core and hence it is not able to produce any interaction with surrounding environments, limiting its application for sensing applications. The issue is usually resolved through the tapering of the fiber, reducing its diameter in the range from micrometers to hundreds of nanometers.[65] Due to the reduced diameter of the fiber, up to the micrometer order, such

https://doi.org/10.1021/acsomega.3c03970
ACS Omega 2024, 9, 3037−3069

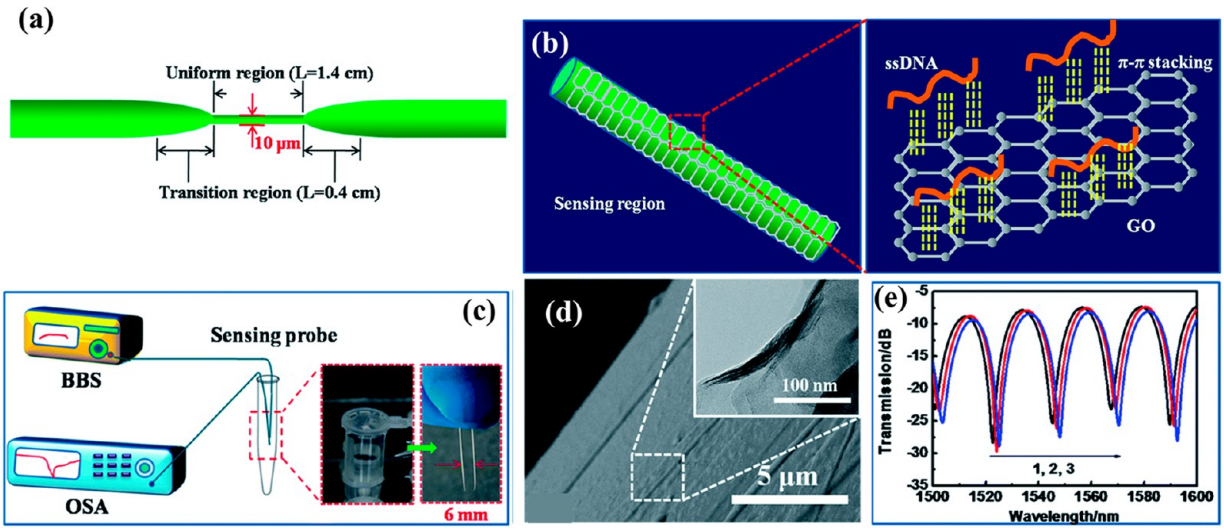

Figure 4. Graphene oxide-functionalized optical microfiber-based ultrasensitive and in situ DNA detection. (a) Schematic geometrical structure of a silica microfiber-based interferometer. (b) Schematic representation of the interaction between ssDNA chains and GO on the fiber surface by $\pi-\pi$ stacking. (c) Experimental setup of the tapered fiber-based biochemical sensor. The inset shows images of the sensing probe. (d) Scanning electron microscope (SEM) image of GO immobilized fiber. The inset shows a magnified view of GO coating by transmission electron microscopy (TEM). (e) Output transmission spectra of the probe for different steps of GO coating process: (1) bared silica fiber after cleaning, (2) after APTES modification on the cleaned fiber surface, and (3) after GO surface immobilization on fiber. Reprinted with permission from ref 75. Copyright 2017 Royal Society of Chemistry.

configuration is called fiber optic microwire or microfiber. Several experimental techniques have been used for the fabrication of microfibers, such as the flame and brush technique,[66] fusion splicer method,[67] laser heating,[68] and chemical etching.[69] In the case of the flame and brush technique, the fiber is heated at the center using optimized flame at its softening temperature, and both ends are pulled simultaneously using two translational stages via a computer-controlled automated system.[70] The length of the microfiber can be controlled by changing the separation of translational stages. The adiabatic or nonadiabatic nature of the microfiber can be controlled by changing the speed of translational stages. In fusion splicer-based microfiber fabrication, the fiber is heated using an electric arc generated between electrodes, and both ends of the fiber are stretched outward using two stepper motors. However, efficient tapering using fiber is a bit tricky due to the limited control of arc power and shifting range of stepper motors in the splicer. Thus, using fusion splicer-based tapering, the length of microfiber cannot increase beyond a few micrometers. Apart from this, the thickness of microfiber cannot be tailored to any desired value. The chemical etching method can produce a very sharp microfiber by dipping the fiber into hydrofluoric acid (HF). However, in this case the fabrication process takes a long time, and it is not well controlled or repeatable. Figure 3 shows the images of different processes of microfiber fabrication.

When the fiber diameter gets reduced, the evanescent field of the core mode propagating to the fiber optic core penetrates the nearby surrounding environment, allowing the possibility of light interaction with the sensing layer. Additionally, the microfiber configuration is also used in several other commendable applications, including low optical loss, outstanding mechanical flexibility, and tight optical confinement.[71] To achieve sensing in these platforms, the specific receptor for the target is immobilized over the microfiber surface. The binding of a guest molecule affects its optical properties, which in turn changes the effective refractive index of the cladding modes significantly. This alters the interference pattern obtained compared to one before molecular binding. By monitoring the difference in interference dips, one can easily monitor the molecular interactions and hence the presence of guest molecules to be sensed.

4. WORKS REPORTED ON VARIOUS MZI PLATFORMS

After understanding the sensing mechanism on several kinds of interferometric configurations, we will discuss a set of studies reported using these platform for biochemical sensing applications. This will provide a brief state-of art of the technology and will help to provide a detailed analysis of translation of the sensing mechanism to a actual sensing device.

4.1. Microfiber-Based MZI Biosensors. In 2015, Huang et al. reported a microfiber-assisted MZI biochemical sensor for the selective recognition of single-stranded DNA (ssDNA) molecules with the help of a conjugated polymer as a sensing agent.[72] A tapered microfiber has a waist diameter of 7.5 μm and a length of 1.4 cm. The transition regions have a length of 0.4 cm. The microfiber surface was functionalized using a conjugated polymer membrane having a thickness of 200 nm. The binding of the ssDNA has been characterized using the wavelength interrogation technique. The sensing probe was used to measure in situ ssDNA with a concentration range of 10^{-12} to 10^{-6} M in PBS solution. This proposed sensing method showed a sensitivity of 2.393 nm/log M with a very good linear response. The sensor showed the lowest detectable concentration of 10^{-10} M. This sensor has a potential for broad utility in biomedical and analytical applications. However, this sensor suffers from poor mechanical instability for its fragile microfiber structure and is not suitable for robust application. A sophisticated mechanical casing is required for low-concentration measurement.

Later in 2016, Song et al. proposed a microfiber-based biosensor for label-free tracking of DNA hybridization kinetics with ultrahigh sensitivity.[73] The sensing probe was fabricated

https://doi.org/10.1021/acsomega.3c03970
ACS Omega 2024, 9, 3037−3069

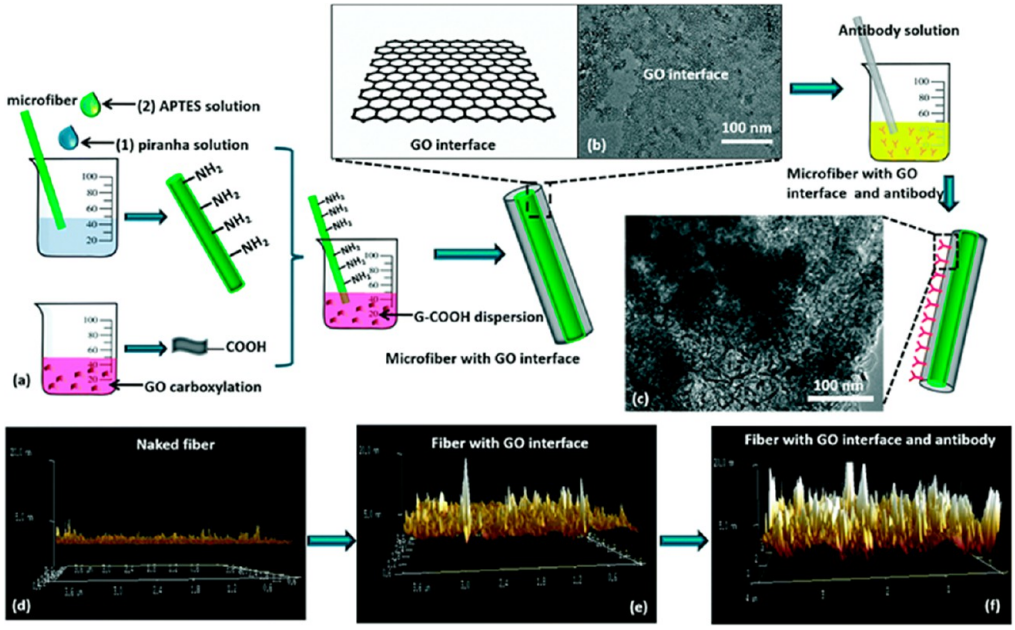

Figure 5. (a) Schematic pictorial description of the biorecognizing synthesis process through GO interface formation on a microfiber surface. TEM images of (b) the GO interface and (c) biorecognizing element immobilization with the GO interface. AFM characterized 3D height view of the (d) silica microfiber surface, (e) microfiber after GO interface formation, and (f) microfiber after GO interface formation with anti-GABA molecules on it. The *Z* scales are 20 nm; the images have been second-order flattened to eliminate the substrate effect. The scan area was 4 μm × 4 μm. Reprinted with permission from ref 77. Copyright 2018 Royal Society of Chemistry.

by preparing a U-shaped microcavity by simply in-line splicing of a tapered microfiber with a small offsetting. The probe was made with different cavity lengths and observed the free spectral range (FSR) for each probe. For biosensing applications, the microcavity region was functionalized using monolayer poly-L-lysine (PLL), followed by probe ssDNA to achieve selective detection of target ssDNA. The ssDNA samples were made in PBS solution with concentrations of 0.0001−1 pmol/μL. The detection limit of the proposed sensor is conservatively as low as 0.0001 pmol/μL. The sensor showed the advantages of compact size, fast response, and high reaction to the DNA hybridization process. However, its suffers from fragility and mechanical instability due to mismatch offsetting and the thin microfiber structure. Apart from this, it is not easy to fabricate and use.

In the same year, Ding et al. represented a micro/nanostructured fiber optic MZI for label-free, ultrasensitive, and selective detection of the neurotransmitter serotonin (5-HT). A modal interferometer was prepared by tapering the conventional SMF with a 6.4 μm waist diameter and 1.5 cm length. The tapered regime of the MZI was coated with silicon dioxide nanospheres, acting as a selective sieve mesoporous structure for the adsorption of 5-HT molecules. The sensitivity of that sensor was 1.04 nm/log M for the target 5-HT sample with a wide dynamic detection range from 100 fM to 1 μM. The proposed sensor shows potential for low-concentration detection and gives great advantages in many application aspects, including biomedical engineering, clinical testing, and nanotechnology.[74] In the following year Huang et al. suggested a microfiber-based biochemical sensor for ultrasensitive in situ measurement of ssDNA. The graphene oxide was coated over the microfiber and provided a strong $\pi-\pi$ interaction with the detected ssDNA, producing the refractive index modulation over the microfiber surface. Figure 4 shows a detailed pictorial description of the study along with a fabricated probe, GO immobilization, and sensor characterization response. The sensor was able to function over a wide range of DNA concentrations, ranging from 10^{-14} to 10^{-6} M, with a satisfactory pH spectrum of 4.3−8.5. The in situ ssDNA measurement procedure provided a detection limit of 10^{-12} M, and a sensitivity of 0.94 nm/log M.[75] However, this sensor is again fragile due to microstructure and bent form. The sensor is also temperature- and bending-sensitive. Therefore, proper care should be taken for low-concentration measurement.

Huang et al. in the year 2017 proposed a tapered microfiber-based ultrasensitive and label-free detection method for γ-aminobutyric acid (GABA).[76] The sensing surface was functionalized by Fe_3O_4@SiO_2@mesoSiO$_2$ microspheres for GABA size-specific adsorption to produce changes in the optical properties of the sensing layer. The sensor was characterized with the wavelength interrogation method over a wide concentration range. The increase in GABA molecular concentrations resulted in more adsorption in the sensing layer, which was reflected by the RI change of the medium around the tapered section of the optical fiber playing an important role in realizing size-dominated GABA sensing. The sensor showed a linear sensitivity of 0.94 nm/log M along with a detection limit of 3.51 × 10^{-13} M. This study was then improved by Jun et al.[77] in 2018 using a similar MZI structure but changing the sensing medium using graphene oxide followed by anti-GABA antibodies, as shown in Figure 5. The improved sensitivity of the modified sensor was found to be 1.03 nm/logM along with an LOD value of 2.91 × 10^{-18} M. The sensor shows very high sensitivity and the potential for trace-level concentration detection. However, this sensor suffers from instability and fragility. The sensor is also sensitive to temperature and bending. Therefore, it is not suitable practically to measure low concentrations precisely without any sophisticated precaution. Moreover, since the recognizing

https://doi.org/10.1021/acsomega.3c03970
ACS Omega 2024, 9, 3037−3069

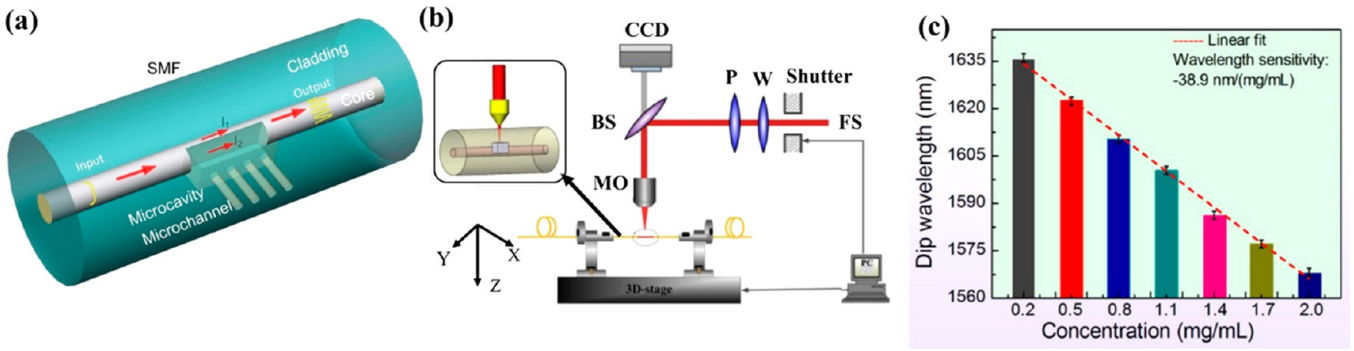

Figure 6. Mach−Zehnder interferometric biosensor for BSA detection. (a) Schematic representation of a MZI-based biochemical sensor. (b) Schematic diagram of the FS laser-based micromachining system utilized to fabricate the in-fiber structure. The system includes an attenuator comprised of a polarizer (P) and half-wave plate (W) for controlling the laser power, a beam splitter (BS), a CCD camera, and an objective lens (MO) to focus the laser beam onto the fiber. (c) Variation of the dip wavelength shift for different concentrations of BSA samples. Reprinted with permission from ref 78. Copyright 2017 Optica.

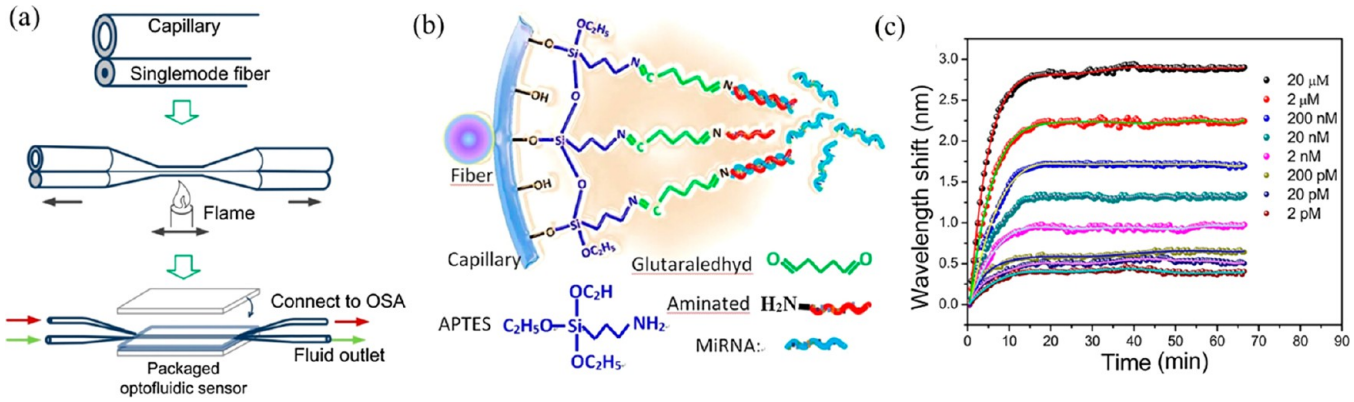

Figure 7. Mach−Zehnder interferometric detection of microRNAs. (a) Schematic diagram of the probe construction process. (b) Functionalization of the sensing probe for microRNA. (c) The kinetic binding curves of different concentrations of miRNA-let7a. Reprinted with permission from ref 80. Copyright 2017 Elsevier.

material is an antibody, proper storage is required to use the sensor multiple times without affecting its sensitivity.

In 2017, Li et al. reported a microcavity-based MZI biochemical sensor for label-free detection of bovine serum albumin (BSA).[78] The microcavity was formed by a femtosecond laser pulse on the surface of the SMF, allowing the external media to interact with the core of the surface. The sensing was achieved using BSA solutions with varying concentrations through microfluidics connected through the microcavity and the sensor surface. The light split into two parts. One part propagates through the fiber core, and another part propagates through the cavity. This light interacts with the analyte in the cavity and suffers from a phase difference and hence produced a shift both in wavelength as well as the intensity in the output. The proposed sensor possessed an ultrahigh RI sensitivity of −10 055 nm/RIU with a detection limit of 3.5×10^{-5} RIU. Figure 6 shows the schematic representation of the proposed structure of the sensor and fabrication steps along with the calibration curve toward varying BSA concentrations. The sensing method for low BSA concentrations showed promising sensing potentials for biochemical applications such as DNA hybridization, medicine examination, and environmental monitoring. The sensor has very high RI sensitivity and a good linear response for BSA detection. The sensor is mechanically stable as compared to microfiber-based MZI sensors and suitable for industrial large-scale manufacturing. However, the fabrication process is time-consuming and not cost-effective. The sensing surface functionalization process is also very challenging. In the same year, Arjmand et al. proposed a new nonadiabatic tapered fiber-based optical MZI for selective detection of methyl parathion, an organophosphate pesticide.[79] The tapered section of the fiber was immobilized by an acetylcholinesterase enzyme acting as a bifunctional cross-linker for guest methyl parathion to realize specific binding. The wavelength interrogation principle is employed for the characterization using the aqueous sample solution of methyl parathion. The sensor showed a red shift in dip wavelength for varying methyl parathion concentrations from 10^{-10} to 5×10^{-5} M along with a LOD value of 2.4×10^{-10} M. This sensor is not durable and mechanically stable. The performance is temperature- and bending-sensitive and thus not practically reliable for low-concentration detection.

Later, Liang et al. demonstrated a capillary-based optofluidic channel coupled with tapered optical fiber as MZI configuration to achieve microRNA(mRNA)-let7a (molecular weight of 6.75 kDa) sensing.[80] The fabricated sensor involved the alignment of SMF and a laterally placed capillary tube, followed by tapering of the obtained structure to form a modal interferometer, as shown in Figure 7a. The capillary interior was modified by several chemical modifications using APTES, glutaraldehyde, and animated NH_2 for mRNA binding (Figure 7b). The biomolecular interaction that occurred between mRNA and animated NH_2 at the capillary interior induced a

https://doi.org/10.1021/acsomega.3c03970
ACS Omega 2024, 9, 3037−3069

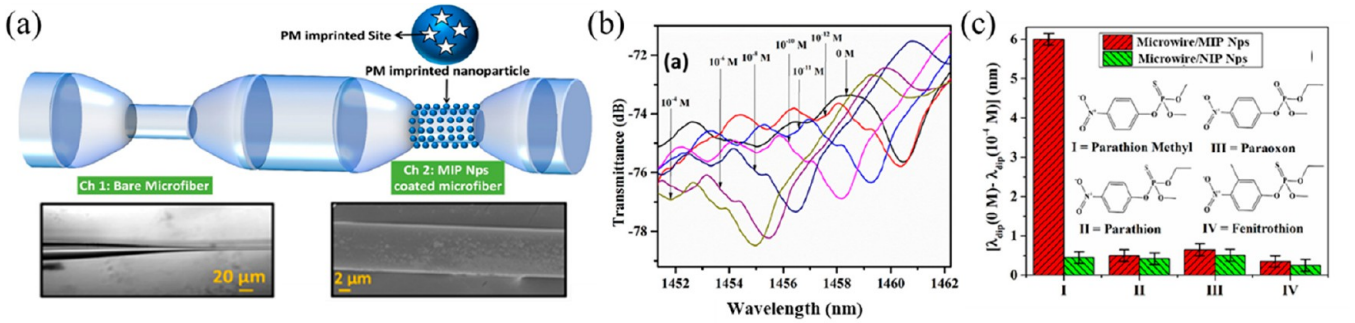

Figure 8. Concatenated microfiber-based MZI for biosensing applications. (a) Schematic image of the concatenated microfiber. The first tapered region is channel-1 used for stable interference patterns, and the second tapered region is channel-2 coated with MIP and used for sensing purposes. The inset shows the microscopic images of the bare microfiber and MIP-coated probe. (b) Variation of interference dip wavelength shifts with the concentration of the sensing analyte (PM). (c) Selectivity performance of the sensor. The red bars represent the comparative shift for different structurally analogous analytes for the MIP-immobilized probe, while the green bars are the same for the NIP-coated probe. Reprinted with permission from ref 83. Copyright 2019 Elsevier.

red spectral shift of the interference spectrum. A log-linear response for mRNA concentrations from 2 nM to 20 μM (Figure 7c) with the lowest measurable concentration of 212 pM (1.43 ng/mL) was obtained by the prepared probe within the response time of approximately 15 min. The sensor shows very good temporal stability and is suitable for real-time measurement. However, it is not mechanically stable due to its fragile microstructure. The inner surface functionalization process is not easy and requires time-consuming steps. However, the fabrication process is easy.

In the year 2018, Zainuddin et al.[81] proposed a MZI-based sensor using a tapered microfiber to detect *Leptospira* bacterial DNA. The highly specific complementary DNA was immobilized over the tapered section of the microfiber probe through several functionalization steps. The sensitivity of the proposed sensor toward DNA was measured as 1.2862 nm/nM with a detection limit of 0.1 fM.[81] The proposed method was able to distinguish between actual DNA of *Leptospira* serovars (Canicola and Copenhageni) with respect to *Clostridium* difficile (control) even at femtomolar concentrations. In the same year, Li et al. proposed another MZI-based biosensor through tapering a multimode fiber for quick and label-free detection of *Escherichia coli* (*E. coli*) bacteria. The sensing probe was fabricated by the immobilization of T4 bacteriophage to capture *E. coli* selectively. The concentration changes of *E. coli* and its binding with T4 bacteriophage resulted in a RI change of the medium around the sensing surface, which was then translated as a shift in interference wavelength dip. The sensor was able to detect *E. coli* with a LOD value of 10^3 CFU/mL along with a dynamic detection range of 10^3–10^7 CFU/mL.[82] The sensor gives a fast and linear detection performance. However, it is not independent of temperature and strain. It needs proper encapsulation for reusable applications. A concatenated structure of single-mode tapered microfiber can be used to observe dual inference. The first microfiber region as a reference channel is used to maintain a stable interference pattern, while other microfiber regions are used as sensing channels. Thus, this concatenated form provides a stable interference pattern irrespective of the RI of the sensing material. Shrivastav et al.[83] first proposed and experimentally demonstrated this structure combined with MIP as recognition agent for selective detection of organophosphorus pesticide parathion methyl (PM), as illustrated in Figure 8. The simulative intensity distribution of this concatenated optical microfiber has been analyzed using the FEM technique. This simulative analysis showed that the intensity of the evanescent electric field was enhanced due to the immobilization of the sensing material. The experimental results of this reported sensor showed a broad dynamic detection range and hypersensitivity of 1.3×10^{12} nm/M for an aqueous PM sample with highly repeatable performance. The essential selectivity property of the biochemical sensor was addressed through the functionalization of the sensing channel with artificial molecular receptor MIP nanoparticles (MIP-NPs). The performance of the sensing probe was optimized via a three-stage optimization process. The presence of MIP-NPs enhances the sensitivity due to the high aspect ratio. The sensor showed an ability to detect a concentration of PM as low as 79.43 fM with high accuracy. The performance of the sensor using a real water sample with a satisfactory recovery rate proved the commercial application possibilities of that sensor.[83] This dual channel microfiber provides a good stability over the functionalized sensing layer's RI. However, the microfibers should be identical in nature, in terms of length and diameter, otherwise there may be a chance of cross-talk between the individual response. In this case, though the sensor is stable from bending due to proper casing, it is not stable from temperature fluctuation.

In 2019, Guan and Huang proposed a microfiber-based biochemical sensor for the detection of γ-amino-butyric acid (GABA), an important neurotransmitter, and cellular cytochrome c.[84] For dual-target analyte detection, the microfiber surface was sensitized with two different functional materials. The sensitivity of the sensor is improved by functionalization and interfacial modification of the microfiber surface by a Ag@ reduced graphene oxide (RGO) nanocomposite, providing high sensitivity and ultralow detection limits of 1.65×10^{-15} and 6.82×10^{-17} M for neurotransmitter γ-amino-butyric acid and for cellular cytochrome c, respectively. The sensor is not durable and suffers from bending and temperature instability. The performance of the sensor fluctuates and hence is not reliable for low-concentration applications. In 2019, Hu et al. reported a novel MZI-based biochemical sensor by utilizing a special type of liquid crystal integrated with a specialty fiber PCF.[85] The MZI structure consisted of an optimized tapered PCF sandwiched between two SMFs. The PCF was functionalized with pH-sensitive material, 4′-pentyl-biphenyl-4-carboxylic acid (PBA)-doped 4-cyano-4′-pentylbiphenyl (5CB), for

https://doi.org/10.1021/acsomega.3c03970
ACS Omega 2024, 9, 3037−3069

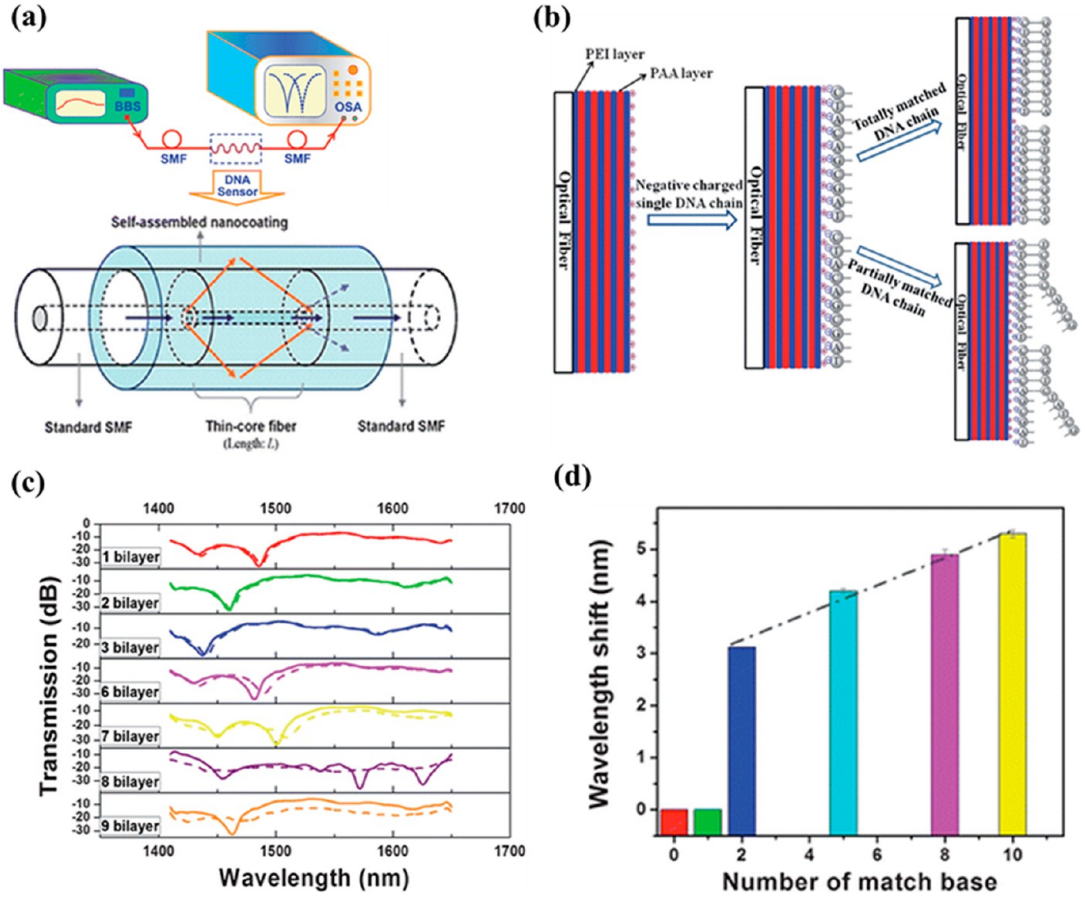

Figure 9. Thin-core optical fiber-based biochemical sensor. (a) Schematic of the experimental setup for probe characterization. (b) Sequential steps for functionalizing the sensing probe. (c) Transmission spectra of the proposed TCFMZI before (solid line) and after (dashed line) the immobilization of (PEI/PAA)n multilayer films with different numbers of bilayers. (d) tSelectivity performance of the proposed TCFMZI-based DNA sensors for a different kinds of target ssDNA detection. Reprinted with permission from ref 87. Copyright 2013 Royal Society of Chemistry.

penicillinase detection. The pH-sensitive element PBA changed the special orientation of the liquid crystal around the tapered PCF through the enzymatic interaction with penicillinase that produced H^+ ions and hence changed the pH value, altering the effective RI of the sensing region. Ling et al. developed a tapered hollow core microfiber-based optical sensor for selective detection of human chorionic gonadotropin (hCG) hormone. Experimental observation showed the shift of 0.5 nm in interference dip wavelength for a concentration change of 0−5 mIU/mL hCG, equivalent to the limit of detection (LOD) value of 0.6 mIU/mL. The sensing method possesses a high degree of selectivity and reproducibility and proves its potential for biomedical employment.[86] The sensor is free from fragility and stable. The sensing transducer is significantly less temperature sensitive. However, proper storage is required for multiple uses. An optical fiber interferometric platform as an immunosensor was proposed by Wang et al. for the selective detection of human IgG in 2018. The sensing probe was fabricated by highly offsetting the core of an SMF segment and splicing between two standard SMFs using a commercial fusion splicer. The sensing region of the sensor was immobilized with staphylococcal protein A, followed by a covalent interaction with goat antihuman IgG antibody. The reported immunosensor showed a highly selective binding affinity for human IgG with a LOD of 2.3 ng/mL. The sensor showed a reusability facility and potential for biosensing applications.[60] The sensor was stable over the microfiber-based sensor and easy to fabricate. The sensor can be made insensitive for bending after proper casing. However, it was not insensitive for temperature. Therefore, proper shielding is required during low=concentration sensing to avoid unwanted fluctuations.

The high sensitivity, compact and small size, and high fringe resolution of MNF-based MZI biochemical sensors have attracted extensive research and attention. On the other hand, the micro- and nanometer order of the fiber increases the biocompatibility and applicability for in vitro application if managed to minimize the fiber damage risks. However, this configuration has certain limitations, most notably the fragile structure due to the micrometer-ordered fiber diameter. Apart from this, the MNF-based biosensors are very much sensitive to bending as well as temperature. Therefore, these sensors require proper casing and shielding to make the sensing structure sensitive only for RI to use for low-concentration detection with good reliability.

4.2. Thin Core Optical Fiber-Based MZI Biochemical Sensor. The thin core fiber (TCF) based MZI is also an extensively used sensing platform for the development of different biochemical sensors. Such fiber consists of a much thinner core compared to conventional single-mode fiber; this leads to the high accessibility of the evanescent wave with the surrounding interface, which makes the fiber applicable for sensing applications. The main advantage as compared to the

https://doi.org/10.1021/acsomega.3c03970
ACS Omega 2024, 9, 3037−3069

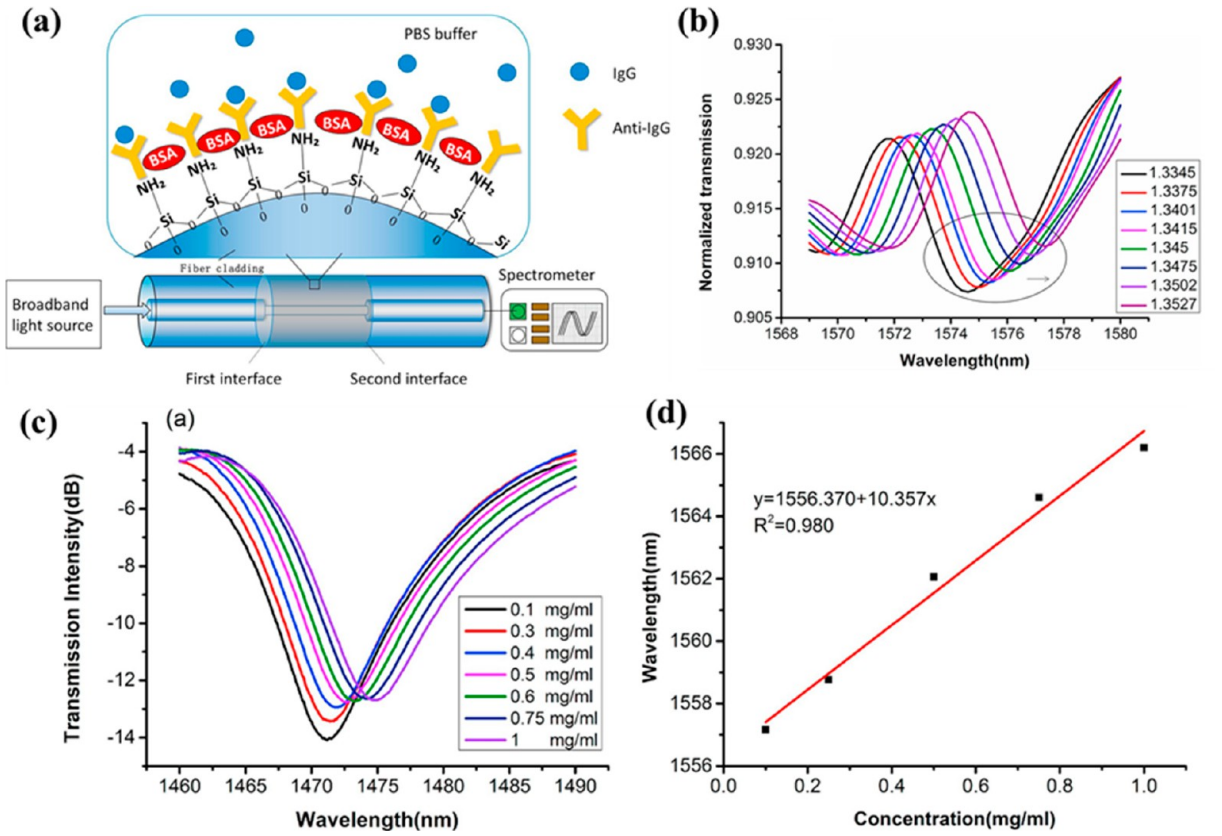

Figure 10. Immunoglobulin G sensor using thin core fiber-based MZI. (a) Schematic image of the sensing probe consisting of a TCF sandwiched between two SMFs. (b) Simulative transmission characterization of the proposed FOB for different refractive index media. (c) Transmission spectra for different concentrations value of IgG. (d) Linear relationship of the dip wavelength shift for different concentration of IgG. Reprinted with permission from ref 89. Copyright 2018 Elsevier.

tapered fiber is its higher mechanical stability, facilitating broad commercial application in various fields.

A TCF-based optical interferometer for selective detection of DNA hybridization was proposed by Yin et al. in 2013.[87] The sensing probe was fabricated by splicing a 1.5 cm long TCF (2.5 μm core, 125 μm cladding) between two standard SMFs, leading to modal interference, as shown in Figure 9. The light from SMF is easily coupled to the core as well as the cladding region of TCF. The subsequent superposition of these two modes produces a stable interference pattern at the output. The sensing transducer was functionalized by a multilayer film of poly(ethylenimine) (PEI), poly(acrylic acid) (PAA), and complementary ssDNA through layer-by-layer deposition over the sensing region for selective DNA detection. The sensing probe was characterized using different types of ssDNA having a concentration of 1 μM. The experimental results showed that the sensitivity of the sensor was about 0.27 nm per matched base. This sensor was easy to fabricate and showed good mechanical stability compared to MNF-based sensors. Moreover, this sensor is not too sensitive to bending, though it is sensitive to the temperature fluctuation of the surrounding medium; hence, proper precautions should be required to avoid unwanted noise during low-concentration measurements.

A similar type of SMF−TCF−SMF structure was utilized for the label-free detection of streptavidin by Yu et al. in the year 2016.[88] The sensing probe was developed by sandwiching TCF between two SMFs, and the electrostatic self-assembly (ESA) technique was used for probe fabrication. For probe functionalization, diallyl dimethylammonium chloride (PDDA) and styrenesulfonate sodium salt (PSS) were utilized as polyelectrolyte self-assembled multilayers (PSAMs) deposited on the TCF surface. The probe was used for selective label-free detection of streptavidin. Further, the specificity of the probe was verified by gelatin and bovine serum albumin (BSA) solutions. The sensor showed a minimum detection limit of 0.02 nM. Another TCF-based modal interferometry technique was used for the selective detection of immunoglobulin-G (IgG) in a study reported by Zhang et al., as shown in Figure 10.[89] The sensing probe was constructed by in-line splicing a 20 mm long TCF with conventional SMF. The bare sensing probe was used for RI sensing and showed a RI sensitivity of 82.7 nm/RIU. To use this fiber structure for biodetection purposes, the sensing probe region was functionalized by APTES. To achieve the selective recognition nature, the probe region was further immobilized with goat antihuman IgG antibody on APTES via covalent bonding. The fabricated probe was then used for selective detection of IgG. The probe was characterized using different concentrations of IgG ranging from 0.1 to 1.0 mg/mL. The sensor showed a good linear response in the given range and sensitivity of 10.4 nm/(mg/mL). The reported sensor showed a very high degree of selectivity. Similarly, Zhang et al. proposed a biochemical sensor using TCF sandwiched by dual s-tapered fiber for label-free selective detection of DNA hybridization.[90] The sensing probe is constructed by splicing a TCF segment with a length of 645 μm in between two normal SMFs. The two joints were then tapered using a commercial fusion splicer to make s-

https://doi.org/10.1021/acsomega.3c03970
ACS Omega 2024, 9, 3037−3069

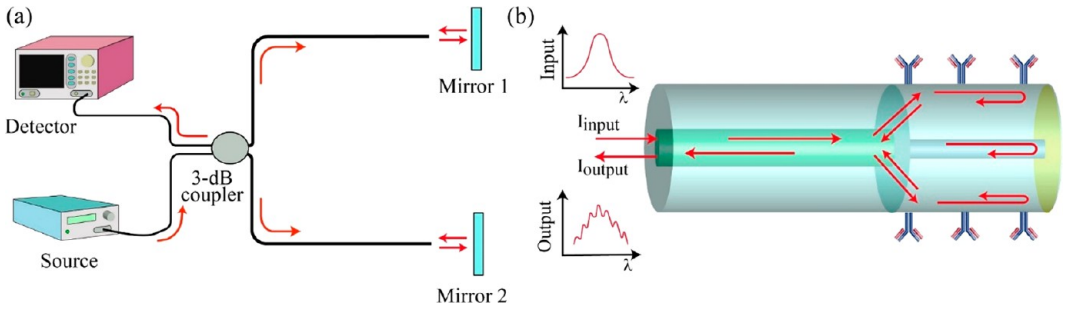

Figure 11. (a) Schematic construction of a basic Michelson interferometer. (b) Modified form of an in-line fiber-based Michelson interferometer.

tapered regions. To use the probe for biosensing applications, the fiber surface was functionalized using monolayer poly-L-lysine (PLL) and single-stranded DNA (ssDNA). The sensor was characterized by a ssDNA sample having a concentration from 0.001 to 1 pmol/μL. The DNA hybridization process was monitored by observing the real-time temporal evolution of the interference spectrum contrast ratio with a detection limit of 1 nM. The proposed sensor shows very good detection specificity. However, this sensor was fragile and very much sensitive to bending for the s-tapered shape. Hence, proper packaging of the sensing probe is required for lower-concentration measurement.

5. OPTICAL FIBER MICHELSON INTERFEROMETER (MI) BASED BIOSENSORS

5.1. The Sensing Principle. The optical fiber-based Michelson interferometers (MIs) are structurally analogous to MZIs. The fundamental approach of MIs is a superposition of light beams in two fiber arms. The configuration of an MI is similar to half of an MZI. Therefore, the construction process and operation mechanism of MIs are almost similar to those of MZIs. The major difference in MIs is the presence of reflecting arrangements. Figure 11a shows the basic form of a MI, where the fiber coupler splits the input light and produces two coherence beams. These coherent lights propagate through the fiber arms and finally incident on the reflecting mirrors. The light reflected from each reflecting end surface and again coupled back into the fiber. The coupling of these reflected lights produces interference at the output after superposition.[91] The utilization of reflection modes makes MIs compact and suitable for practical applications. The multiplexing facility of several sensing probes is another structural benefit of MIs. The single-fiber-based in-line structure of MI is also possible as depicted in Figure 11b, in which a fraction of the fundamental core mode is coupled to excite higher-order cladding modes. These modes are reflected from a common reflecting surface placed at the end of the fiber and recoupled to the core of the fiber. The superposition of these modes produces interference spectra. The reflected interference spectra are monitored at the output instead of transmission spectra as compared to the fiber-based MZI sensor. The MI sensors are more compact, durable in structure and, most importantly, capable of point of care (POC) applications.[92−94]

5.2. Micro/nanostructured Optical Fiber-Based MI Biochemical Sensor. The basic configuration of MI-based biochemical sensors is quite similar to that of MZI-based sensors, except for the addition of a reflected film at the fiber end face. This MI-based sensing transducer can be obtained in a compact in-line form using micro/nanostructured fiber. A few examples are as follows.

In the year 2018, Li et al. reported a glucose sensor by combining a tapered microfiber-based MI as a transducing platform and glucose oxidase as a specific receptor.[95] A SMF was tapered nonadiabatically to support the higher-order modes. The microfiber was then bent in a U-shaped structure. The second end of this fiber structure was coupled back into the interrogator to observe the output. The pictorial representation of the functionalization process and the obtained results are summarized in Figure 12. The sensing

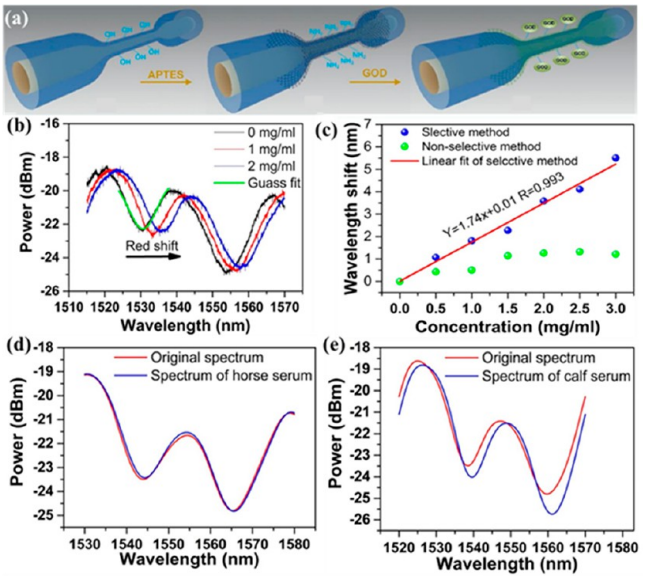

Figure 12. Sensitive detection of glucose using a microfiber-based MI. (a) Schematic diagram of the GOD immobilization process on a multimode microfiber. (b) Transmission interference spectra for different concentrations of glucose solution. (c) Linear relationship between wavelength shift and sample concentration. Detected transmittance spectra for (d) horse serum and (e) calf serum. Reprinted with permission from ref 95. Copyright 2018 Elsevier.

probe was a U-shaped microfiber immobilized with a graphene quantum dot (GQD) for enhanced sensitivity along with biocompatibility. The sensor possesses the linear detection range of glucose concentration of 0−3.0 mg/mL with a sensitivity of 1.74 nm/(mg/mL). The sensor can detect glucose specifically from animal serum samples very accurately, which indicates the suitability of the sensor in clinical diagnostic sectors. However, the sensing transducer suffers from fragility and is sensitive to bending as well as temperature fluctuations.

5.3. Photonic Crystal Fiber (PCF) Based MI Biochemical Sensor. Photonic crystal fiber (PCF) is a special type of

https://doi.org/10.1021/acsomega.3c03970
ACS Omega 2024, 9, 3037−3069

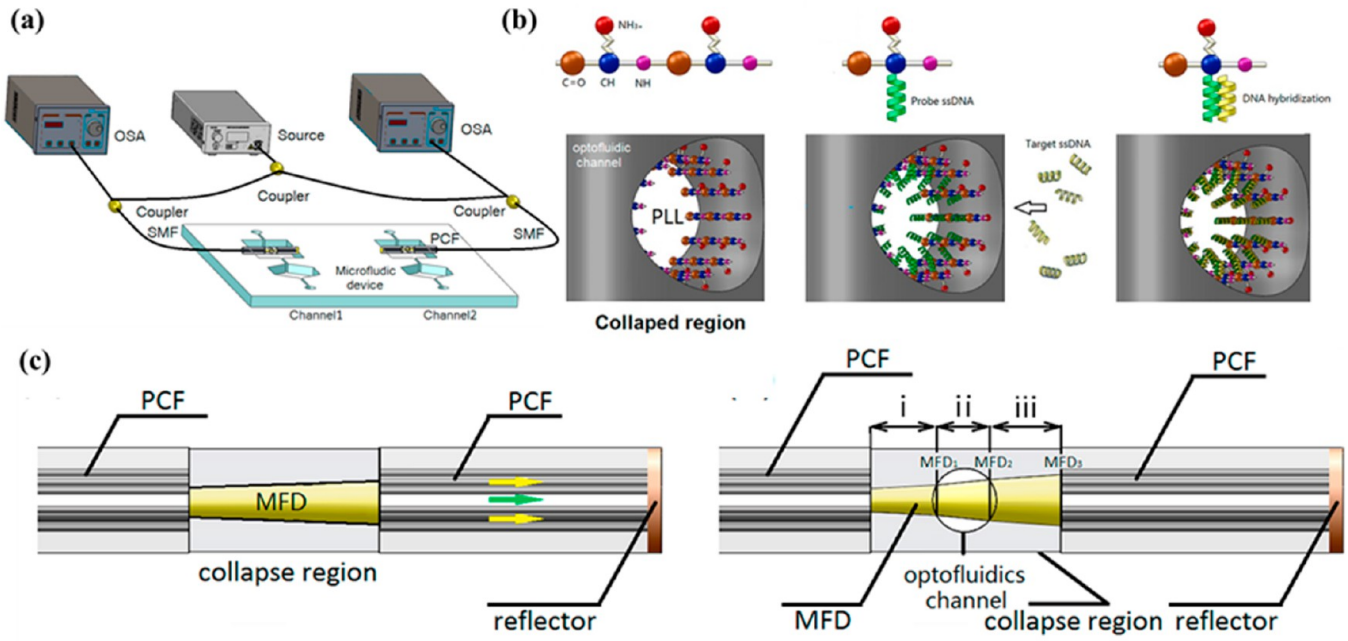

Figure 13. Optofluidic fiber-based biochemical sensor using a MI. (a) Schematic experimental setup consisting of a common broadband source coupled with two optical spectrum analyzers (OSA). (b) Systematic probe functionalization process. (c) Schematic structure of the fabricated probes. Reprinted with permission from ref 96. Copyright 2016 Elsevier.

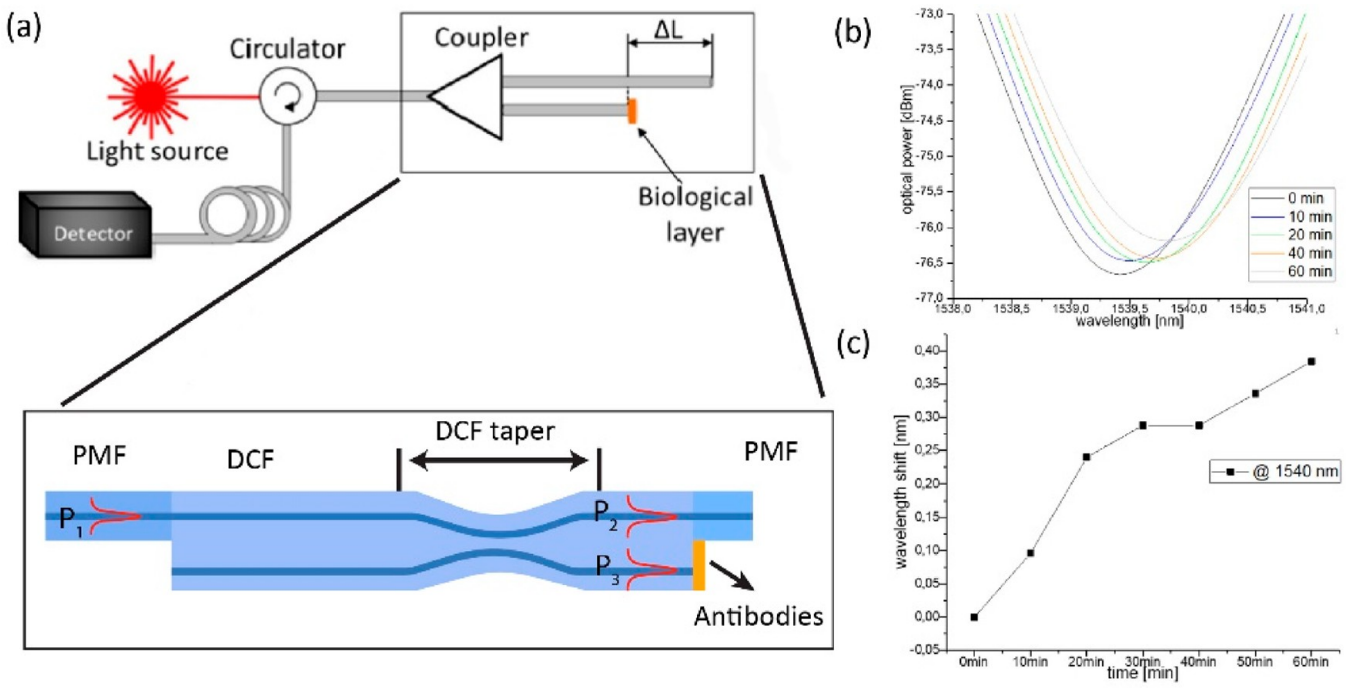

Figure 14. In-line dual-core fiber-based MI for biochemical sensing. (a) Schematic experimental setup with a magnified view of the dual-core fiber. (b) Transmission characteristics curve for different binding times between anti-IgG and IgG. (c) Variation of the dip wavelength shift for different binding times. Reprinted with permission from ref 99. Copyright 2018 Elsevier.

optical fiber that consists of using periodic stacking of air channels along the length of the fiber. The core of the fiber may be hollow or solid silica. The hollow air channels and silica form an effective cladding region of the fiber. The in-line fiber-based MI can be obtained using this specialty fiber (PCF). In 2016, Gao et al. reported a fiber optic biochemical sensor using MI interferometry for the identification of DNA molecules.[96] The sensing probe was fabricated by splicing a PCF section with the SMF. The collapsed region diffracts the light and excites higher-order cladding modes. These modes propagate through the PCF and are reflected from the cleaved end face. A thin gold coating was made at the end face of the PCF to increase the reflection power. The sensing region was made by making a microcavity in the collapsed region using a high-power pulsed laser. The inner surface of the cavity was functionalized by complementary ssDNA followed by a coating

https://doi.org/10.1021/acsomega.3c03970
ACS Omega 2024, 9, 3037−3069

of a poly-L-lysine layer inside the inner surface of the microcavity formed, as shown in Figure 13. The experimental observations showed that the detection limit of the sensor was 5 nM. This sensor was compact and very much stable as compared to microfiber-based sensors. Moreover, it not sensitive to bending. However, it is a little bit complex and costly. Another group, Sandhu et al., reported an MI-based biochemical sensor. The sensing probe was formed by fabricating a long-period fiber grating (LPG) inside the core of SMF near its end face. The light gets diffracted from this grating and excites the higher-order cladding modes. These modes are further reflected from the end face of SMF by the gold mirror and finally recombine with the core mode and produce interference. A thin film of nanocomposite polymer was used as a recognizing layer as well as for enhancing the evanescent electric field intensity of the cladding mode, resulting in increased sensitivity with refractive index resolution of 3×10^{-3} RIU.[97]

5.4. Dual-Core-Fiber (DCF) Based MI Biochemical Sensor. Another configuration of MI-based interferometry uses DCF fibers. In such fibers, the multipath evolutions of light through different core induces an interference pattern. This can be used for measurement purposes. DCF is minimally sensitive to short-range temperature variations for similar thermal expansion coefficients of the core and cladding material and has a good linear response, providing a high RI sensitivity and proving itself a suitable candidate for biosensing applications.[98] Wysokiński et al. proposed a fiber optic MI sensor for the detection of specific proteins, antigens, and biologically relevant molecules.[99] The interferometer was made using DCF with a tapered form having two arms with a precise length difference between them. This was achieved by splicing a fragment of polarization-maintaining fiber (PMF) onto one of the fiber ends. The schematic configuration and characterization curves of the sensor are shown in Figure 14. To fabricate the sensing region, the DCF was tapered using a fusion splicer. One end face of DCF was functionalized by dipping the probe into an IgG antibody in rabbit serum solution for surface immobilization. The sensor was used to measure goat antirabbit IgG protein. The thickness of the sensing layer increased due to the binding of guest IgG protein. The small change in thickness due to this binding with IgG antigen was measured using all-fiber interferometry. The sensor showed good mechanical stability.

6. SAGNAC INTERFEROMETRY (SI) BASED BIOCHEMICAL SENSORS

6.1. Sensing Principle. Fiber-based Sagnac interferometers (SIs) are ring-shaped or fiber loop configurations, where a 3 dB coupler is used to split the input light into two coherent beams. The light beam propagates through the fiber and is superposed with the counter-propagating beam.[100] Due to this superposition, a stable interference pattern is produced at the output. Generally, a small section of polarization-maintaining fiber (PMF) or birefringent fiber is inserted within the fiber loop, causing polarization-dependent interference between two counter-propagating light beams.

The transmitted intensity of the SI sensor can be expressed as

$$I_G = \frac{1}{2}\left(1 - \cos\frac{2\pi BL}{\lambda}\right)$$

where L corresponds to birefringent fiber length, B ($= n_{\mathrm{eff}}^{x} - n_{\mathrm{eff}}^{y}$) stands for modal birefringence, where n_{eff}^{x} and n_{eff}^{y} represent the x- and y-polarized mode indices, respectively. Figure 15 represents a schematic of a generic optical fiber SI

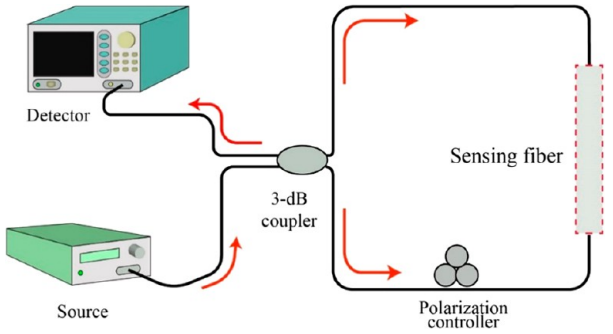

Figure 15. Schematic representation of a fiber-optic Sagnac interferometer.

interferometer. Sensing using a SI relies on the change in effective the refractive index contrast between the slow and fast axis birefringence, as the refractive index around the birefringent fiber changes due to molecular binding. This will cause a change in the interference pattern. In other words, the change in interference pattern depends on the phase difference introduced due to the additional birefringent fiber, which is expressed as $\Phi = (2\pi/\lambda)BL$. Any change of the external RI may change the refractive index difference between the fast axis and slow axis of the birefringence (B) via the evanescent field and hence shift the interferometric wavelength determined by Φ.

The phase difference between the polarization can be approximately expressed as $\Phi = (2\pi/\lambda)BL$. Additionally, the wavelength sensitivity (S) for a small RI change of the surrounding medium is given by $S = \mathrm{d}\lambda/\mathrm{d}n = (\lambda/G)\,(\partial B/\partial n)$. Here n is the external RI and $G = B - \lambda\bullet(\partial \mathrm{B}/\partial\lambda)$ stands for the group birefringence. Hence, one can conclude that the sensitivity of the sensor depends one the light wavelength (λ), group birefringence (G), and RI-induced birefringence variation ($\partial B/\partial n$). The main advantages of these sensors are ease in the fabrication process, input polarization insensitivity, and minimal insertion loss. These SI-based sensing transducers show good RI sensitivity to the external analyte medium and thus have been used by many research groups to fabricate different biosensors after functionalizing them with biorecognizing materials. Some examples are given in the following section.

6.2. Microfiber-Based SI Biosensors. In the year 2017, Gao et al. proposed a high-sensitivity, label-free SI-based optical fiber sensor for ssDNA detection using a high-birefringence (Hi-Bi) micro/nanostructured fiber.[101] The details pictorial description of the proposed sensor is shown in Figure 16. The sensing probe was constructed with a small segment of Hi-Bi microfiber sandwiched between the SMFs. The sensing probe region was encapsulated in a microfluidic chip having an inlet and outlet that enable the analyte sample to interact with the recognizing layer. The intensity distribution of this microfiber has been studied using the FEM technique, showing the enhancement of the evanescent light as for the tapering. The detection specificity of this sensor was achieved by functionalizing the microfiber region with monolayer poly-L-lysine (PLL) and ssDNA having a concentration of 10 μM. The sensor showed a dynamic

https://doi.org/10.1021/acsomega.3c03970
ACS Omega 2024, 9, 3037−3069

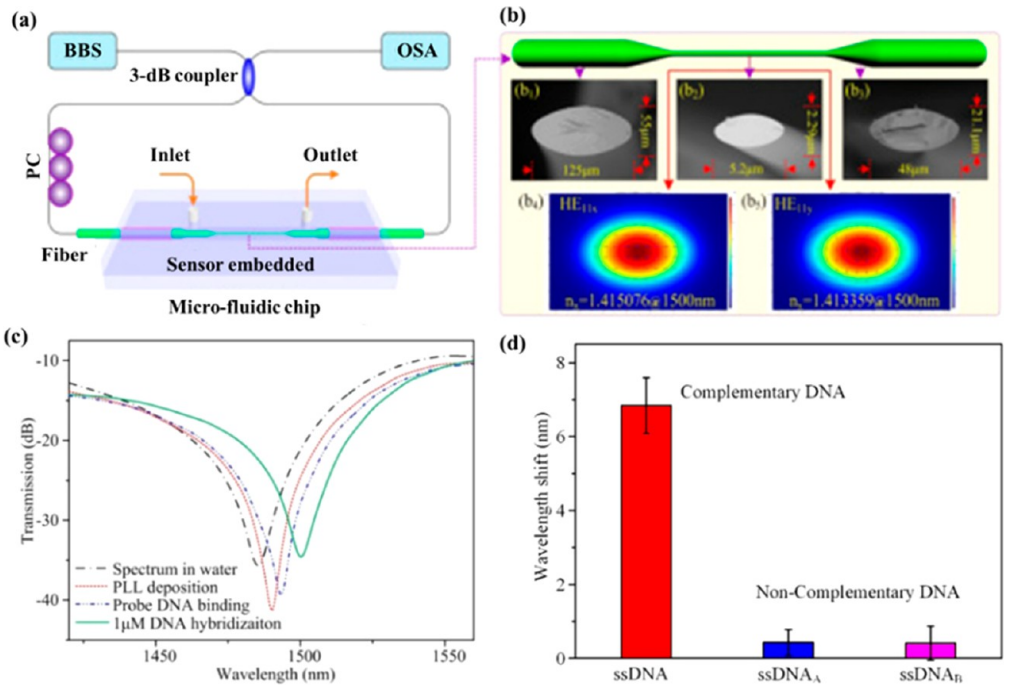

Figure 16. High-sensitivity microfiber-based SI for DNA detection. (a) Schematic experimental setup for probe characterization. (b) Elliptical high-birefringence (Hi-Bi) microfiber cross-sectional view and simulative intensity distributions profile of the *x*- and *y*-polarized transverse modes. (c) Output transmission spectrum of the probe at each stage of surface functionalization. (d) Performance of the sensor for constant concentration value of matched and mismatched (ssDNAA and ssDNAB) DNA. Reprinted with permission from ref 101. Copyright 2017 Optica.

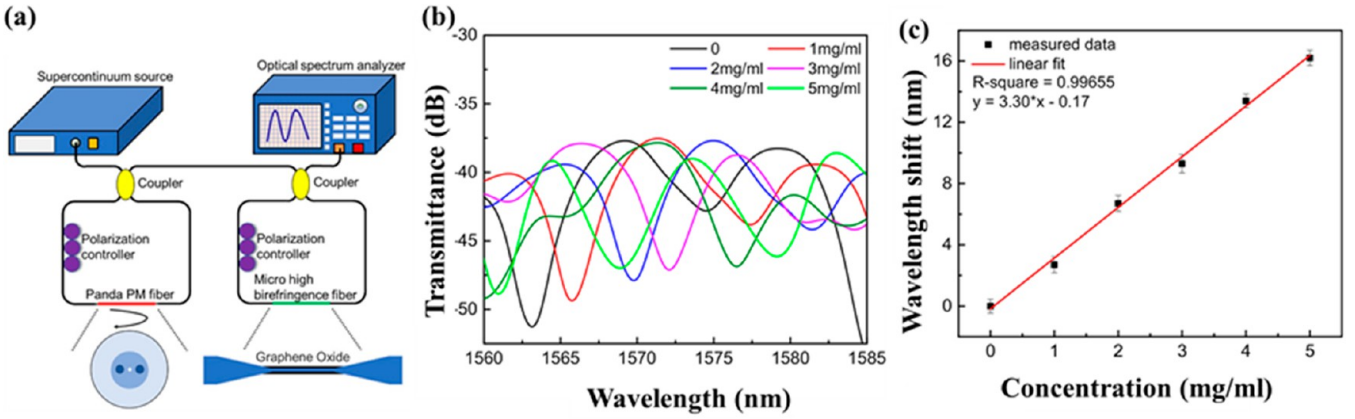

Figure 17. A high-birefringence (Hi-Bi) microfiber Sagnac interferometer biochemical sensor using the Vernier effect. (a) Schematic experimental setup of measurement. (b) Transmission spectra of the sensor for different concentrations of BSA solutions. (c) Experimental data for the shift with a linear fit. Reprinted with permission from ref 102. Copyright 2018 MDPI.

detection range from 100 pM to 1 μM for the target ssDNA, and the detection limit was 75 pM. The probe revealed a high degree of detection specificity due to its complementary DNA structure. However, due to the microstructured sensing probe, the sensor was fragile.

The sensitivity of SI-based biochemical sensors can be improved by cascading two SIs serially, which in turn forms a single ultrasensitive sensor for biological sample analysis. In 2018, Wang et al. reported a similar type of Hi-Bi microfiber sensor utilizing the Vernier effect to detect BSA.[102] Figure 17 shows the schematic experimental setup consisting of two similar types of SIs in cascaded form. One sensing probe was fabricated using a Panda polarization-maintaining fiber (PMF) segment, and another probe was made via tapering a birefringence fiber immobilized with a GO layer. The sensor possessed an ultrahigh refractive index sensitivity of 2429 nm/RIU as well as a BSA detection sensitivity up to 9.097 nm/(mg/mL). The proposed sensing probe showed a wide linear detection range of 0−5 mg/mL. The sensor was a little bit bulky because of its cascaded form and also mechanically unstable due to its microfiber structure. Since, the working principle of this sensor is polarization dependent hence, a costly PMF is required in this sensor.

6.3. Specialty Fiber-Based SI Biosensors. In the year 2017, An et al. suggested PCF-based biosensors for the selective detection of glucose using the SI technique. The proposed sensor was small in size, compact in structure, and sensitive in performance.[103] Figure 18 shows the schematic experimental setup and characterization curves of the sensing probe. The sensitivity achieved using this SI-based biochemical

https://doi.org/10.1021/acsomega.3c03970
ACS Omega 2024, 9, 3037−3069

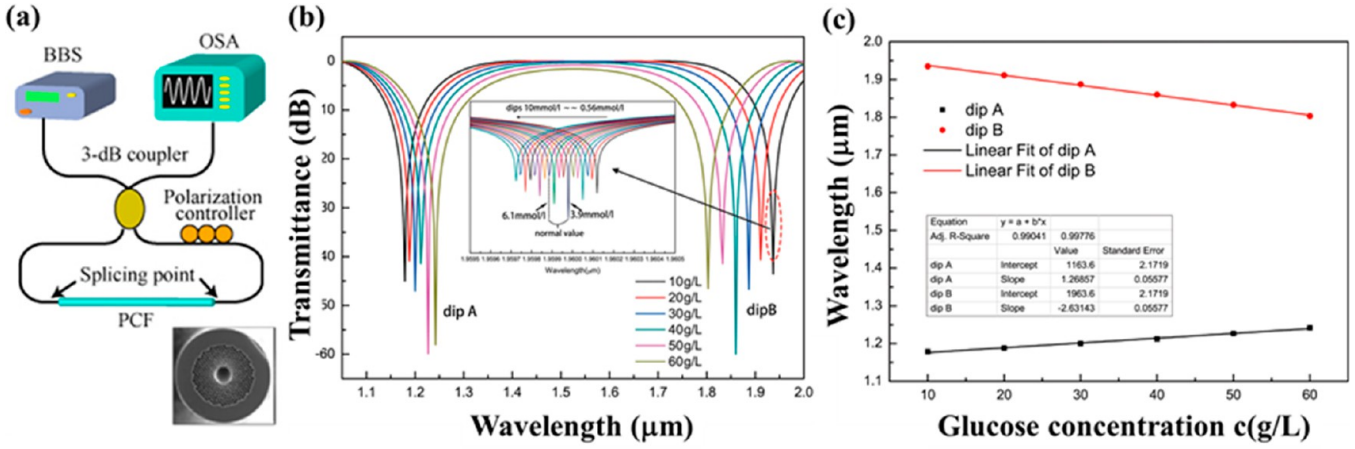

Figure 18. Glucose sensing using a PCF-based SI biochemical sensor. (a) Experimental setup for probe characterization. (b) Output spectra of the sensor for different concentrations of sensing analyte (glucose). (c) Experimental data and corresponding linear shift. Reprinted with permission from ref 103. Copyright 2017 Elsevier.

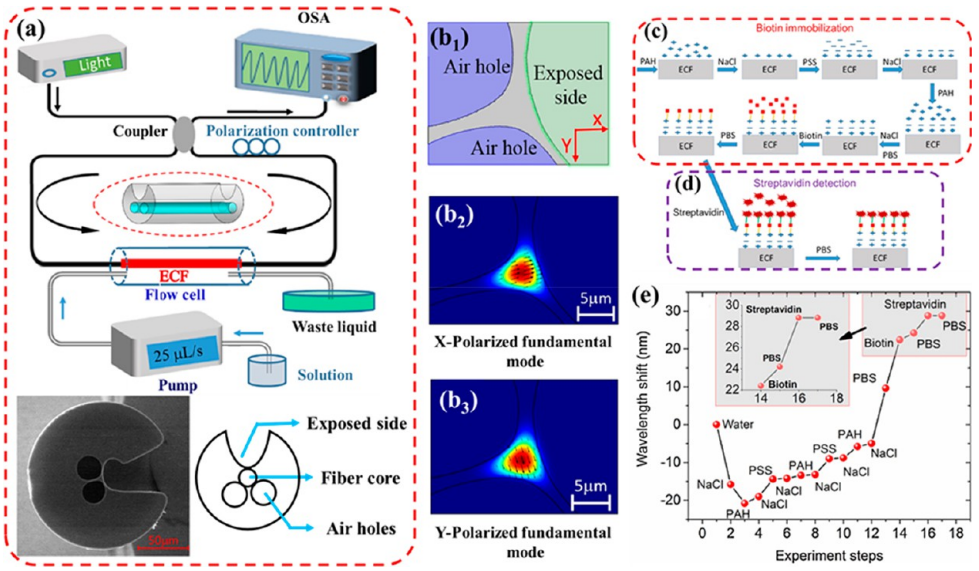

Figure 19. High-sensitivity free SI-based biochemical sensor using an exposed core microstructure optical fiber. (a) Schematic experimental setup for probe characterization. The inset shows the microscopic view of the ECF cross-section. (b_1–b_3) Geometry of the theoretical simulation and the simulated electric field intensity distribution profiles of the *x*- and *y*-polarized fundamental modes. (c) Sequential steps of the probe functionalization procedure. (d) Biochemical sensing process. (e) Wavelength shift of the transmission spectra for each working step. Reprinted with permission from ref 104. Copyright 2018 Elsevier.

sensor was 22130 nm/RIU. The sensor showed a broad linear detection range from 10 to 60 g/L. The sensor has good biocompatible behavior with an easy operation capability and simple structure, making it useful for commercial fabrication.

Li et al, . in the year 2018, presented an exposed core fiber (ECF) based novel, label-free, and high-sensitivity SI biochemical sensor to detect streptavidin.[104] ECF is a specially designed microstructure optical fiber where one side of the fiber core can interact directly with the surrounding analyte medium, as shown in Figure 19. This makes ECF, with an asymmetric structure in the fiber core, realize a birefringence property in terms of output characteristics. This birefringence property of ECF can be used for sensing purposes. When the core of the fiber is in direct contact with a certain external analyte, the RI distribution around the sensing probe becomes particularly asymmetric, giving rise to polarization-based interference. This phenomenon can be effectively used for biochemical sensing purposes.[105] The study reported by Li et al. demonstrates a RI sensitivity of 3137 nm/RIU using ECF-based SI. For the detection of streptavidin, the sensing probe was immobilized with biotin as the sensing material. Figure 19a shows the schematic experimental setup and detailed probe fabrication procedure. The interaction of light from the fiber core with the external medium along the exposed side of the fiber has been studied using the FEM technique. The sensor has a compact and durable size as compared to micro/nanostructured fiber. This sensor did not require any sample holder due to the presence of an in-line exposed core.

The SI-based biochemical sensors have been used in various application fields due to their structural robustness, ease of fabrication, and label-free sensitivity in biodetection. For the study of polarization-dependent biochemical detection, the Hi-Bi fiber can be used as the sensing part. However, the birefringence phenomena are strongly hampered by the high-

https://doi.org/10.1021/acsomega.3c03970
ACS Omega 2024, 9, 3037−3069

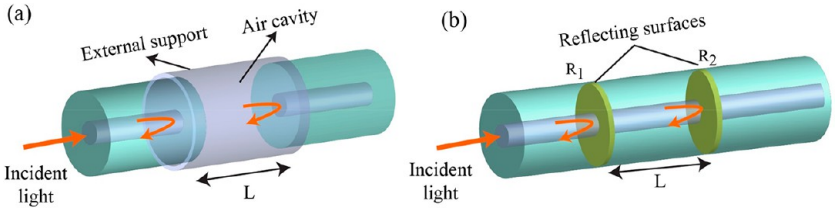

Figure 20. (a) Extrinsic FPI sensor made by forming an external air cavity. (b) Intrinsic FPI sensor formed by two reflecting components, R1 and R2, along with a fiber.

temperature variation. Therefore, to study the temperature-dependent biological activity, the Hi-Bi fiber can be replaced by a simple microstructure fiber. However, microfibers are very fragile. The SI-based biochemical sensors with some of the newly developed fiber-based sensing transducers have the great advantage of label-free detection. However, these types of sensors have comparatively larger volumes, are bulky for the formation of ring-type of structures, and are unable to be used in vivo biological measurements.

7. FABRY−PEROT INTERFEROMETRY-BASED BIOCHEMICAL SENSORS

7.1. Sensing Principle. Fabry−Perot interferometry is another interesting interferometric technique that has been used on a large scale for the fabrication of different fiber-based sensing platforms. In general, the Fabry−Perot interferometer (FPI) consists of two parallel reflecting surfaces separated by a certain distance.[106,107] The multiple reflections and their superposition of the beam between the parallel surfaces cause the interference. For optical fiber-based FPI configurations, the cavity is prepared by designing two reflectors, either intrinsically or extrinsically, based on which the fiber optic FPIs are categorized.[108] In the extrinsic FPI sensor, the reflecting cavity is formed outside of the fiber, while the intrinsic FPI consists of a reflecting cavity within the fiber.[28,109] Figure 20a shows a schematic representation of an extrinsic FPI, where an air cavity is created using a supporting structure; due to the highly reflective surfaces, this structure provides a high finesse interference spectrum.[110] Additionally, such structure requires a comparatively easy fabrication process without any high-cost equipment, but these types of FPIs suffer from alignment refinement, low coupling efficiency, and costly packaging.[28] On the other hand, the intrinsic nature of FPIs is fabricated by the creation of the micrometer dimension cavity inside the fiber, as shown in Figure 20b. A few methods have been utilized for the fabrication of such intrinsic FPI, namely micromachining,[111−113] chemical etching,[114] fiber Bragg gratings (FBGs),[115−117] and thin film deposition.[118−120] However, these methods are still limited due to the requirement of high-cost instrumentation to create a cavity.

The resultant transmission or reflection spectra of an FPI can be realized using the wavelength interrogation of the input light spectrum and obtained due to the phase difference between the reflected or transmitted beams. The phase difference of the FPI may be expressed as

$$\delta = \frac{2\pi}{\lambda} 2nL$$

Here, λ corresponds to the wavelength of input light, n represents the RI for material within the cavity, and L indicates the physical length of the cavity. The peaks and dips generated in the output spectrum are due to in and out of phase of light at that wavelength, respectively, in the modulus of 2π. When any perturbation is introduced through changing the cavity dimension or via altering the RI of the cavity material, the interference shift occurs in terms of the free spectral range. Therefore, the influencing change can be predicted through spectral shift observations. This basic principle of FPI has been utilized for the fabrication of different biochemical sensors after functionalizing the sensing region with suitable recognition materials, as discussed in the following section.

7.2. Micro/nanostructured Optical Fiber-Based FPI Biochemical Sensor. The optical fiber-based FPI sensor can be realized by making an ultrasmall optical cavity on the fiber surface. In 2017, Warren-Smith et al. demonstrated an FPI-based biochemical sensor using an optical microcavity with a diameter of 2.8 μm.[121] The cavity facilitates the ability of the fluid analyte to flow easily into this cavity, thus modulating the RI of the cavity and acting as an RI sensor for ultrahigh sensitivity. The estimated sensitivity of the proposed sensor was 57.3 rad/RIU while a minimum detection limit was of the order of 10^{-4} RIU. The biological activity of that sensor was carried out by coating the cavity surface using a polyelectrolyte layer.

In the year 2018, Khan et al. suggested a single-mode fiber tip-based FPI sensor for the selective detection of glucose and pH with high sensitivity.[122] The sensor was composed of a highly polished uncladded SMF tip immobilized with gold nanoparticles, followed by the deposition of a polymer membrane mixed with three different glucose sensing dyes: Nile red, rhodamine B, and 4-ANMP. In this sensor, when the polar glucose solution comes in contact with the Nile red dye, its sensitivity increases due to the abrupt change of dipole moment of Nile red dye. This change of the dipole moment occurs for large charge transfer between donor and acceptor moieties. Hence, the energy gap decreases with the increase in solvent polarity. For the change of the energy gap between the ground and excited states, the permittivity and hence refractive index of the dye molecule are altered. This produces the shift in dip wavelength of the spectra that depends on the concentration of glucose solution. The maximum pH sensitivity obtained was 1.95 nm/pH, and the glucose detection sensitivity was 3.25 nm/mM.

7.3. C-type Optical Fiber-Based FPI Biochemical Sensor. A C-type fiber is one kind of specialty fiber where one side is open to air, allowing interaction of the external media with the fiber core and modulating the propagation of light. In this type of FPI sensor, a section of C-type fiber is spliced between two normal SMFs, thus the open side makes a cavity between two SMFs. This cavity allows the fluidic samples to enter into the gap. Hence, by proper functionalization of this inner cavity surface, this sensing transducer can be made sensitive to the desired analyte. In the year 2014, Wu et al. fabricated a cavity-based FPI sensor by splicing a small

https://doi.org/10.1021/acsomega.3c03970
ACS Omega 2024, 9, 3037−3069

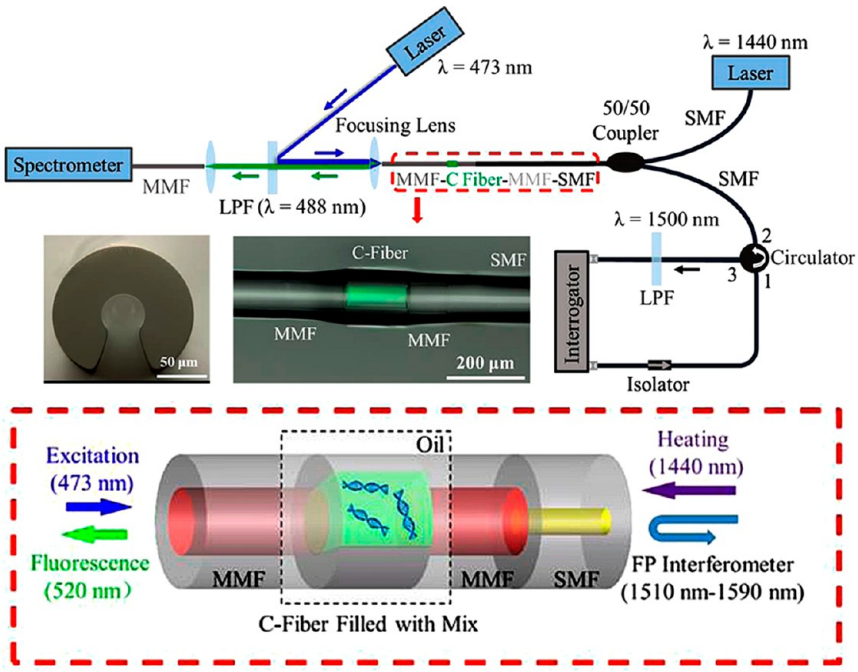

Figure 21. Schematic experimental setup and sensing mechanism of a C-type fiber-based Fabry–Perot interferometer for all-fiber qPCR. Reprinted with permission from ref 125. Copyright 2020 Elsevier.

section of C-shaped specialty fiber between two SMFs using a fusion splicer.[123] The RI sensitivity of that sensor was checked using an ethanol–water mixture with varying concentrations. The sensor showed a RI sensing response in the range of 1.33 to 1.36. Its RI sensitivity was obtained as 1368 nm/RIU for a 1600 nm wavelength of input light with negligible temperature cross-sensitivity of 3.04×10^{-7} RIU/°C.

In the year 2019, Xie et al. adopted the same principle of C-shaped optical fiber and proposed a dual cavity-based FPI sensor for selective detection of streptavidin.[124] The sensing probe was constructed by forming a dual cavity using two C-shaped optical fibers through serially arranged in-line splicing with conventional single-mode fiber. The lengths of the two cavities were taken as 80 and 183 μm. The first cavity was taken as a reference cavity and the other one was used as a target cavity for measurement or vice versa. The experimental observations showed minimum cross-talk effect between the two cavities, which confirmed the independent nature of both probes. To use this sensing transducer for biosensing applications, both cavity regions were immobilized with layer-by-layer polymer nanofilms. The first cavity region, called the control probe, was then immersed in PBS solution. The second cavity was also coated with polyelectrolyte nanofilm using the same technique, followed by functionalization with biotin. The biotin–streptavidin binding property was utilized for the detection of streptavidin with high specificity. Due to this binding interaction, the RI of the cavity region of the target probe changes. This alters the phase difference in the output fast Fourier transform (FFT) spectra. The minimum cross-talk effect showed the capability of the probe for independent dual parameter sensing and also shows the possibility of multiple biochemical sensing. This in-line cavity-based sensor shows the potential of multiplexing more cavities. However, this sensor was limited from separating the FFT for different cavities. The light beam was divergent for the open cavity and prevented the multiplexing of a greater number of cavities. This makes the output intensity lossy. Another remarkable limitation of this sensor was the minimum cavity length that supports the sensor. For a further decrease of cavity length, the FSR increased. That makes it very difficult to demodulate the signal using FFT.

In 2020, Li et al. demonstrated a C-type fiber-based all-fiber all-optical biosensor for quantitative polymerase chain reaction (qPCR) detection.[125] In this sensor, the C-type fiber cavity was used as a sensing transducer where the qPCR process was performed and the real-time fluorescence was monitored, as shown in Figure 21. The experimental results showed the real-time fluorescence capability of the sensor for quantitative amplification of DNA. The proposed sensing platform showed a new strategy for remote diagnosis and real-time data collection. The biochemical sensor based on the C-type specialty fiber showed high sensitivity due to the direct interaction of the fluidic analyte medium with the core of the fiber through an open microfluidic cavity. Therefore, this type of sensor allows on-site real-time measurements. However, this type of sensor suffers from serious optical loss due to the direct interaction of propagating light inside the resonating fiber cavity. Moreover, this sensor is not suitable for any in vivo biological observations.

7.4. Hollow Core Optical Fiber-Based FPI Biochemical Sensor. The FPI phenomena can be achieved by forming multiple cavities within the in-line fiber structure. This in-line fiber cavity can be formed using a hollow core specialty fiber or tube in combination with normal SMF. In 2005, Zhang et al. reported a fiber optic in-line FPI sensor for selective biochemical sensing using multicavity structures.[126] The sensing probe was constructed by simple splicing of a hollow core silica tube with an approximate length of 10 μm at the end of an SMF. The inner and outer diameters of the tube are 50 and 125 μm, respectively.

Another segment of SMF was spliced at the end of the silica tube and cleaved. Thus, two optical cavities are formed at the

https://doi.org/10.1021/acsomega.3c03970
ACS Omega 2024, 9, 3037–3069

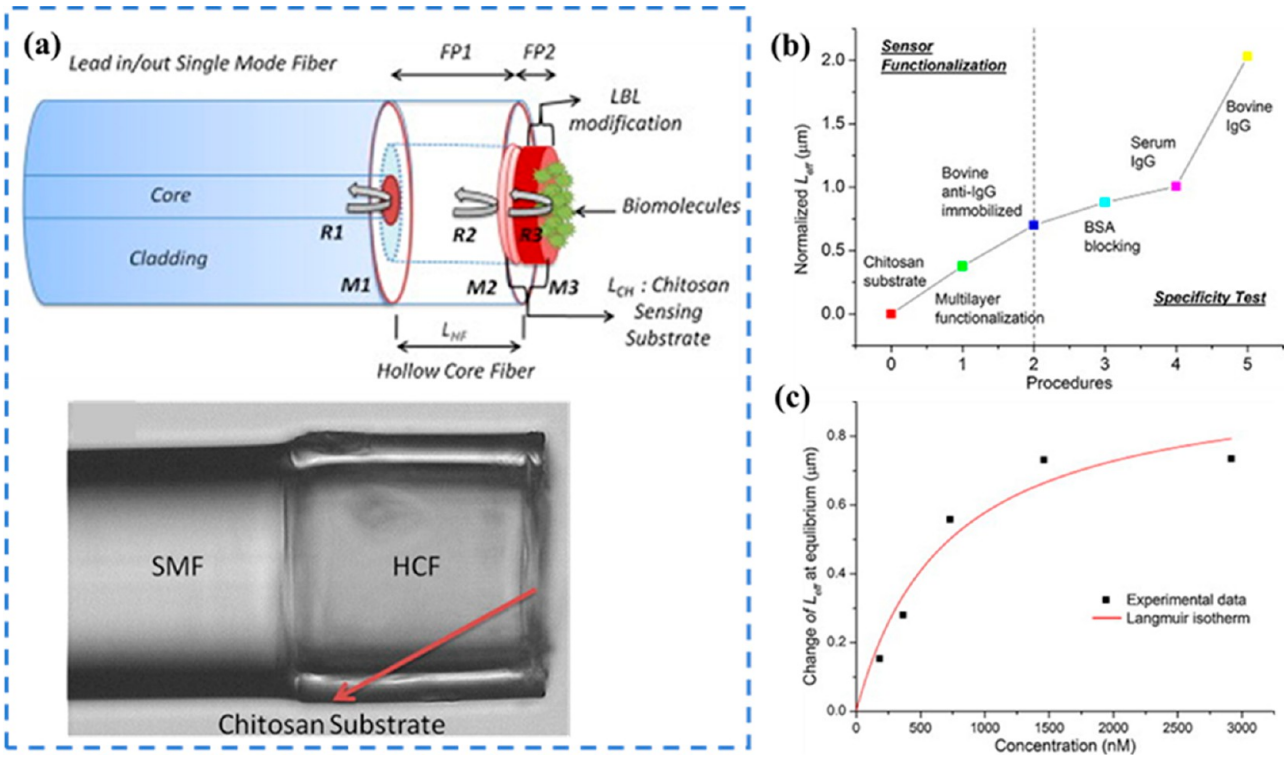

Figure 22. Fiber optic Fabry–Perot interferometer-based biochemical immunosensor. (a) Schematic presentation of the sensing probe with a microscopic view. (b) Spectral response of the probe during the layer-by-layer functionalization process. (c) Spectral response for different IgG concentrations. Reprinted with permission from ref 127. Copyright 2013 Elsevier.

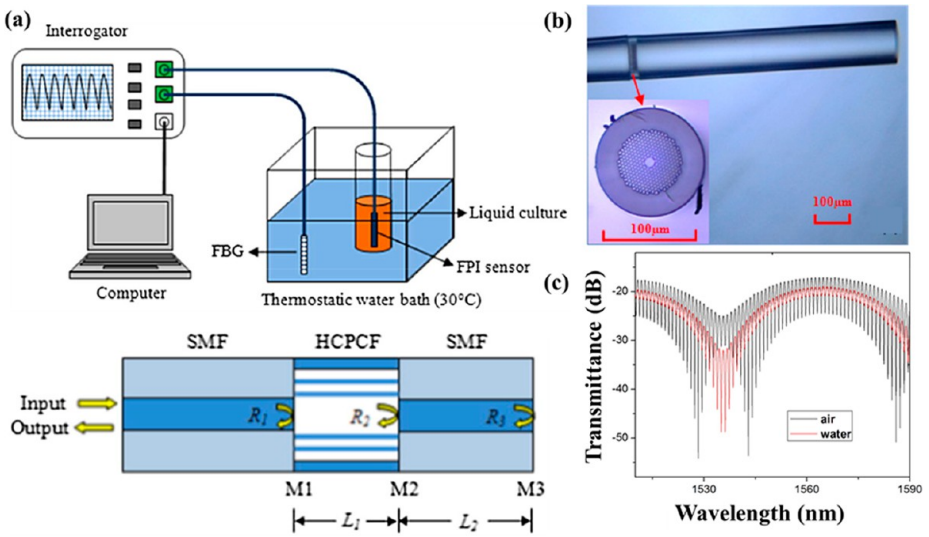

Figure 23. Fiber optic FPI sensor for microorganism detection. (a) Schematic experimental setup and basic working principle. (b) Microscopic image of the sensing probe. (c) Transmission interference spectra of the fabricated sensor. Reprinted with permission from ref 128. Copyright 2016 Elsevier.

end of SMF. The incident light reflected from the front and back walls of these two cavities and for superpositions of them produced a stable interference pattern. This cavity-based transducing platform was functionalized and used for selective biochemical sensing applications. In this process, self-assembled polyelectrolyte layers were immobilized for the specific detection of immunoglobulin G (IgG). The compact, flexible structure of the sensor gives the potential for in situ sensing applications. However, this sensitive tip-based sensor is difficult to fabricate. Moreover, proper storage is required for repeated use. A similar type of cavity-based FPI sensor was reported in 2013 by Chen et al.[127] The sensor was fabricated by splicing a hollow core fiber (HCF) segment having an inner diameter of 70 μm with a standard SMF, as shown in Figure 22. The end face of HCF was coated with a self-assembled chitosan and polystyrenesulfonate membrane. This coated membrane formed an optical cavity at the end of the fiber and produced interference at the reflected output. The chitosan membrane was immobilized with protein through a layer-by-layer self-assembly technique. The surface modification of

https://doi.org/10.1021/acsomega.3c03970
ACS Omega 2024, 9, 3037−3069

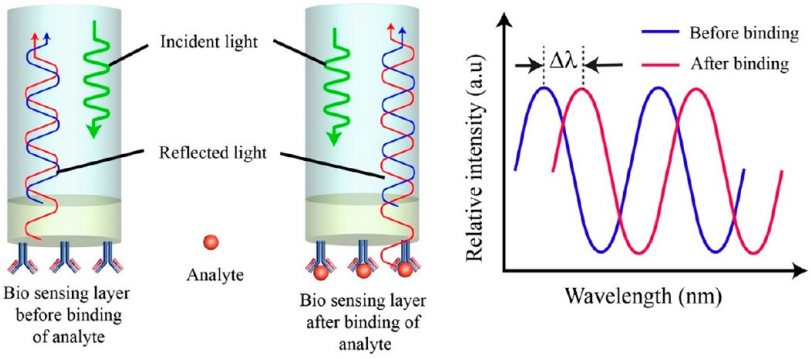

Figure 24. Schematic representation of a biolayer interferometry (BLI) based biochemical sensor.

chitosan preserved the biospecific activity of the adsorber. This FPI-based single-ended immunosensor was characterized for specific label-free detection of anti-IgG. The effect of each step of the immunoassay process was monitored. The experimental results confirmed the negligible response for unrelated anti-IgG. The sensitivity of the fabricated sensor was found to be 0.033 μm/(pg/mm^2) with a limit of detection of 0.005 nM.

Hollow core PCF (HCPCF) is an exclusive type of specialty fiber that can be used with normal SMF to make FP-based biochemical sensors. In the year 2016, Liu et al. developed an FPI-based biochemical sensor for the detection of micro-organ activities.[128] Here, HCPCF was used with conventional SMF to fabricate the FP cavity at the end of SMF, as shown in Figure 23. This cavity supports multiple reflection-based interference spectra. The proposed sensor showed a very high refractive sensitivity of −136 dB/RIU. The single-ended sensing probe was functionalized and immersed vertically into the liquid culture medium to detect the growth of yeast. However, this cavity-based sensor suffered from insertion loss due to the leakage of light.

The above examples show that, in comparison with MZI, MI, and SI-based biochemical sensors, the FPI-based biochemical sensors are more compact in terms of volumes and lengths. The typical size of this type of biochemical sensor is only a few tens of micrometers or even a few micrometers. Therefore, these sensors require very low amounts of analyte samples for measurement. The single-ended sensors are more convenient to use for long-distance monitoring and remote biosensing applications. Moreover, these are very suitable for insertion in in situ and in vivo measurements. Besides, these microcavity-based FPI biosensors facilitate the microresonance phenomenon inside the in-line cavity, achieving PCR amplification. Apart from this, the cascading facility of such a biochemical sensor provides simultaneous measurement of multiple biochemicals.

8. BIOLAYER INTERFEROMETRY (BLI) BASED BIOCHEMICAL SENSOR

Another important interferometric technique that is widely used for the detection of different biological elements is biolayer interferometry (BLI). This technique was first developed by ForteBio, focusing on qualifying and quantifying the protein−protein interaction. This BLI technique analyzes the real-time biomolecular interaction kinetics without any requirement of fluorescent labeling of the sensing probe.[129−131] It is based on thin film interference as produced by two reflecting surfaces at the tip of the sensor. To construct this BLI sensor, the free end of the sensor tip is first immobilized with the ligand that will bind the desired analyte. Due to the immobilization of the ligand molecule, a thin film is formed at the end of the sensor tip. Now, when the white light is incident on this thin film, part of the light gets reflected from the first surface of the film while another part of the light as transmitted light is again reflected from the second face of the thin film. Thus, these two reflected lights with different intensities propagate through the sensor and produce an interference pattern at the detector.[132] The interference wavelength shift depends on the thickness of the sensing film instead of the RI of the external medium. To use this BLI sensor for biosensing applications, the sensing tip is dipped into the sample solution containing the desired analyte. The analyte from the sample binds with the ligand at the tip of sensor. Due to the association of the target analyte, the thickness of the biological layer increases. This will shift the interference dip wavelength toward the high-wavelength region, while for dissociation of the target analyte a blue shift occurs. Thus, any shift in output spectra is directly linked with the association or dissociation of the desired analyte. The schematic construction and working principle of a BLI sensor is shown in Figure 24. Here the wavelength shift $\Delta\lambda$ shows the interference shift for increasing the biological layer thickness due to association of the target analyte. This interferometric technique allows for real-time monitoring of biological interaction. In order to suppress any nonspecific molecular interaction, the sensor tip can be functionalized with specific biorecognizing elements like enzymes, antibodies, aptamer, and cells that improve the binding specificity of the sensor.[130,133,134] The BLI sensor has been used extensively in the pharmaceutical industry for drug characterization, molecular interaction kinetics monitoring, and characterization due to its easy construction, small compact structure, label-free performance, and disposable nature.

9. BIOCHEMICAL SENSORS BASED ON OPTOTHERMAL EFFECTS

Optothermal-based biosensors correspond to identifying the change in the refractive index of the sensing material through varying the temperature at the surface, which is then transferred to a readable signal through any refractive index sensing method such as interferometry,[135] whispering gallery modes,[136] etc. This surface heat can be changed through the effects of laser irradiation, the chemical interaction between the a sensing layer and target analyte,[137] etc. Recently, Yang et al., reported one such sensor, where a MZI-based fiber optic probe is proposed to identify the optothermal effects of ionic liquids by laser illumination.[135] The sensor consists of a U-shaped

https://doi.org/10.1021/acsomega.3c03970
ACS Omega 2024, 9, 3037−3069

Table 1. Summarized Tabulated Description Depicting the Yearwise Growth of Several Interferometric-Based Biochemical Sensors[a]

category and configuration of sensor	target analyte	sensing layer	concentration range	detection limit	remarks	publication year
MZI biosensors: microfiber based						
MZI: tapered fiber[72]	single-stranded DNA (ssDNA)	conjugated polymer membrane		10^{-4} μM	potential for biochemical applications	2015
MZI: tapered fiber[74]	neurotransmitter serotonin (5-HT)	mesoporous structures of SiO_2	10^{-10} to 1 μM (10^{-7} to 1 μM linear range)	84×10^{-9} μM	response time: 20 min	2016
MZI: tapered fiber coupled with laterally aligned microcapillary[80]	MicroRNA-let7a	APTES/glutaraldehyde/animated NH_2	0.002−20 μM (log-linear range)	2.12×10^{-4} μM	response time: 15 min	2017
MZI: tapered fiber[75]	single-stranded DNA (ssDNA)	graphene oxide layer	10^{-8} to 1 μM (10^{-6} to 1 μM linear range)	10^{-6} μM	wide pH range: 4.3−8.5	
MZI: tapered fiber[76]	γ-aminobutyric acid (GABA)	Fe_3O_4@SiO_2@mesoporous SiO_2 microspheres	10^{-7} to 10^{3} μM (linear range)	3.51×10^{-7} μM	size-based selectivity	
MZI: tapered fiber[79]	methyl parathion	acetylcholinesterase enzyme	(10^{-4} to 50) μM	2.4×10^{-4} μM	response time: 5 min	
MZI: tapered fiber[82]	*Escherichia coli* (*E. coli*).	T4 bacteriophage	10^{3} to 10^{7} CFU/mL	10^{3} CFU/mL	applications in food industry	2018
MZI: tapered fiber[81]	*Leptospira* bacterial DNA	complementary DNA	10^{-10} to 10^{-3} μM (linear range)	10^{-10} μM	highly specific	
MZI: tapered fiber[77]	γ-aminobutyric acid (GABA)	graphene oxide/anti-GABA antibodies	10^{-12} to 1 μM (linear range)	2.91×10^{-12} μM	demonstrated real application	
MZI: tapered fiber[84]	γ-aminobutyric acid (GABA) cellular cytochrome c	anti-GABA/Ag@RGO	10^{-12} to 10^{3} μM (linear range)	1.65×10^{-9} to 6.82×10^{-11} μM	highly selective with real-time monitoring	2019
MZI: tapered PCF[85]	enzymatic reaction of penicillinase	PCF coated with APG and LC based on pH change of PBA	6.1−8.5 pH (linear range)		potential for biological applications	
MZI: concatenated tapered fiber[83]	parathion methyl (PM)	MIP	10^{-6} to 10^{2} μM (log-linear range)	79.43×10^{-9} μM	potential for real sample analysis	
MZI: tapered fiber[138]	urea	MIP	10^{-5} − 10^{2} μM (log-linear range)	17.1×10^{-9} μM	potential for real applications	2021
MZI: tapered microfiber[139]	BOD material (glucose and glutamate)	fiber surface immobilized with Nb_2CT_X MXene	0.2−1 mg/mL (linear range)	5.7×10^{-4} mg/mL	temperature sensitive	
MZI: tapered microfiber[140]	dengue virus (DENV) II E protein	fiber surface/chitosan/anti-DENV II E protein	1 pM to 0.1 μM	1 pM	applicable in clinical analysis	
MZI: S-tapered microfiber[141]	human IgG	fiber surface/dopamine/protein A/BSA/IgG	0.25−2 μg/mL (linear range)	28 ng/mL	specific in nature	
MZI: cascade of tapered fibers[142]	*Staphylococcus aureus*	EDC/IgG antibody/BSA	7×10^{1} to 7×10^{5} CFU/mL	11 CFU/mL	specific in nature	2022
MZI: tapered fiber[143]	cholesterol	polydopamine-β-CD membrane	0.001−1 mM		highly specific	2023
MZI: tapered fiber[144]	glucose	carboxy phenylboric acid film	0.1−20 mM	12.6 ppm	specific in nature	
MZI: tapered fiber[145]	CAIX protein biomarker	Ti_3C_2 MXene@Au nanorod	10^{-21} to 10^{-8} M	13.8 zM	potential for cancer cell detection	
MZI: double tapered microfiber[146]	4-nitrophenol	MIP nanoparticles	10^{-6} to 10^{2} μM (log-linear range)	1.63×10^{-9} μM	selective and repeatable	
MZI biosensors: TCF-based						
MZI: TCFMI[87]	DNA (ssDNA)	self-assembly of PEI, PAA, and ssDNA		10^{3} μM	highly selective	2013
MZI: SMF−TCF−SMF[88]	htreptavidin	PSAMs functionalized with biotin	(1.67−83.3)× 10^{-3} μM	2×10^{-5} μM	selective	2016
MZI: SMF−TCF−SMF[89]	human IgG	APTES/glutaraldehyde/goat anti-IgG	0.67−6.7 μM (linear range)		highly specific	2018
MZI: dual S-tapered TCF[90]	DNA hybridization	PLL/ssDNA	10^{-3} to 1 μM	10^{-3} μM	selective	2019
MZI: TCMF@microfluidic chip[147]	*Toxoplasma gondii*	MoS_2 functionalized with *T. gondii* antigens	0.001−10 ng/mL	87 fg/mL	potential for clinical application	2023
MZI biosensors: offset fiber-based						
MZI: core offset[60]	human IgG	goat antihuman IgG	(3.3−333) × 10^{-3} μM	3×10^{-4} μM	suitable for biomedical fields	2018
MZI: bent offset fiber[148]	2,4-DCP	fiber surface/MIP nanoparticles	0.1−100 μM	8.77 nM	fast and specific in nature	2023

https://doi.org/10.1021/acsomega.3c03970
ACS Omega 2024, 9, 3037−3069

Table 1. continued

category and configuration of sensor	target analyte	sensing layer	concentration range	detection limit	remarks	publication year
MZI biosensors: offset fiber-based						
MZI: cascaded SMF-DSMF-SMF structures[149]	canine distemper virus	functionalized with APTES/CDV antibody	0.1−10^4 pg/mL	0.1687 pg/mL	selective and suitable for clinical testing	
MZI biosensors: cavity-based						
MZI: U-shaped microcavity[73]	ssDNA binding kinetics	poly-L-lysine (PLL)/complementary ssDNA	10^{-4} to 10^{-2} μM	10^{-4} μM	suitable for medical diagnosis	2016
MZI: microcavity within SMF[78]	bovine serum albumin (BSA	based on RI changes of BSA solutions	3−30 μM (linear range)	3.9 × 10^{-3} μM		2017
MZI biosensors: specialty fiber-based						
MZI: ECF[150]	streptavidin	biotin-functionalized			selective	2015
MZI: STHS[86]	hCG	hCG-β-mAb	(1.2−117) × 10^{-6} μM	1.4 × 10^{-7} μM	highly specific	2020
MZI: SMF−PCF−SMF with small core offset[151]	glucose	immobilized PCF with GO-GOD	10−70 g/L (linear range)		shows good stability	2021
MZI: etched SMF−MMF−SMF[152]	anti-BSA	functionalized with APTES and BSA	0.01−100 μg/mL	0.7 μg/mL	robust in nature	2022
MZI: SMF−PCF−SMF[153]	nitrate ion	graphene−PVA membrane	0−100 ppm	3.33 ppm	fast in nature and selective	
MZI: SMF−ECF−SMF[154]	cDNA	APTES/p-DNA	10−60 nM	0.31 nM	specific and sensitive	
MZI: SMF−NCF−SMF[155]	protamine	functionalized with chitosan/heparin	6.25−1000 μg/mL	0.48 μg/mL	selective	2023
MZI: ECF[156]	deafness gene DNA	fiber surface/PLL/p-DNA	1−10^4 nM	0.046 nM	sensitive, robust, and specific	
MZI: SMF−PCF−SMF[157]	*p*-cresol	MIP nanoparticles	10^{-2}−10^3 μM (log-linear range)	1.55 × 10^{-3} μM	fast responsive and repeatable	
MZI: SMF−TNCF−MMF−SMF[158]	deafness gene DNA	black phosphorus nanointerface	1 pM to 1 μM	0.24 pM	potential of clinical applications	
MZI: SMF−COF−SMF[159]	*Staphylococcus aureus*	porcine IgG antibody	10−10^5 CFU/mL	1.0 CFU/mL	highly selective and repeatable	
MI biosensors: microfiber-based						
MI: multimode tapered fiber[95]	glucose	APTES/GOD-functionalized	(0−2) × 10^4 μM		potential for practical application	2018
MI: tapered microfiber[160]	anti-IgG	human IgG-functionalized using PDA	0−14 ng/mL	2 ng/mL	potential of micron label localization	2023
MI biosensors: specialty fiber-based						
MI: optofluidic channel in PCF collapse region[96]	DNA hybridization	PLL-functionalized	10^{-3}−10^{-1} μM	5 × 10^{-3} μM	highly specific, potential for biosensing	2016
MI: DCF[99]	anti-IgG	antibody-functionalized		4 μg/mL	specific	2018
MI: SMF−SHSCTCF[161]	DNA	APTES and probe DNA		29 nM	compact size and selective	2022
MI: TCF−NCF[162]	fluoride ion	α-Fe2O3/ZrO2 sensing film	0−1.5 ppm	0.06 ppm	selective with temperature and pH stability	
MI: SMF−PCF single-ended[163]	lead ion	functionalized with Chitosan-PVA and glutathione AuNp	0−50 ppb	1.6 ppb	compact, fast, and selective	
MI: TCF−SMF−NCF[164]	lead ion	MXene (Ti3C2) functionalized	0−100 μM	0.001 μM	fast response and highly selective	2023
SI biosensors: microfiber-based						
SI: Hi-Bi microfiber[101]	DNA	PLL/ssDNA functionalized	10^{-4} to 1 μM	75 × 10^{-6} μM	utility for practical applications	2017
SI: panda PM fiber and Hi-Bi microfiber[102]	BSA	APTES/GO immobilized	15 to 75 μM		potential for biosensing applications	2018
SI biosensors: specialty fiber-based						
SI: ECF microstructured fiber[104]	streptavidin	biotin-functionalized			capable of biosensing	2018
SI: PCF[103]	glucose		(6−33) × 10^4 μM		potential of clinical testing	2017
SI: PCF[165]	cancer cell				high resolution	2020
SI: PMF and ExTFG[166]	canine distemper virus	GO functionalized with anti-CDV MAbs	0.001−50 ng/mL	1 pg/mL	highly specific and suitable for clinical measurement	2023

https://doi.org/10.1021/acsomega.3c03970
ACS Omega 2024, 9, 3037−3069

Table 1. continued

category and configuration of sensor	target analyte	sensing layer	concentration range	detection limit	remarks	publication year
FPI biosensors: microfiber-based						
FPI: AuNP coated on core[122]	glucose	Nile red, rhodamine-B, 4-ANMP-functionalized	1 to 10^6 μM		specific	2017
FPI: splicing MF at SMF end[167]	thrombus	thin film of blood on MF tip	0.5−3.4 μL		fast performance	2023
FPI biosensensors: C-type fiber-based						
FPI: cascaded C-type fiber[124]	streptavidin	biotin-functionalized		1.01 μM	suitable for biochemical sensing	2019
FPI: C-fiber microcavity[125]	DNA				fluorescence free operation	2020
FPI: SMF−C-type fiber−SMF[168]	cDNA	functionalized with APTES and probe DNA		67.5 nM	highly selective and fast performance	2022
FPI biosensors: hollow core fiber-based						
FPI: splicing of SMF-HCF single-ended[127]	anti-IgG	IgG/chitosan/polystyrenesulfonate functionalized		5×10^{-6} μM	biomedical applications	2013
FPI: SMF-HCF-SMF[128]	yeast growth				real time monitoring potential	2016
FPI biosensors: thin film cavity-based						
FPI: thin film-based cavity[169]	perfluorooctanoic acid	graphene-doped alginate thin film	0.2−2 ppb	0.4 ppb	fast response and sensitive	2023
FPI: SMF-based open cavity[170]	carcinoembryonic antigen	functionalized with anti-CEA antibody	500 fg/mL to 5 ng/mL	36.14 fg/mL	highly sensitive and specific	
FPI: multilayered thin film cavity[171]	cholesterol	epoxy resin/GO /β-CD	0−8 mM	3.48 μM	selective, stable, and reusable	
FPI: SMF-Mg-silicate NPs doped fiber[172]	CCL5 cancer biomarker	Fiber tip/APTES/GAG/antibodies	1 aM to 100 nM	17.6 aM	potential of real-time detection	2024
BLI-based biosensors						
BLI: SELEX[173]	patulin	streptavidin/biotin/PAT C3 aptamer	0.045 to 100 ng/mL	0.173 ng/mL	potential for real sample analysis	2022
BLI: aptamer−antibody receptor pair[174]	TNF-α	biotin/streptavidin/aptamer	0.25−32 nM	0.0625 nM	clinical point-of-care-testing	
BLI: immunoassay platform[175]	NS1 protein	Z-domain Sup35NM/*E. coli* cell	1−10^4 ng/mL	0.82 ng/mL	highly selective and sensitive	2023
BLI: peptide−-nucleic acid aptamer pair[176]	biomarker $VEGF_{165}$	fiber end surface/biotin−streptavidin/AuNP	0.01−1 nM	6 pM	applicable for point-of-care clinical testing	
BLI-ELASA[177]	glaucoma biomarker GDF15	biotin/streptavidin	10−810 pg/mL	5−6 pg/mL	suitable for real-time monitoring	

[a]APTES, (3-aminopropyl) triethoxysilane; PSAM, polyelectrolyte self-assembled multilayers; RGO, Reduced Graphene Oxide; ANMP, amino-*N*-methylphthalimide; PAA, poly(acrylic acid); PEI, poly(ethylenimine); hCG, human chorionic gonadotropin; IgG, immunoglobulin G; PMF, polarization-maintaining fiber; ExTFG, excessively tilted fiber grating; COF, core-only fiber; β-CD, β-cyclodextrin; SHSCTCF, single hole suspended core twin-core fiber; PDA, polydopamine; TCMF, thin core microfiber; STHC, single mode-tapered hollow core-single mode; EDC, 1-(3-(dimethylamino)propyl)-3-ethylcar-bodiimide hydrochloride; DCF, dual core fiber; SELEX, systematic evolution of ligands by exponential enrichment; TNF, tumor necrosis factor; DSMF, dislocation single mode fiber; GAG, glutaraldehyde; CCL5, CC chemokine ligand 5; VEGF, vascular endothelial growth factor; ELASA, enzyme-linked aptamer sandwich assay; NCF, no core fiber; TNF, tumor necrosis factor; GO-GOD, graphene oxide−glucose oxidase; BOD, biological oxygen demand; DCP, dichlorophenol; BSA, bovine serum albumin.

https://doi.org/10.1021/acsomega.3c03970
ACS Omega 2024, 9, 3037−3069

Table 2. Critical Comparison among Different Interferometric-Based Biochemical Sensors

working principle	fiber configuration	advantages	disadvantages	refs
MZI	MNF	ultrasensitive, high resolution, small size	fragile structure, temperature, and bending cross-reference	74
	MOF	high sensitivity, stable configure	complex fabrication, temperature, strain cross reference	83
	TCF	easy fabrication, stable structure, easy to use	low sensitivity, temperature cross-reference	88
MI	MNF	compact size, reflective type structure, high sensitivity	fragile structure, temperature, bending cross reference	95
	PCF	compact size, reflective type structure, high sensitivity	complex fabrication	96
	DCF	compact size, stable structure	complex fabrication	99
SI	MNF	ultrasensitive, fine structure	fragile structure, temperature, bending cross reference, lossy	101
	ECF	ultrasensitive, compact size	complex manufacturing, lossy	104
FPI	MNF	ultrasmall size, reflection-type probe structure, high sensitivity, cascading facility	complex fabrication, lossy, poor repeatability	121
	MOF			124
	HCF			128
BLI	SMF/MMF	ultrasensitive, point-of-care application	complex manufacturing, lossy	132

microcavity between two laterally shifted coreless fiber optic segments, which helps to improve the refractive index sensitivity as well as the visibility of the interference. Through changing the refractive index of ionic liquid, the sensitivity of the sensor was found to be able to be −9.6525 nm/(mW·mm^{-2}) for laser irradiation power from 0.00 to 11.67 mW/mm^2. Although only a few studies have reported interferometric and optothermal-based fiber optic biosensors, this technique holds several potential applications, such as thermal-functionalized applications like temperature-dependent biosensing, ionic-liquid-functionalized applications, optical tweezing, wavelength tuning, etc.

A comprehensive comparison of all interferometric-based biochemical sensors is summarized in Table 1, in terms of the sensing probe configuration, nature of the sensing layer, detection range, and limit of detection.

10. COMPARISON OF DIFFERENT INTERFEROMETRIC-BASED BIOCHEMICAL SENSORS

A summarized critical comparison among different fiber optic interferometric-based biochemical sensors is given in Table 2. Here one can see a brief classification of the four types of interferometric sensors based on the category of optical fiber that is used for sensing probe fabrications process. The optical fiber interferometric-based biochemical sensors have the potential to provide very sophisticated experimental data consistent with theoretical analysis. These biochemical sensors have the advantages of being label-free and biocompatible, along with allowing real-time measurements. MI and FPI have smaller and more compact sizes as compared to MZI- and SI-based biochemical sensors. Apart from this, the reflective structure of MI and FPI sensors has potential for online in vivo measurements. In addition, owing the cascading facility of the FPI sensors, simultaneous measurement of multiple analytes can be realized. The MNF-based interferometric biosensors have high sensitivity, but they have fragile structures and very poor temperature cross-sensitivity. The MOF-based interferometers have the advantages of high sensitivity and fast response, but they suffer from a more complex fabrication process. All these optical fibers based biochemical sensors have a significant role in label-free, sensitive biochemical detection with high specificity.

11. CHALLENGES AND POSSIBLE SOLUTIONS

The main challenge to develop these sensors for transfer to real devices is the sensitivity toward mechanical fluctuations such as bending, stretching, and and temperature variations. The reason for this cross-sensitivity with external fluctuations is the change in the effective index of the higher-order modes propagating across the sensing layer, which depends on the refractive index of the sensing layer and the optical and structural properties of the optical waveguide. These unwanted noise signals can easily alter the actual result, especially in the case of low-concentration measurements or evaluating the sensor's detection limit. Therefore, in the current scenario, these sensors should be fabricated in such a way that any unwanted bending effect as well as the temperature fluctuations cannot influence the sensor's performance significantly during biosensing measurements. Considering the existing techniques, the most broadly used method is using fiber optic distributed sensors, which are sensitive to temperature, stress, and and with vibrations.[178] To minimize these effects, herein we propose a few possible solutions. First solution is that, after the sensor fabrication, one should fix the sensing regime within a thin cylindrical casing made of Teflon, PDMS, or PMMA having the facility of a microfluidic channel to ease transportation of sensing molecules. The casing will help to minimize the temperature fluctuations/mechanical vibrations and other external influences. Several properties such as flexibility, hardness, and temperature coefficient are important while designing such a casing. One of the possible solutions, which researchers have utilized broadly in fiber-based configurations, is where a fiber bragg grating is fabricated very near to the sensing region and the temperature response is recorded.[179−181] After the measurements, with a correlation of temperature change in sensor response, one can easily diminish the response obtained due to the temperature fluctuations. A similar study has also been performed using dual fiber bragg grating on the tip of microfiber. Chen et al. reported a temperature compensation enabled refractive index sensor where two different fiber bragg gratings were fabricated using ultrashot pulses on a microfiber platform.[180] The grating showed the response toward changes in the surrounding refractive index and also showed a response with changes in the surrounding environments. Hence, by compiling the results, the authors succeed in minimizing the temperature

https://doi.org/10.1021/acsomega.3c03970
ACS Omega 2024, 9, 3037−3069

cross-talk.[180] In a similar manner, a number of studies can be found in the literature.[180,182] However, this method has not been utilized yet in the case of optical fiber interferometry-based refractive index or biochemical sensors. The reason may be the fabrication of FBG on microfiber platforms, PCF, especially designed microstructure fiber is tricky. Hence, it will be interesting to fabricate such sensor where FBG and interferometry are integrated toward compensating the external influence. The designed FBG should have fabricated on/very near to the sensing channel and as well as the operating wavelength should not overlap with the operating wavelength of the fiber optic interferometer.

Another kind of temperature compensation study for fiber-based multimode interference was reported by Oe et al.[183] Here, the authors used an optical frequency comb (OFC) sensing cavity along with multimode interference (MMI) fiber, with two different sensors enabling concurrent monitoring of sample temperature and as well as material-dependent RI. Then, by decoding the results, the authors were able to realize the temperature compensation RI sensing with a precision of 1.6×10^{-4} RIU along with a temperature stability of 0.08 °C. Additionally, we feel that it is also worth trying with distributed sensing, since this is also quite sensitive for measuring thermal and mechanical fluctuations. Similar to FBG, the distributed sensors could help to nullify the external influence, which can obviously improve the performance of the fiber optic interferometric sensors. The preference of distributed sensing over the FBG will be due to the fact that in this case you do not need many changes in the fiber configurations. Initially, after fabricating the fiber, one should check the response with respect to the external influences and characterize the sensor one by monitoring these changes; using this method, one can nullify the response corresponding to the external fluctuations. Furthermore, one should also focus on the several works on the acousto-optic devices[184] and elasto-optic devices with fiber bragg grating,[185] which have been used to find the effect of mechanical fluctuations to apply them for biomedical applications. Although, these works are not focused for biochemical sensing applications, they show the potential toward developing the fiber optic devices toward biomedical devices. For example, the first papers[184] provide the details of using a fiber optic material and its components for acousto-optic modulation applications where the mechanical fluctuations modulate the light signal and one can identify the surface changes on the fiber platform by monitoring the changes; it may also provide an insight into identify the changes when an interferometric platform is used. However, we would to like to mention again that the solutions provided are still not reported in the literature for incorporation with fiber optic interferometry, but we believe in the recent few years the technology will provide more options to diminish the external fluctuation response from the signal. We believe that the most feasible solution from above is the use of cylindrical sheath around the sensing region to make it isolated.

12. SUMMARY AND FUTURE SCOPE OF RESEARCH

To conclude, a comprehensive survey on interferometry-based fiber optic biosensors has been presented, providing fabrication methods, sensing mechanisms, and advanced structures with advantages/disadvantages. A variety of interferometric configurations such as the Mach−Zehnder interferometer (MZI), Michelson interferometer (MI), Sagnac interferometer (SI), and Fabry−Perot interferometer (FPI) are discussed fundamentally along with their biosensing applications. A brief description of generic biosensors is also provided for better understanding for the readers. In the end, a tabulated comparison of various reported optical fiber interferometry-based biosensors is done, keeping in mind their performance parameters such as sensing configuration and linear dynamic concentration ranges, along with a comparison of the detection limits. Finally, the drawbacks and advantages of several special optical fiber interferometric structures have been tabulated to predict the further needs and scope for the improvement in bioengineering field. These critical examples employing optical fiber-based biochemical sensors are demonstrating the huge potential for these sensors for the biomedical industry, clinical laboratories, online water quality monitoring, and many more. This also shows the potential for high sensitivity, response time, and biocompatibility. The high sensitivity, compact size, and applicability of online monitoring and remote sensing provide a huge advantage to these devices for biocompatibility and in vitro and in vivo monitoring of biochemical entities, in addition to the point-of-care (POC) applications for the case of Fabry−Perot configurations. However, although several investigations have been done utilizing fiber-based interferometric structures, these are still limited to the laboratory research level and still not fully developed for commercialized devices. The first reason is the fragile nature of microfiber structures that causes the huge possibility of sensor damage for a slightly higher degree of bending, even occurring due to a small fan. Hence, the efficient packaging of such a device is a little critical, but it is not impossible to resolve this problem using a specific sealing of the probe near the active regime. The second critical point is the presence of several dips obtained in the interference pattern, which happens due to interference occurring at certain wavelengths realizing various dips, the sensitivity of each dip not being the same as the effective index contrast of core, and cladding mode changes with the wavelength. In such a case, the dip wavelength corresponding to the maximum sensitivity is traced, which is to be selected wisely. The third and most problematic issue hindering the commercialization of such sensors is the integration of these devices with the microfluidic channels with the sensing channel of the optical fiber due to fiber cylindrical geometry.

Apart from the discussion on several benefits and issues with fiber optic interferometry-based sensors, we would like to put thoughts while reviewing a broad range of sensors. While talking about the performance of generic biosensors, a number of reports agree with the physical and chemical laws of naturel; however, due to a race for a high number of publications and to prove their superiority, a large number of studies also claim the false results. The reason is very clear that to claim a high-performance sensor one should always take care of all the aspects such as sensitivity, selectivity, interference study, signal broadening, temperature effects, minimum detection limits, etc., and it can be easily found that many reports do not perform all the studies and do not take care about the actual surface effects such as the number of possible molecules at the surface, numbers of unbound molecules on the surface, surface affinity, molecular transport, mass transfer, and many more.[186] Further, one issue arises from the several definitions reported for calculating parameters; for example, in case of limit of detection, there are a number of formulas available including three times of standard deviation,[187] and it can also be calculated by taking the ratio of the device resolution and the sensitivity at minimum concentration.[15] Hence for each

https://doi.org/10.1021/acsomega.3c03970
ACS Omega 2024, 9, 3037−3069

experiment, there is a possibility of different LODs which can lead to the wrong numbers. Hence each definition has certain limitations and cannot be applied to each experiment. Additionally, one more possibility is that, while calculating the LODs, researchers consider the resolution of the device from the ideal case, which also in turn to the wrong claims from the physically possible numbers.[188] Hence, we would like to conclude that researchers should always take care of the formulas and definitions according to the practical application and be advised to use the numbers obtained from the experiments without considering the ideal case. To measure the minimum detection limit of a sensing device, one should take care of a few important things using the ideal instrument as a benchmark: temperature drift and blank signal, nonspecific binding, biomolecule dynamics, mass transfer, and optical signal-to-noise ratio. Yang et al. reported a quite comprehensive study on measuring the ultralow detection limit, and more details on this can be found elsewhere.[189]

On the other hand, it is quite challenging to take care of all the experimental validations for real biosensors applied to clinical diagnosis, sometimes due to experimental facilities available and sometimes due to the fact that it is difficult to find the actual situations where the study is feasible and shows the best performance. There are several real hurdles while working with these label-free technologies such as surface plasmon resonance (SPR), localized SPR, interferometry, etc. First is the action of the sensing device in complex media, since the identification of a rare protein in the presence of hundreds of other proteins may affect the sensor result. It is hard to develop such surface chemistry that can bind only with one specific analyte without nonspecific binding. The second issue arises from the limited receptor affinity. Consider that a sensor is able to enhance the surface sensitivity but the number of molecules that can bind to the surface is limited. Therefore, even if the sensitivity of the sensor is higher one cannot improve the higher concentration to be detected, and one needs to improve the surface chemistry instead of instrumentation and methods. The next possible issue while working with the real devices to control the temperature and mechanical fluctuations in the sensing device, which is a hard challenge faced to convert these in-lab devices to commercial sensing devices. A more detailed analysis of these issues can be found elsewhere.[186,189]

Although there are several issues the technology is facing, as discussed above, exponential technological growth will surely find the solutions to these issues, and in the near future we hope for the possibility of extending these devices from the research level to compact biosensing industrial devices. In addition to these possibilities, we would to add further possible developments in the recent future. For example, in case of FPI, there are two main challenges: first is the designing the cavity in a manner such that the biosensing medium should deposit uniformly along the sensing channel inside the FP cavity, while the other issue stays with the limited size of the cavity, making it less sensitive and as well as making it more difficult to pour the sensing channel/analyte within the cavity. However, the technological developments with the sophisticated liquid input/output technique along with external auxiliary equipment can better improve the issues. Further, the advancements in the deposition methods and nanotechnology can improve the uniform deposition as well. Solving these issues, FPI-based sensors can prove themselves promising candidates in the near future for biosensing applications. In case of MZI, as we mentioned earlier, the issue corresponding to the temperature sensitivity is the big hurdle limiting its application as a commercial device. Still, a few solutions have been suggested by the researchers, such as two cascaded interferometers, but the still the complete elimination of temperature cross-sensitivity is still cannot be ignored. We hope that we can get a better solution to the issue as one of most awaited works in near future.

For the tapered interferometric configuration (microfiber), we would like to mention that the evanescent field during the tapered region plays a very important role to achieve sensing. Thus, the sensitivity of the sensor can further be improved if the shape of the tapered portion can be improved as such the more the evanescent field comes out, and one such method is to use the elliptical core. Further, integration with the microfluidic platform, low mechanical strength, and external environment sensitivity are the additional challenges, which need to be rectified. We hope that in the near future the technology will come up with a solution for these issues, since microfiber is one of the promising candidate for future biosensing. In addition to all above-mentioned challenges and the possible solution in the technology, we would like mention that despite the technology having several issues with technological problems, with a modern day solution we will sure find a way to make the interferometric platform a better candidate, since optical fiber platform provides an extra edge of advantages comparing to the conventional sensing methods in terms of in vivo sensing, compactness, increased flexibility, remote sensing, and online monitoring.

Apart from the sensing application, we also hope that the rapid growth in science and technology will lead to the use of microfiber-based techniques for quantum optics studies to uncover the light−matter interactions.[190] When the fiber diameter is reduced from microlevel to the nanoscale (termed as nanofiber), it offers unprecedented potentials for a wide range of quantum applications like tight optical mode confinement, intense evanescent fields, flexibility, low loss, unique light geometries provided through fiber modes, and diffraction-free propagation, promising improved atom−light interaction[191−194] for a variety of quantum applications.[195,196] The evanescent field associated with guided modes of these nanofiber/tapered fiber interferometers provides an intensity gradient suitable for generating an optical dipole trap.[191,194] The development of atom traps around optical nanofibers affords new avenues of research including loss-limited hybrid quantum systems.[192−194] However, there are still several competing realizations of such qubits (trapped ions, cold atoms, electrospinning, etc.), and the research community is still exploring the pros and cons of these processes for future nanofiber-based quantum systems. For example, in the case of trapped ions, atomic force interferometry is introduced, which is used to measure the weak forces by employing time-dependent spin-dependent forces.[197] In addition, an example of miniaturized cold atom interferometry is proposed by Lee et al.[198] The study successfully designed a compact and customized titanium vacuum package incorporating a tetrahedral grating magneto-optical trap (GMOT) chip using a single cooling beam. Due to the ultrafast progressing research works in this field, soon there will be studies utilizing the mechanism for various biomedical applications, including optical tweezers, molecular trapping, and single-molecule sensing.

https://doi.org/10.1021/acsomega.3c03970
ACS Omega 2024, 9, 3037−3069

■ ASSOCIATED CONTENT

Data Availability Statement

All the data is already available with corresponding references mentioned in various sections of the manuscript.

■ AUTHOR INFORMATION

Corresponding Author

Rajan Jha − *Nanophotonics and Plasmonics Laboratory, School of Basic Sciences, Indian Institute of Technology, Bhubaneswar, Odisha 752050, India;* orcid.org/0000-0003-1626-8071; Email: rjha@iitbbs.ac.in, rajaniitd@gmail.com

Authors

Pintu Gorai − *Nanophotonics and Plasmonics Laboratory, School of Basic Sciences, Indian Institute of Technology, Bhubaneswar, Odisha 752050, India*

Anand Shrivastav − *Department of Physics and Nanotechnology, SRM Institute of Science and Technology, Kattankulthar, Tamil Nadu 603203, India;* orcid.org/0000-0002-3257-2818

Anand Pathak − *School of Physics, University of Hyderabad, Hyderabad, Telangana 500046, India*

Complete contact information is available at: https://pubs.acs.org/10.1021/acsomega.3c03970

Author Contributions

P.G. wrote the manuscript. R.J. and A.M.S. revised the manuscript.

Notes

The authors declare no competing financial interest.

■ ACKNOWLEDGMENTS

R.J. would like to thank the SPARC program of MHRD, Government of India, for this collaborative work. P.G. thanks DST INSPIRE for financial support. R.J. acknowledges the support of the SERB-STAR fellowship. A.P.P. thanks the National Academy of Sciences India (NASI) for the award of the NASI Senior Scientist Platinum Jubilee Fellowship.

■ REFERENCES

(1) Jayanthi, V. S. A.; Das, A. B.; Saxena, U. Recent Advances in Biosensor Development for the Detection of Cancer Biomarkers. *Biosens. Bioelectron.* **2017**, *91*, 15−23.

(2) Wang, Y.; Zeng, S.; Humbert, G.; Ho, H. P. Microfluidic Whispering Gallery Mode Optical Sensors for Biological Applications. *Laser Photonics Rev.* **2020**, *14* (12), 1−20.

(3) Hung, P.-S.; Wang, G.-R.; Chung, W.-A.; Chiang, T.-T.; Wu, P.-W. Green Synthesis of Ni@ PEDOT and Ni@ PEDOT/Au (Core@ Shell) Inverse Opals for Simultaneous Detection of Ascorbic Acid, Dopamine, and Uric Acid. *Nanomaterials* **2020**, *10* (9), 1722.

(4) Nehru, R.; Hsu, Y.-F.; Wang, S.-F.; Dong, C.-D.; Govindasamy, M.; Habila, M. A.; AlMasoud, N. Graphene Oxide@ Ce-Doped TiO2 Nanoparticles as Electrocatalyst Materials for Voltammetric Detection of Hazardous Methyl Parathion. *Microchim. Acta* **2021**, *188* (6), 216.

(5) Bhargava, A.; Bansal, A. Novel Coronavirus (COVID-19) Diagnosis Using Computer Vision and Artificial Intelligence Techniques: A Review. *Multimed. Tools Appl.* **2021**, *80* (13), 19931−19946.

(6) Taha, B. A.; Al Mashhadany, Y.; Hafiz Mokhtar, M. H.; Dzulkefly Bin Zan, M. S.; Arsad, N. An Analysis Review of Detection Coronavirus Disease 2019 (COVID-19) Based on Biosensor Application. *Sensors* **2020**, *20* (23), 6764.

(7) Shrivastav, A. M.; Mishra, S. K.; Gupta, B. D. Fiber Optic SPR Sensor for the Detection of Melamine Using Molecular Imprinting. *Sensors Actuators B Chem.* **2015**, *212*, 404−410.

(8) Song, Y.; Xu, M.; Li, Z.; He, L.; Hu, M.; He, L.; Zhang, Z.; Du, M. Ultrasensitive Detection of Bisphenol A under Diverse Environments with an Electrochemical Aptasensor Based on Multicomponent AgMo Heteronanostructure. *Sensors Actuators B Chem.* **2020**, *321*, 128527.

(9) Zhou, W.; Hu, K.; Kwee, S.; Tang, L.; Wang, Z.; Xia, J.; Li, X. Gold Nanoparticle Aggregation-Induced Quantitative Photothermal Biosensing Using a Thermometer: A Simple and Universal Biosensing Platform. *Anal. Chem.* **2020**, *92* (3), 2739−2747.

(10) Mészáros, G.; Akbarzadeh, S.; De La Franier, B.; Keresztes, Z.; Thompson, M. Advances in Electromagnetic Piezoelectric Acoustic Sensor Technology for Biosensor-Based Detection. *Chemosensors* **2021**, *9* (3), 58.

(11) Hu, Z.; Zhou, X.; Duan, J.; Wu, X.; Wu, J.; Zhang, P.; Liang, W.; Guo, J.; Cai, H.; Sun, P.; et al. Aptamer-Based Novel Ag-Coated Magnetic Recognition and SERS Nanotags with Interior Nanogap Biosensor for Ultrasensitive Detection of Protein Biomarker. *Sensors Actuators B Chem.* **2021**, *334*, 129640.

(12) Srinivasan, R.; Umesh, S.; Murali, S.; Asokan, S.; Siva Gorthi, S. Bare Fiber Bragg Grating Immunosensor for Real-time Detection of Escherichia Coli Bacteria. *J. Biophotonics* **2017**, *10* (2), 224−230.

(13) Quero, G.; Consales, M.; Severino, R.; Vaiano, P.; Boniello, A.; Sandomenico, A.; Ruvo, M.; Borriello, A.; Diodato, L.; Zuppolini, S.; et al. Long Period Fiber Grating Nano-Optrode for Cancer Biomarker Detection. *Biosens. Bioelectron.* **2016**, *80*, 590−600.

(14) Khalil, I.; Yehye, W. A.; Julkapli, N. M.; Sina, A. A. I.; Rahmati, S.; Basirun, W. J.; Seyfoddin, A. Dual Platform Based Sandwich Assay Surface-Enhanced Raman Scattering DNA Biosensor for the Sensitive Detection of Food Adulteration. *Analyst* **2020**, *145* (4), 1414−1426.

(15) Gupta, B. D.; Shrivastav, A. M.; Usha, S. P. Surface Plasmon Resonance-Based Fiber Optic Sensors Utilizing Molecular Imprinting. *Sensors* **2016**, *16* (9), 1381.

(16) Xu, Y.; Xiong, M.; Yan, H. A Portable Optical Fiber Biosensor for the Detection of Zearalenone Based on the Localized Surface Plasmon Resonance. *Sensors Actuators B Chem.* **2021**, *336*, 129752.

(17) Li, X.; Chen, N.; Zhou, X.; Gong, P.; Wang, S.; Zhang, Y.; Zhao, Y. A Review of Specialty Fiber Biosensors Based on Interferometer Configuration. *J. Biophotonics* **2021**, *14*, No. e202100068.

(18) Riza, M. A.; Go, Y. I.; Harun, S. W.; Maier, R. R. J. FBG Sensors for Environmental and Biochemical Applications—A Review. *IEEE Sens. J.* **2020**, *20* (14), 7614−7627.

(19) Balbinot, S.; Srivastav, A. M.; Vidic, J.; Abdulhalim, I.; Manzano, M. Plasmonic Biosensors for Food Control. *Trends Food Sci. Technol.* **2021**, *111*, 128−140.

(20) Ambartsumyan, O.; Gribanyov, D.; Kukushkin, V.; Kopylov, A.; Zavyalova, E. SERS-Based Biosensors for Virus Determination with Oligonucleotides as Recognition Elements. *Int. J. Mol. Sci.* **2020**, *21* (9), 3373.

(21) Wang, X.; Wolfbeis, O. S. Fiber-Optic Chemical Sensors and Biosensors (2015−2019). *Anal. Chem.* **2020**, *92* (1), 397−430.

(22) Li, L.; Zhang, Y.; Zhou, Y.; Zheng, W.; Sun, Y.; Ma, G.; Zhao, Y. Optical Fiber Optofluidic Bio-chemical Sensors: A Review. *Laser Photon. Rev.* **2021**, *15* (7), 2000526.

(23) Barsan, M. M.; Diculescu, V. C. An Antibody-Based Amperometric Biosensor for 20S Proteasome Activity and Inhibitor Screening. *Analyst* **2021**, *146* (10), 3216−3224.

(24) Hianik, T. Advances in Electrochemical and Acoustic Aptamer-Based Biosensors and Immunosensors in Diagnostics of Leukemia. *Biosensors* **2021**, *11* (6), 177.

(25) Quintanilla-Villanueva, G. E.; Luna-Moreno, D.; Blanco-Gámez, E. A.; Rodríguez-Delgado, J. M.; Villarreal-Chiu, J. F.; Rodríguez-Delgado, M. M. A Novel Enzyme-Based SPR Strategy for Detection of the Antimicrobial Agent Chlorophene. *Biosensors* **2021**, *11* (2), 43.

(26) Kim, D.; Han, S.; Ji, Y.; Youn, H.; Kim, H.; Ko, O.; Lee, J. B. RNA Polymerization Actuating Nucleic Acid Membrane (RANAM)-Based Biosensing for Universal RNA Virus Detection. *Biosens. Bioelectron.* **2022**, *199*, 113880.
(27) Ndunda, E. N. Molecularly Imprinted Polymers—A Closer Look at the Control Polymer Used in Determining the Imprinting Effect: A Mini Review. *J. Mol. Recognit.* **2020**, *33* (11), No. e2855.
(28) Lee, B. H.; Kim, Y. H.; Park, K. S.; Eom, J. B.; Kim, M. J.; Rho, B. S.; Choi, H. Y. Interferometric Fiber Optic Sensors. *sensors* **2012**, *12* (3), 2467−2486.
(29) Zhao, K.; Veksha, A.; Ge, L.; Lisak, G. Near Real-Time Analysis of Para-Cresol in Wastewater with a Laccase-Carbon Nanotube-Based Biosensor. *Chemosphere* **2021**, *269*, 128699.
(30) Nayak, J. K.; Parhi, P.; Jha, R. Graphene Oxide Encapsulated Gold Nanoparticle Based Stable Fibre Optic Sucrose Sensor. *Sensors Actuators B Chem.* **2015**, *221*, 835−841.
(31) Hua, Z.; Yu, T.; Liu, D.; Xianyu, Y. Recent Advances in Gold Nanoparticles-Based Biosensors for Food Safety Detection. *Biosens. Bioelectron.* **2021**, *179*, 113076.
(32) Kamaci, U. D.; Kamaci, M. Selective and Sensitive ZnO Quantum Dots Based Fluorescent Biosensor for Detection of Cysteine. *J. Fluoresc.* **2021**, *31* (2), 401−414.
(33) Iannazzo, D.; Espro, C.; Celesti, C.; Ferlazzo, A.; Neri, G. Smart Biosensors for Cancer Diagnosis Based on Graphene Quantum Dots. *Cancers (Basel).* **2021**, *13* (13), 3194.
(34) Dilgin, Y.; Karakaya, S.; Dilgin, D. G. Quantum Dots-Based Photoelectrochemical Sensors and Biosensors. In *Electroanalytical Applications of Quantum Dot-Based Biosensors*; Uslu, B., Ed.; Elsevier, 2021; pp 209−269.
(35) Wen, Z.; Guan, Z.; Dong, J.; Li, H.; Cai, Y.; Gao, S. A Review of Sensitivity Enhancement in Interferometer-Based Fiber Sensors. *Sensors* **2022**, *22* (7), 2506.
(36) Tekinay, M.; Sylvester, T.; Brunton, M.; Ganesh, T. Applications of Fiber Optic Sensors in Traffic Monitoring: A Review. *Integrated Roadways* **2022**, DOI: 10.13140/RG.2.2.28700.77447.
(37) Pathak, A. K.; Viphavakit, C. A Review on All-Optical Fiber-Based VOC Sensors: Heading Towards the Development of Promising Technology. *Sensors Actuators A Phys.* **2022**, *338*, 113455.
(38) Kirsch, J.; Siltanen, C.; Zhou, Q.; Revzin, A.; Simonian, A. Biosensor Technology: Recent Advances in Threat Agent Detection and Medicine. *Chem. Soc. Rev.* **2013**, *42* (22), 8733−8768.
(39) Tuerk, C.; Gold, L. Systematic Evolution of Ligands by Exponential Enrichment: RNA Ligands to Bacteriophage T4 DNA Polymerase. *Science (80-.).* **1990**, *249* (4968), 505−510.
(40) Majdinasab, M.; Hayat, A.; Marty, J. L. Aptamer-Based Assays and Aptasensors for Detection of Pathogenic Bacteria in Food Samples. *TrAC Trends Anal. Chem.* **2018**, *107*, 60−77.
(41) Dehghani, S.; Nosrati, R.; Yousefi, M.; Nezami, A.; Soltani, F.; Taghdisi, S. M.; Abnous, K.; Alibolandi, M.; Ramezani, M. Aptamer-Based Biosensors and Nanosensors for the Detection of Vascular Endothelial Growth Factor (VEGF): A Review. *Biosens. Bioelectron.* **2018**, *110*, 23−37.
(42) Ferri, S.; Kojima, K.; Sode, K. Review of Glucose Oxidases and Glucose Dehydrogenases: A Bird's Eye View of Glucose Sensing Enzymes. *J. Diabetes Sci. Technol.* **2011**, *5* (5), 1068−1076.
(43) Wang, S.; Chen, S.; Shang, K.; Gao, X.; Wang, X. Sensitive Electrochemical Detection of Cholesterol Using a Portable Paper Sensor Based on the Synergistic Effect of Cholesterol Oxidase and Nanoporous Gold. *Int. J. Biol. Macromol.* **2021**, *189*, 356−362.
(44) Rienda, B.; Elexpe, A.; Tolentino-Cortez, T.; Gulak, M.; Bruzos-Cidón, C.; Torrecilla, M.; Astigarraga, E.; Barreda-Gómez, G. Analysis of Acetylcholinesterase Activity in Cell Membrane Microarrays of Brain Areas as a Screening Tool to Identify Tissue Specific Inhibitors. *Analytica* **2021**, *2* (1), 25−36.
(45) Usha, S. P.; Shrivastav, A. M.; Gupta, B. D. FO-SPR Based Dextrose Sensor Using Ag/ZnO Nanorods/GOx for Insulinoma Detection. *Biosens. Bioelectron.* **2016**, *85*, 986−995.
(46) Gupta, B. D.; Shrivastav, A. M.; Usha, S. P. *Optical Sensors for Biomedical Diagnostics and Environmental Monitoring*; CRC Press: Boca Raton, FL, 2017.
(47) Wang, Y.; Liu, X.; Chen, C.; Chen, Y.; Li, Y.; Ye, H.; Wang, B.; Chen, H.; Guo, J.; Ma, X. Magnetic Nanorobots as Maneuverable Immunoassay Probes for Automated and Efficient Enzyme Linked Immunosorbent Assay. *ACS Nano* **2022**, *16*, 180.
(48) Puttananjegowda, K.; Takshi, A.; Thomas, S. Silicon Carbide Nanoparticles Electrospun Nanofibrous Enzymatic Glucose Sensor. *Biosens. Bioelectron.* **2021**, *186*, 113285.
(49) Briones, M.; Casero, E.; Vázquez, L.; Pariente, F.; Lorenzo, E.; Petit-Domínguez, M. D. Diamond Nanoparticles as a Way to Improve Electron Transfer in Sol-Gel l-Lactate Biosensing Platforms. *Anal. Chim. Acta* **2016**, *908*, 141−149.
(50) Semwal, V.; Shrivastav, A. M.; Verma, R.; Gupta, B. D. Surface Plasmon Resonance Based Fiber Optic Ethanol Sensor Using Layers of Silver/Silicon/Hydrogel Entrapped with ADH/NAD. *Sensors Actuators B Chem.* **2016**, *230*, 485−492.
(51) Gupta, B. D.; Pathak, A.; Shrivastav, A. M. Optical Biomedical Diagnostics Using Lab-on-Fiber Technology: A Review. *Photonics* **2022**, *9*, 86.
(52) Zheng, S.; Kim, D.-K.; Park, T. J.; Lee, S. J.; Lee, S. Y. Label-Free Optical Diagnosis of Hepatitis B Virus with Genetically Engineered Fusion Proteins. *Talanta* **2010**, *82* (2), 803−809.
(53) Altintas, Z.; Gittens, M.; Guerreiro, A.; Thompson, K.-A.; Walker, J.; Piletsky, S.; Tothill, I. E. Detection of Waterborne Viruses Using High Affinity Molecularly Imprinted Polymers. *Anal. Chem.* **2015**, *87* (13), 6801−6807.
(54) Ponzo, I.; Möller, F. M.; Daub, H.; Matscheko, N. A DNA-Based Biosensor Assay for the Kinetic Characterization of Ion-Dependent Aptamer Folding and Protein Binding. *Molecules* **2019**, *24* (16), 2877.
(55) Shen, L.; Wang, P.; Ke, Y. DNA Nanotechnology-Based Biosensors and Therapeutics. *Adv. Healthc. Mater.* **2021**, *10* (15), 2002205.
(56) Hua, Y.; Ma, J.; Li, D.; Wang, R. DNA-Based Biosensors for the Biochemical Analysis: A Review. *Biosensors* **2022**, *12* (3), 183.
(57) Khan, S.; Le Calvé, S.; Newport, D. A Review of Optical Interferometry Techniques for VOC Detection. *Sensors Actuators A Phys.* **2020**, *302*, 111782.
(58) Miliou, A. In-Fiber Interferometric-Based Sensors: Overview and Recent Advances. *Photonics* **2021**, *8*, 265.
(59) Murphy, R. P.; James, S. W.; Tatam, R. P. Multiplexing of Fiber-Optic Long-Period Grating-Based Interferometric Sensors. *J. Light. Technol.* **2007**, *25* (3), 825−829.
(60) Wang, B.-T.; Wang, Q. An Interferometric Optical Fiber Biosensor with High Sensitivity for IgG/Anti-IgG Immunosensing. *Opt. Commun.* **2018**, *426*, 388−394.
(61) Xia, F.; Zhao, Y. RI Sensing System with High Sensitivity and Large Measurement Range Using a Microfiber MZI and a Photonic Crystal Fiber MZI. *Measurement* **2020**, *156*, 107603.
(62) Azmi, A. I.; Abdullah, A. S.; Mohd Noor, M. Y.; Mohd Supa'at, A. S.; Kassim, N. M.; Ngajikin, N. H. Intensity-modulated Temperature Sensor Based on Fiber Interferometer with Optical Bandpass Filtering. *Microw. Opt. Technol. Lett.* **2016**, *58* (6), 1458−1462.
(63) Yu, F.; Xu, B.; Zhang, Y.; Wang, D. Fiber Ring Laser Based on SMF-TCF-SMF Structure for Strain and Refractive Index Sensing. *Opt. Eng.* **2017**, *56* (12), 126105.
(64) Talataisong, W.; Ismaeel, R.; Brambilla, G. A Review of Microfiber-Based Temperature Sensors. *Sensors* **2018**, *18* (2), 461.
(65) Dass, S.; Jha, R. Square Knot Resonator-Based Compact Bending Sensor. *Ieee Photonics Technol. Lett.* **2018**, *30* (18), 1649−1652.
(66) Kumar, A.; Sahu, S.; Jha, R. Small Angles Vector Magnetometer Based on Anisotropic Ferromagnetic Nanofluid Functionalized Fiber Interferometer. *J. Phys. D. Appl. Phys.* **2022**, *55* (40), 405102.
(67) Dong, S.; Pu, S.; Wang, H. Magnetic Field Sensing Based on Magnetic-Fluid-Clad Fiber-Optic Structure with Taper-like and

Lateral-Offset Fusion Splicing. *Opt. Express* **2014**, *22* (16), 19108−19116.
(68) Vitullo, D. L. P.; Gardosi, G.; Zaki, S.; Tokmakov, K. V.; Brodsky, M.; Sumetsky, M. Discovery of Parabolic Microresonators Produced via Fiber Tapering. *Opt. Lett.* **2018**, *43* (20), 4977−4980.
(69) Kaur, M.; Hohert, G.; Lane, P. M.; Menon, C. Fabrication of a Stepped Optical Fiber Tip for Miniaturized Scanners. *Opt. Fiber Technol.* **2021**, *61*, 102436.
(70) Dass, S.; Jha, R. Tapered Fiber Attached Nitrile Diaphragm-Based Acoustic Sensor. *J. Light. Technol.* **2017**, *35* (24), 5411−5417.
(71) Lee, D.; Lee, K. J.; Kim, J.-H.; Park, K.; Lee, D.; Kim, Y.-H.; Shin, H. Fabrication Method for Ultra-Long Optical Micro/Nano-Fibers. *Curr. Appl. Phys.* **2019**, *19* (12), 1334−1337.
(72) Huang, Y.; Tian, Z.; Sun, L.-P.; Sun, D.; Li, J.; Ran, Y.; Guan, B.-O. High-Sensitivity DNA Biosensor Based on Optical Fiber Taper Interferometer Coated with Conjugated Polymer Tentacle. *Opt. Express* **2015**, *23* (21), 26962−26968.
(73) Song, B.; Zhang, H.; Liu, B.; Lin, W.; Wu, J. Label-Free in-Situ Real-Time DNA Hybridization Kinetics Detection Employing Microfiber-Assisted Mach-Zehnder Interferometer. *Biosens. Bioelectron.* **2016**, *81*, 151−158.
(74) Ding, M.; Huang, Y.; Guo, T.; Sun, L.-P.; Guan, B.-O. Mesoporous Nanospheres Functionalized Optical Microfiber Biosensor for Low Concentration Neurotransmitter Detection. *Opt. Express* **2016**, *24* (24), 27152−27159.
(75) Huang, Y.; Yu, B.; Guo, T.; Guan, B.-O. Ultrasensitive and in Situ DNA Detection in Various PH Environments Based on a Microfiber with a Graphene Oxide Linking Layer. *RSC Adv.* **2017**, *7* (22), 13177−13183.
(76) Huang, Y.; Ding, M.; Guo, T.; Zhang, N.; Tian, Z.; Sun, L.-P.; Guan, B.-O. Ultrasensitive and Label-Free Detection of γ-Aminobutyric Acid Using Fiber-Optic Interferometric Sensors Functionalized with Size-Selective Molecular Sieve Arrays. *Sensors Actuators B Chem.* **2017**, *244*, 934−940.
(77) Zhou, J.; Huang, Y.; Chen, C.; Xiao, A.; Guo, T.; Guan, B.-O. Improved Detection Sensitivity of γ-Aminobutyric Acid Based on Graphene Oxide Interface on an Optical Microfiber. *Phys. Chem. Chem. Phys.* **2018**, *20* (20), 14117−14123.
(78) Li, Z.; Liao, C.; Chen, D.; Song, J.; Jin, W.; Peng, G.-D.; Zhu, F.; Wang, Y.; He, J.; Wang, Y. Label-Free Detection of Bovine Serum Albumin Based on an in-Fiber Mach-Zehnder Interferometric Biosensor. *Opt. Express* **2017**, *25* (15), 17105−17113.
(79) Arjmand, M.; Saghafifar, H.; Alijanianzadeh, M.; Soltanolkotabi, M. A Sensitive Tapered-Fiber Optic Biosensor for the Label-Free Detection of Organophosphate Pesticides. *Sensors Actuators, B Chem.* **2017**, *249*, 523−532.
(80) Liang, L.; Jin, L.; Ran, Y.; Sun, L.-P.; Guan, B.-O. Interferometric Detection of MicroRNAs Using a Capillary Optofluidic Sensor. *Sensors Actuators B Chem.* **2017**, *242*, 999−1006.
(81) Zainuddin, N. H.; Chee, H. Y.; Ahmad, M. Z.; Mahdi, M. A.; Abu Bakar, M. H.; Yaacob, M. H. Sensitive Leptospira DNA Detection Using Tapered Optical Fiber Sensor. *J. Biophotonics* **2018**, *11* (8), No. e201700363.
(82) Li, Y.; Ma, H.; Gan, L.; Gong, A.; Zhang, H.; Liu, D.; Sun, Q. Selective and Sensitive Escherichia Coli Detection Based on a T4 Bacteriophage-immobilized Multimode Microfiber. *J. Biophotonics* **2018**, *11* (9), No. e201800012.
(83) Shrivastav, A. M.; Sharma, G.; Jha, R. Hypersensitive and Selective Biosensing Based on Microfiber Interferometry and Molecular Imprinted Nanoparticles. *Biosens. Bioelectron.* **2019**, *141*, 111347.
(84) Guan, B.-O.; Huang, Y. Interface Sensitized Optical Microfiber Biosensors. *J. Light. Technol.* **2019**, *37* (11), 2616−2622.
(85) Hu, J.; Fu, D.; Xia, C.; Long, S.; Lu, C.; Sun, W.; Liu, Y. Fiber Mach-Zehnder-Interferometer-Based Liquid Crystal Biosensor for Detecting Enzymatic Reactions of Penicillinase. *Appl. Opt.* **2019**, *58* (17), 4806−4811.
(86) Chen, L.; Liu, B.; Liu, J.; Wan, S.-P.; Wu, T.; Yuan, J.; Zhou, X.; Long, K.; Shao, L.; Fu, Y. Q.; et al. Novel Microfiber Sensor and Its Biosensing Application for Detection of HCG Based on a Single-mode-Tapered Hollow Core-Singlemode Fiber Structure. *IEEE Sens. J.* **2020**, *20* (16), 9071−9078.
(87) Yin, M.; Wu, C.; Shao, L.; Chan, W. K. E.; Zhang, A. P.; Lu, C.; Tam, H. Label-Free, Disposable Fiber-Optic Biosensors for DNA Hybridization Detection. *Analyst* **2013**, *138* (7), 1988−1994.
(88) Yu, W.; Lang, T.; Bian, J.; Kong, W. Label-Free Fiber Optic Biosensor Based on Thin-Core Modal Interferometer. *Sensors Actuators B Chem.* **2016**, *228*, 322−329.
(89) Zheng, Y.; Lang, T.; Shen, T.; Shen, C. Simple Immunoglobulin G Sensor Based on Thin Core Single-Mode Fiber. *Opt. Fiber Technol.* **2018**, *41*, 104−108.
(90) Zhang, X.; Liu, B.; Zhang, H.; Zhang, X.; Song, B.; Wu, J.; Duan, S. Label-Free Detection of DNA Hybridization Utilizing Dual S-Tapered Thin-Core Fiber Interferometer. *J. Light. Technol.* **2019**, *37* (11), 2762−2767.
(91) Zhang, T.; Pang, F.; Liu, H.; Cheng, J.; Lv, L.; Zhang, X.; Chen, N.; Wang, T. A Fiber-Optic Sensor for Acoustic Emission Detection in a High Voltage Cable System. *Sensors* **2016**, *16* (12), 2026.
(92) Wang, J.; Liu, B.; Wu, Y.; Mao, Y.; Zhao, L.; Sun, T.; Nan, T. A Novel Fiber In-Line Michelson Interferometer Based on End Face Packaging for Temperature and Refractive Index Measurement. *Optik (Stuttg).* **2019**, *194*, 163094.
(93) Shao, M.; Zhang, R.; Zhao, X.; Zhang, W.; Lu, Q.; Qiao, X. Dual-Core Fiber Based in-Line Michelson Interferometer for Humidity Sensing. *Opt. Fiber Technol.* **2021**, *64*, 102570.
(94) Liu, Y.; Wang, D. N. Fiber In-Line Michelson Interferometer Based on Inclined Narrow Slit Crossing the Fiber Core. *IEEE Photonics Technol. Lett.* **2018**, *30* (3), 293−296.
(95) Li, Y.; Ma, H.; Gan, L.; Liu, Q.; Yan, Z.; Liu, D.; Sun, Q. Immobilized Optical Fiber Microprobe for Selective and High Sensitive Glucose Detection. *Sensors Actuators B Chem.* **2018**, *255*, 3004−3010.
(96) Gao, R.; Lu, D.-F.; Cheng, J.; Jiang, Y.; Jiang, L.; Xu, J.-D.; Qi, Z.-M. Fiber Optofluidic Biosensor for the Label-Free Detection of DNA Hybridization and Methylation Based on an in-Line Tunable Mode Coupler. *Biosens. Bioelectron.* **2016**, *86*, 321−329.
(97) Sandhu, P.; Yang, J.; Xu, C.-Q. In-Fiber Michelson Interferometer with Polymeric/Nanoparticle Thin-Film Overlay as a Platform for Biosensing. *IEEE J. Sel. Top. Quantum Electron.* **2010**, *16* (3), 685−690.
(98) Zhang, C.; Ning, T.; Li, J.; Zheng, J.; Gao, X.; Lin, H.; Pei, L. Etching Twin Core Fiber for the Temperature-Independent Refractive Index Sensing. *J. Opt.* **2018**, *20* (4), 045802.
(99) Wysokiński, K.; Budnicki, D.; Fidelus, J.; Szostkiewicz, Ł.; Ostrowski, Ł.; Murawski, M.; Staniszewski, M.; Staniszewska, M.; Napierała, M.; Nasiłowski, T. Dual-Core All-Fiber Integrated Immunosensor for Detection of Protein Antigens. *Biosens. Bioelectron.* **2018**, *114*, 22−29.
(100) Culshaw, B. The Optical Fibre Sagnac Interferometer: An Overview of Its Principles and Applications. *Meas. Sci. Technol.* **2006**, *17* (1), R1.
(101) Gao, S.; Sun, L.-P.; Li, J.; Jin, L.; Ran, Y.; Huang, Y.; Guan, B.-O. High-Sensitivity DNA Biosensor Based on Microfiber Sagnac Interferometer. *Opt. Express* **2017**, *25* (12), 13305−13313.
(102) Wang, X.-Z.; Wang, Q. A High-Birefringence Microfiber Sagnac-Interferometer Biosensor Based on the Vernier Effect. *Sensors* **2018**, *18* (12), 4114.
(103) An, G.; Li, S.; An, Y.; Wang, H.; Zhang, X. Glucose Sensor Realized with Photonic Crystal Fiber-Based Sagnac Interferometer. *Opt. Commun.* **2017**, *405*, 143−146.
(104) Li, X.; Nguyen, L. V.; Zhao, Y.; Ebendorff-Heidepriem, H.; Warren-Smith, S. C. High-Sensitivity Sagnac-Interferometer Biosensor Based on Exposed Core Microstructured Optical Fiber. *Sensors Actuators B Chem.* **2018**, *269*, 103−109.
(105) Warren-Smith, S. C.; Kostecki, R.; Nguyen, L. V.; Monro, T. M. Fabrication, Splicing, Bragg Grating Writing, and Polyelectrolyte Functionalization of Exposed-Core Microstructured Optical Fibers. *Opt. Express* **2014**, *22* (24), 29493−29504.

https://doi.org/10.1021/acsomega.3c03970
ACS Omega 2024, 9, 3037−3069

(106) Elster, J. L.; Jones, M. E.; Evans, M. K.; Lenahan, S. M.; Boyce, C. A.; Velander, W. H.; VanTassell, R. Optical Fiber Extrinsic Fabry-Perot Interferometric (EFPI)-Based Biosensors. *Proc. SPIE* **2000**, *3911*, 105−112.
(107) Islam, M. R.; Ali, M. M.; Lai, M. H.; Lim, K. S.; Ahmad, H. Chronology of Fabry-Perot Interferometer Fiber-Optic Sensors and Their Applications: A Review. *Sensors (Switzerland)* **2014**, *14* (4), 7451−7488.
(108) Zhang, Y.; Huang, J.; Lan, X.; Yuan, L.; Xiao, H. Simultaneous Measurement of Temperature and Pressure with Cascaded Extrinsic Fabry-Perot Interferometer and Intrinsic Fabry-Perot Interferometer Sensors. *Opt. Eng.* **2014**, *53* (6), 067101.
(109) Dash, J. N.; Jha, R. Fabry-Perot Cavity on Demand for Hysteresis Free Interferometric Sensors. *J. Light. Technol.* **2016**, *34* (13), 3188−3193.
(110) Ma, W.; Jiang, Y.; Hu, J.; Jiang, L.; Zhang, T.; Zhang, T. Microelectromechanical System-Based, High-Finesse, Optical Fiber Fabry-Perot Interferometric Pressure Sensors. *Sensors Actuators A Phys.* **2020**, *302*, 111795.
(111) Ran, Z.; Rao, Y.; Zhang, J.; Liu, Z.; Xu, B. A Miniature Fiber-Optic Refractive-Index Sensor Based on Laser-Machined Fabry-Perot Interferometer Tip. *J. Light. Technol.* **2009**, *27* (23), 5426−5429.
(112) Liao, C. R.; Hu, T. Y.; Wang, D. N. Optical Fiber Fabry-Perot Interferometer Cavity Fabricated by Femtosecond Laser Micromachining and Fusion Splicing for Refractive Index Sensing. *Opt. Express* **2012**, *20* (20), 22813−22818.
(113) Wang, M.; Yang, M.; Cheng, J.; Zhang, G.; Liao, C. R.; Wang, D. N. Fabry-Perot Interferometer Sensor Fabricated by Femtosecond Laser for Hydrogen Sensing. *IEEE Photonics Technol. Lett.* **2013**, *25* (8), 713−716.
(114) Chen, S.-H.; Dai, Y.-T.; Xiao, X.; Ding, L.-Y. Investigation on Laser Polishing of GaN Film Using Deep Ultraviolet Laser. *Laser Technol.* **2012**, *36* (1), 13−15.
(115) Luo, J.; Liu, S.; Chen, P.; Lu, S.; Zhang, Q.; Chen, Y.; Du, B.; Tang, J.; He, J.; Liao, C.; et al. Fiber Optic Hydrogen Sensor Based on a Fabry-Perot Interferometer with a Fiber Bragg Grating and a Nanofilm. *Lab Chip* **2021**, *21* (9), 1752−1758.
(116) Yoshino, T.; Sano, Y.; Ota, D.; Fujita, K.; Ikui, T. Fiber-Bragg-Grating Based Single Axial Mode Fabry-Perot Interferometer and Its Strain and Acceleration Sensing Applications. *J. Light. Technol.* **2016**, *34* (9), 2241−2250.
(117) Jiang, Y.; Yang, D.; Yuan, Y.; Xu, J.; Li, D.; Zhao, J. Strain and High-Temperature Discrimination Using a Type II Fiber Bragg Grating and a Miniature Fiber Fabry-Perot Interferometer. *Appl. Opt.* **2016**, *55* (23), 6341−6345.
(118) Peng, J.; Qu, Y.; Wang, W.; Sun, T.; Yang, M. Thin-Film-Based Optical Fiber Fabry-Perot Interferometer Used for Humidity Sensing. *Appl. Opt.* **2018**, *57* (12), 2967−2972.
(119) Su, D.; Qiao, X.; Rong, Q.; Sun, H.; Zhang, J.; Bai, Z.; Du, Y.; Feng, D.; Wang, Y.; Hu, M.; et al. A Fiber Fabry-Perot Interferometer Based on a PVA Coating for Humidity Measurement. *Opt. Commun.* **2013**, *311*, 107−110.
(120) Abbas, L. G.; Mumtaz, F.; Dai, Y.; Zhou, A.; Hu, W.; Ashraf, M. A. Highly Sensitive Polymer Based Fabry-Perot Interferometer for Temperature Sensing. *Prog. Electromagn. Res. Lett.* **2021**, *97*, 87−94.
(121) Warren-Smith, S. C.; André, R. M.; Dellith, J.; Eschrich, T.; Becker, M.; Bartelt, H. Sensing with Ultra-Short Fabry-Perot Cavities Written into Optical Micro-Fibers. *Sensors Actuators, B Chem.* **2017**, *244*, 1016−1021.
(122) Khan, M. R. R.; Watekar, A. V.; Kang, S.-W. Fiber-Optic Biosensor to Detect PH and Glucose. *IEEE Sens. J.* **2018**, *18* (4), 1528−1538.
(123) Wu, C.; Liu, Z.; Zhang, A. P.; Guan, B.-O.; Tam, H.-Y. In-Line Open-Cavity Fabry-Pérot Interferometer Formed by C-Shaped Fiber Fortemperature-Insensitive Refractive Index Sensing. *Opt. Express* **2014**, *22* (18), 21757−21766.
(124) Xie, L.; Nguyen, L. V.; Ebendorff-Heidepriem, H.; Warren-Smith, S. Multiplexed Optical Fiber Biochemical Sensing Using Cascaded C-Shaped Fabry-Perot Interferometers. *IEEE Sens. J.* **2019**, *19* (22), 10425−10431.
(125) Li, X.; Nguyen, L. V.; Hill, K.; Ebendorff-Heidepriem, H.; Schartner, E. P.; Zhao, Y.; Zhou, X.; Zhang, Y.; Warren-Smith, S. C. All-Fiber All-Optical Quantitative Polymerase Chain Reaction (QPCR). *Sensors Actuators B Chem.* **2020**, *323*, 128681.
(126) Zhang, Y.; Shibru, H.; Cooper, K. L.; Wang, A. Miniature Fiber-Optic Multicavity Fabry-Perot Interferometric Biosensor. *Opt. Lett.* **2005**, *30* (9), 1021−1023.
(127) Chen, L. H.; Chan, C. C.; Menon, R.; Balamurali, P.; Wong, W. C.; Ang, X. M.; Hu, P. B.; Shaillender, M.; Neu, B.; Zu, P.; et al. Fabry-Perot Fiber-Optic Immunosensor Based on Suspended Layer-by-Layer (Chitosan/Polystyrene Sulfonate) Membrane. *Sensors Actuators B Chem.* **2013**, *188*, 185−192.
(128) Liu, X.; Jiang, M.; Sui, Q.; Luo, S.; Geng, X. Optical Fiber Fabry-Perot Interferometer for Microorganism Growth Detection. *Opt. Fiber Technol.* **2016**, *30*, 32−37.
(129) Concepcion, J.; Witte, K.; Wartchow, C.; Choo, S.; Yao, D.; Persson, H.; Wei, J.; Li, P.; Heidecker, B.; Ma, W.; et al. Label-Free Detection of Biomolecular Interactions Using BioLayer Interferometry for Kinetic Characterization. *Comb. Chem. High Throughput Screen.* **2009**, *12* (8), 791−800.
(130) Kumaraswamy, S.; Tobias, R. Label-Free Kinetic Analysis of an Antibody-Antigen Interaction Using Biolayer Interferometry. In *Protein-Protein Interactions*; Meyerkord, C. L., Fu, H., Eds.; Springer, 2015; pp 165−182.
(131) Sultana, A.; Lee, J. E. Measuring Protein-protein and Protein-nucleic Acid Interactions by Biolayer Interferometry. *Curr. Protoc. Protein Sci.* **2015**, *79*, 19.25.1−19.25.26.
(132) Müller-Esparza, H.; Osorio-Valeriano, M.; Steube, N.; Thanbichler, M.; Randau, L. Bio-Layer Interferometry Analysis of the Target Binding Activity of CRISPR-Cas Effector Complexes. *Front. Mol. Biosci.* **2020**, *7*, 98.
(133) Ott, W.; Durner, E.; Gaub, H. E. Enzyme-Mediated, Site-Specific Protein Coupling Strategies for Surface-Based Binding Assays. *Angew. Chem.* **2018**, *130* (39), 12848−12851.
(134) Ziu, I.; Laryea, E. T.; Alashkar, F.; Wu, C. G.; Martic, S. A Dip-and-Read Optical Aptasensor for Detection of Tau Protein. *Anal. Bioanal. Chem.* **2020**, *412* (5), 1193−1201.
(135) Yang, M.; Zhang, H.; Yao, Y.; Lin, W.; Duan, S.; Liu, B. Characterization of Light-Sensitive Refractive Indices for Ionic Liquids Based on a Coreless-Fiber-Coupled Microcavity Interferometric Sensor. *IEEE Sens. J.* **2023**, *23* (13), 14142−14152.
(136) Chen, J.; Xiong, Y.; Xu, F.; Lu, Y. Silica Optical Fiber Integrated with Two-Dimensional Materials: Towards Opto-Electro-Mechanical Technology. *Light Sci. Appl.* **2021**, *10* (1), 78.
(137) Hulanicki, A.; Glab, S.; Ingman, F. Chemical Sensors: Definitions and Classification. *Pure Appl. Chem.* **1991**, *63* (9), 1247−1250.
(138) Gorai, P.; Jha, R. Artificial Receptor-Based Optical Sensors (AROS): Ultra-Sensitive Detection of Urea. *Adv. Photonics Res.* **2021**, *2* (8), 2100044.
(139) Bi, M.; Miao, Y.; Li, W.; Fei, C.; Zhang, K. Ultrasensitive BOD Detection of Fiber Integrated with Nb 2 CT X MXene for Water Pollution. *J. Light. Technol.* **2022**, *40* (7), 2173−2180.
(140) Amin, N. M.; Kamil, Y. M.; Abidin, N. H. Z.; Mustafa, F. H.; Bakar, M. H. A. Chitosan-Integrated Single-Mode Tapered Optical Fiber DENV II e Protein Sensor. *IEEE Sens. J.* **2021**, *21* (18), 20069−20077.
(141) Liu, H.; Sun, Y.; Guo, J.; Liu, W.; Liu, L.; Meng, Y.; Yu, X. Temperature-Insensitive Label-Free Sensors for Human IgG Based on S-Tapered Optical Fiber Sensors. *IEEE Access* **2021**, *9*, 116286−116293.
(142) Li, H.-C.; Leng, Y.-K.; Liao, Y.-C.; Liu, B.; Luo, W.; Liu, J.; Shi, J.-L.; Yuan, J.; Xu, H.-Y.; Xiong, Y.-H.; et al. Tapered Microfiber MZI Biosensor for Highly Sensitive Detection of Staphylococcus Aureus. *IEEE Sens. J.* **2022**, *22* (6), 5531−5539.
(143) Hou, Z.; Sun, D.; Wang, G.; Ma, J. Highly Sensitive Cholesterol Concentration Trace Detection Based on a Microfiber

https://doi.org/10.1021/acsomega.3c03970
ACS Omega 2024, 9, 3037−3069

Optic-Biosensor Enhanced Specificity with Beta-Cyclodextrin Film. *Spectrochim. Acta Part A Mol. Biomol. Spectrosc.* **2023**, *300*, 122881.
(144) Ma, C.; Sun, K.; Wang, G.; Wang, G.; Sun, D.; Ma, J. A Nonenzymic Microfiber Optic-Biosensor Modified Phenylboric Acid for Sensitively and Specifically Detecting Low Glucose Concentration. *Spectrochim. Acta Part A Mol. Biomol. Spectrosc.* **2023**, *303*, 123197.
(145) Li, H.; Huang, T.; Yuan, H.; Lu, L.; Cao, Z.; Zhang, L.; Yang, Y.; Yu, B.; Wang, H. Combined Ultrasensitive Detection of Renal Cancer Proteins and Cells Using an Optical Microfiber Functionalized with Ti3C2MXene and Gold Nanorod-Nanosensitized Interfaces. *Anal. Chem.* **2023**, *95* (11), 5142−5150.
(146) Gorai, P.; Kumar, S.; Marques, C.; Singh, P. K.; Jha, R. Imprinted Polymer Functionalized Concatenated Optical Microfiber (COM): Hypersensitive & Selective. *IEEE Sens. J.* **2023**, *23* (1), 329−336.
(147) Chen, H.; Luo, B.; Wu, S.; Shi, S.; Dai, Q.; Peng, Z.; Zhao, M. Microfluidic Biosensor Based on Molybdenum Disulfide (MoS2) Modified Thin-Core Microfiber for Immune Detection of Toxoplasma Gondii. *Sensors* **2023**, *23* (11), 5218.
(148) Gorai, P.; Brambilla, G.; Jha, R. Fast, Selective, and Sensitive Detection of 2,4-Dichlorophenol by an Imprinted Polymer Functionalized Core-Offset U-Shaped Fiber Sensor. *Opt. Lett.* **2023**, *48* (20), 5391−5394.
(149) Zhang, X.; Hou, X.; Feng, W. Trace Detection of Canine Distemper Virus Based on Surface-Functionalized Optic-Fiber Mach-Zehnder Interferometer and the Vernier Effect. *J. Phys. D. Appl. Phys.* **2023**, *56* (43), 435401.
(150) Nguyen, L. V.; Hill, K.; Warren-Smith, S.; Monro, T. Interferometric-Type Optical Biosensor Based on Exposed Core Microstructured Optical Fiber. *Sensors Actuators B Chem.* **2015**, *221*, 320−327.
(151) Li, J.; Zhang, W.; Tong, Z.; Liu, J. Fiber Optic Sensor Modified by Graphene Oxide-Glucose Oxidase for Glucose Detection. *Opt. Commun.* **2021**, *492*, 126983.
(152) Patiño-Jurado, B.; Cardona-Maya, Y.; Jaramillo-Grajales, M.; Montagut-Ferizzola, Y. J.; Botero-Cadavid, J. F. A Label-Free Biosensor Based on E-SMS Optical Fiber Structure for Anti BSA Detection. *Opt. Fiber Technol.* **2022**, *74*, 103116.
(153) Al Noman, A.; Dash, J. N.; Cheng, X.; Tam, H.-Y.; Yu, C. Mach-Zehnder Interferometer Based Fiber-Optic Nitrate Sensor. *Opt. Express* **2022**, *30* (21), 38966−38974.
(154) Li, X.; Chen, N.; Zhou, X.; Zhang, Y.; Zhao, Y.; Nguyen, L. V.; Ebendorff-Heidepriem, H.; Warren-Smith, S. C. In-Situ DNA Detection with an Interferometric-Type Optical Sensor Based on Tapered Exposed Core Microstructured Optical Fiber. *Sensors actuators B Chem.* **2022**, *351*, 130942.
(155) Yan, M.; Wang, R.; Wang, Q.; Li, Y.; Liu, B.; Li, Y.; Jiang, M. Label-Free and Highly-Sensitive Protamine Detection by Layer-by-Layer Assembled Chitosan/Heparin Functionalized Optical Fiber Mode Interferometer. *Sensors Actuators B Chem.* **2023**, *395*, 134414.
(156) Lu, J.; Duan, T.; Wang, L.; Geng, Y.; Yi, D.; Tong, Z.; Zhu, X.; Li, X.; Hong, X. In-Situ DNA Detection Using a Phase-Demodulated High-Order Intermodal Interferometer Based on an Exposed-Core Microstructure Fiber. *IEEE Sens. J.* **2023**, *23* (12), 12736−12742.
(157) Gorai, P.; Mizuno, Y.; Kumar, M.; Jha, R. Molecular Imprinting Polymer Nanoparticles Coupled with an Optical Sensor for Sensitive and Label-Free Detection of p-Cresol. *ACS Appl. Nano Mater.* **2023**, *6* (14), 12946−12956.
(158) Wang, L.; Yi, D.; Geng, Y.; Duan, T.; Tong, Z.; Chen, S.; Ning, Z.; Du, Y.; Hong, X.; Li, X. Ultrasensitive Deafness Gene DNA Hybridization Detection Employing a Fiber Optic Mach-Zehnder Interferometer: Enabled by a Black Phosphorus Nanointerface. *Biosens. Bioelectron.* **2023**, *222*, 114952.
(159) Liu, J.; Liu, B.; Liu, J.; He, X.-D.; Yuan, J.; Ghassemlooy, Z.; Torun, H.; Fu, Y.-Q.; Dai, X.; Ng, W. P.; et al. Integrated Label-Free Erbium-Doped Fiber Laser Biosensing System for Detection of Single Cell Staphylococcus Aureus. *Talanta* **2023**, *257*, 124385.
(160) Hua, P.; Ding, Z.; Liu, K.; Guo, H.; Pan, M.; Zhang, T.; Li, S.; Jiang, J.; Liu, T. Distributed Optical Fiber Biosensor Based on Optical Frequency Domain Reflectometry. *Biosens. Bioelectron.* **2023**, *228*, 115184.
(161) Hu, X.; Zhao, Y.; Peng, Y.; Tong, R.; Zheng, H.; Zhao, J.; Hu, S. In-Fiber Optofluidic Michelson Interferometer for Detecting Small Volume and Low Concentration Chemicals with a Fiber Ring Cavity Laser. *Sensors Actuators B Chem.* **2022**, *370*, 132467.
(162) Yue, Z.; Feng, W. Fiber-Optic Michelson Interferometer Based on α-Fe2O3/ZrO2 Sensing Membrane and Its Application in Trace Fluoride-Ion Detection. *Zeitschrift für Naturforsch. A* **2022**, *77* (3), 269−278.
(163) Al Noman, A.; Dash, J. N.; Cheng, X.; Tam, H.-Y.; Yu, C. PCF Based Modal Interferometer for Lead Ion Detection. *Opt. Express* **2022**, *30* (4), 4895−4904.
(164) Xiong, G. L.; Zhuang, J. H.; Feng, W. L. Fiber-Optic Lead Ion Sensor Based on MXene Film Integrated Michelson Interference Structure. *Phys. Scr.* **2023**, *98* (2), 025708.
(165) Mollah, M. A.; Usha, R. J.; Tasnim, S.; Ahmed, K. Detection of Cancer Affected Cell Using Sagnac Interferometer Based Photonic Crystal Fiber Refractive Index Sensor. *Opt. Quantum Electron.* **2020**, *52* (9), 421.
(166) Gu, H.; Luo, B.; Wu, S.; Shi, S.; Zou, X.; Dai, Q.; Zhao, M.; Zhang, L. Novel Optical Fiber Vernier Immunosensor Based on Cascading Sagnac Loops Embedded with Excessively Tilted Fiber Grating for Specific Detection of Canine Distemper Virus. *J. Biophotonics* **2023**, *16* (4), No. e202200294.
(167) Ghasemi, M.; Oh, J.; Jeong, S.; Lee, M.; Bohlooli Darian, S.; Oh, K.; Kim, J. K. Fabry-Perot Interferometric Fiber-Optic Sensor for Rapid and Accurate Thrombus Detection. *Biosensors* **2023**, *13* (8), 817.
(168) Li, F.; Li, X.; Zhou, X.; Gong, P.; Zhang, Y.; Zhao, Y.; Nguyen, L. V.; Ebendorff-Heidepriem, H.; Warren-Smith, S. C. Plug-in Label-Free Optical Fiber DNA Hybridization Sensor Based on C-Type Fiber Vernier Effect. *Sensors Actuators B Chem.* **2022**, *354*, 131212.
(169) Faiz, F.; Cran, M. J.; Zhang, J.; Muthukumaran, S.; Sidiroglou, F. Graphene Oxide Doped Alginate Coated Optical Fiber Sensor for the Detection of Perfluorooctanoic Acid in Water. *IEEE Sens. J.* **2023**, *23* (12), 12861.
(170) Chen, L.; Li, J.; Xie, F.; Tian, J.; Yao, Y. High-Sensitivity Carcinoembryonic Antigen Detection Using Open Cavity Fabry-Perot Immunosensor Based on Vernier Effect. *J. Light. Technol.* **2023**, *41* (13), 4547.
(171) Wang, R.; Yan, M.; Jiang, M.; Li, Y.; Kang, X.; Hu, M.; Liu, B.; He, Z.; Kong, D. Label-Free and Selective Cholesterol Detection Based on Multilayer Functional Structure Coated Fiber Fabry-Perot Interferometer Probe. *Anal. Chim. Acta* **2023**, *1252*, 341051.
(172) Rakhimbekova, A.; Seitkamal, K.; Kudaibergenov, B.; Nazir, F.; Pham, T.; Blanc, W.; Vangelista, L.; Tosi, D. Fiber-Optic Semi-Distributed Fabry-Perot Interferometer for Low-Limit Label-Free Detection of CCL5 Cancer Biomarker. *Opt. Laser Technol.* **2024**, *168*, 109953.
(173) Mukherjee, M.; Appaiah, P.; Sistla, S.; Bk, B.; Bhatt, P. Bio-Layer Interferometry-Based SELEX and Label-Free Detection of Patulin Using Generated Aptamer. *J. Agric. Food Chem.* **2022**, *70* (20), 6239−6246.
(174) Gao, S.; Cheng, Y.; Zhang, S.; Zheng, X.; Wu, J. A Biolayer Interferometry-Based, Aptamer-Antibody Receptor Pair Biosensor for Real-Time, Sensitive, and Specific Detection of the Disease Biomarker TNF-α. *Chem. Eng. J.* **2022**, *433*, 133268.
(175) Qin, T.; Wang, M.; Wu, P.; Zhang, Q.; Kang, K.; Ma, Y.; Lin, Z.; Wang, J. Escherichia Coli Surface-Displayed by Sup35NM Nanofibrils and Z-Domains Fusion Protein for Signal Enhancement in a Biolayer Interferometry-Based Immunoassay. *Sensors Actuators B Chem.* **2023**, *390*, 133938.
(176) Gao, S.; Li, Q.; Zhang, S.; Sun, X.; Zhou, H.; Zhang, Y.; Wu, J. Peptide-Nucleic Acid Aptamer Pair Biosensor for Disease Biomarker Detection in Clinical Samples. *Chem. Eng. J.* **2023**, *458*, 141499.
(177) Gao, S.; Li, Q.; Zhang, S.; Sun, X.; Zhou, H.; Wang, Z.; Wu, J. A Novel Biosensing Platform for Detection of Glaucoma Biomarker

https://doi.org/10.1021/acsomega.3c03970
ACS Omega 2024, 9, 3037−3069

GDF15 via an Integrated BLI-ELASA Strategy. *Biomaterials* **2023**, *294*, 121997.
(178) Bao, X.; Chen, L. Recent Progress in Distributed Fiber Optic Sensors. *sensors* **2012**, *12* (7), 8601−8639.
(179) Díaz-Herrera, N.; Viegas, D.; Jorge, P. A. S.; Araújo, F. M.; Santos, J.-L.; Navarrete, M.-C.; González-Cano, A. Fibre-Optic SPR Sensor with a FBG Interrogation Scheme for Readout Enhancement. *Sensors Actuators B Chem.* **2010**, *144* (1), 226−231.
(180) Chen, M.; He, T.; Zhao, Y.; Yang, G. Ultra-Short Phase-Shifted Fiber Bragg Grating in a Microprobe for Refractive Index Sensor with Temperature Compensation. *Opt. Laser Technol.* **2023**, *157*, 108672.
(181) Wei, Y.; Wu, P.; Zhu, Z.; Liu, L.; Liu, C.; Hu, J.; Wang, S.; Zhang, Y. Surface-Plasmon-Resonance-Based Optical-Fiber Micro-Displacement Sensor with Temperature Compensation. *Sensors 2018, Vol. 18, Page 3210* **2018**, *18* (10), 3210.
(182) Shiratsuchi, T.; Imai, T. Development of Fiber Bragg Grating Strain Sensor with Temperature Compensation for Measurement of Cryogenic Structures. *Cryogenics (Guildf).* **2021**, *113*, 103233.
(183) Oe, R.; Minamikawa, T.; Taue, S.; Koresawa, H.; Mizuno, T.; Yamagiwa, M.; Mizutani, Y.; Yamamoto, H.; Iwata, T.; Yasui, T. Refractive Index Sensing with Temperature Compensation by a Multimode-Interference Fiber-Based Optical Frequency Comb Sensing Cavity. *Opt. Express* **2019**, *27* (15), 21463.
(184) Pannell, C. N.; Wacogne, B. F.; Abdulhalim, I. In-Fiber and Fiber-Compatible Acoustooptic Components. *J. Light. Technol.* **1995**, *13* (7), 1429−1434.
(185) Abdulhalim, I.; Pannell, C. N. Photoelastic In-Fiber Birefringence Modulator Operating at the Fundamental Transverse Acoustic Resonance. *IEEE photonics Technol. Lett.* **1993**, *5* (10), 1197−1199.
(186) Dahlin, A. Biochemical Sensing with Nanoplasmonic Architectures: We Know How but Do We Know Why? *Annu. Rev. Anal. Chem.* **2021**, *14*, 281−297.
(187) Little, T. Method Validation Essentials, Limit of Blank, Limit of Detection, and Limit of Quantitation. *BioPharm. Int.* **2015**, *28* (4). https://www.biopharminternational.com/view/method-validation-essentials-limit-blank-limit-detection-and-limit-quantitation
(188) Kabashin, A. V.; Evans, P.; Pastkovsky, S.; Hendren, W.; Wurtz, G. A.; Atkinson, R.; Pollard, R.; Podolskiy, V. A.; Zayats, A. V. Plasmonic Nanorod Metamaterials for Biosensing. *Nat. Mater.* **2009**, *8* (11), 867−871.
(189) Yang, T.; Chen, S.; He, X.; Guo, H.; Sun, X. How to Convincingly Measure Low Concentration Samples with Optical Label-Free Biosensors. *Sensors Actuators B Chem.* **2020**, *306*, 127568.
(190) Kimble, H. J. The Quantum Internet. *Nature* **2008**, *453* (7198), 1023−1030.
(191) Solano, P.; Grover, J. A.; Xu, Y.; Barberis-Blostein, P.; Munday, J. N.; Orozco, L. A.; Phillips, W. D.; Rolston, S. L. Alignment-Dependent Decay Rate of an Atomic Dipole near an Optical Nanofiber. *Phys. Rev. A* **2019**, *99* (1), 13822.
(192) Pierini, S.; D'Amato, M.; Joos, M.; Glorieux, Q.; Giacobino, E.; Lhuillier, E.; Couteau, C.; Bramati, A. Hybrid Devices for Quantum Nanophotonics. *J. Phys.: Conf. Ser.* **2020**, *1537*, 012005.
(193) Solano, P.; Grover, J. A.; Hoffman, J. E.; Ravets, S.; Fatemi, F. K.; Orozco, L. A.; Rolston, S. L. Optical Nanofibers: A New Platform for Quantum Optics. *Adv. At., Mol., Opt. Phys.* **2017**, *66*, 439−505.
(194) Ding, C.; Loo, V.; Pigeon, S.; Gautier, R.; Joos, M.; Wu, E.; Giacobino, E.; Bramati, A.; Glorieux, Q. Optical Nanofiber Interferometer and Resonator. *arXiv* **2019**, 1903.09735.
(195) Murmu, S.; Kumar, A.; Jha, R. Bidirectional Coupling of Diamond Emitters to Optical Nanowire: Tunable and Efficient. *JOSA B* **2021**, *38* (12), F170−F177.
(196) Sahu, S.; Jha, R. Efficient Coupling of Single Photons into Tilted Nanofiber Bragg Gratings. *Indian J. Pure Appl. Phys.* **2023**, *61* (7), 546−553.
(197) Martínez-Garaot, S.; Rodriguez-Prieto, A.; Muga, J. G. Interferometer with a Driven Trapped Ion. *Phys. Rev. A* **2018**, *98* (4), 043622.
(198) Lee, J.; Ding, R.; Christensen, J.; Rosenthal, R. R.; Ison, A.; Gillund, D. P.; Bossert, D.; Fuerschbach, K. H.; Kindel, W.; Finnegan, P. S.; et al. A Compact Cold-Atom Interferometer with a High Data-Rate Grating Magneto-Optical Trap and a Photonic-Integrated-Circuit-Compatible Laser System. *Nat. Commun.* **2022**, *13*, 5131.

https://doi.org/10.1021/acsomega.3c03970
ACS Omega 2024, 9, 3037−3069